Alma Mater Studiorum - Università di Bologna

DOTTORATO DI RICERCA IN

MECCANICA E SCIENZE AVANZATE DELL'INGEGNERIA

Ciclo 35

Settore Concorsuale: 09/A1 - INGEGNERIA AERONAUTICA, AEROSPAZIALE E NAVALE

Settore Scientifico Disciplinare: ING-IND/04 - COSTRUZIONI E STRUTTURE AEROSPAZIALI

VIBRO-ACOUSTIC ANALYSIS AND DESIGN OPTIMIZATION TO IMPROVE COMFORT AND SUSTAINABILITY OF FUTURE PASSENGER AIRCRAFT

Presentata da: Martino Carlo Moruzzi

Coordinatore Dottorato

Lorenzo Donati

Supervisore

Sara Bagassi

Co-supervisore

Marco Carricato

Esame finale anno 2023

Abstract

Due to the interest of general public and the industrial stakeholders, new challenges and demands are rising in aircraft design. The sustainability is taking its place amongst more traditional design factors, such as safety, performances and costs. Sustainability is both environmental and economic, and among the factors contributing to economic sustainability, there is also passengers' comfort. In order to win these two challenges, they must be considered in the early stages of aircraft design. In this work, the focus is on emissions generation and acoustic comfort, aiming at reducing pollution and internal noise in the preliminary design phases. These results can be achieved with both unconventional aircraft configurations and advanced materials, which also require new numerical formulations to be assessed. In this research, on one hand, the windowless configuration for a commercial aircraft is studied with traditional preliminary design methods in order to achieve a weight reduction and consequently a return in terms of emissions and costs. On the other hand, a new class of insulating materials, the acoustic metamaterials, is applied on the passenger cabin lining panels. The complex kinematic behaviour of these advanced materials is studied through the Carrera's Unified Formulation, that enhances a wide class of powerful refined shell and beam theories with a unique formulation.

A piè del monte la cui neve è rosa
In su 'l mattino candido e vermiglio,
Lucida, fresca, lieve, armoniosa
Traversa un'acqua ed ha nome dal giglio.

Giosuè Carducci, In riva al Lys

Contents

List of Figures

List of Tables

Introduction

The last thirty years have seen the rise of new demands and needs in the aviation sector from citizens, politics and industry. These requests can be subsumed under the concept of dual sustainability, which ranges from environmental sustainability, stemming from concern about rising global temperatures and reducing local air quality, to economic sustainability, that includes also requirements defined by the needs of users in their environment. The aviation sector can not avoid this challenge, because it participates in the production of pollutant emissions, around the 3-5 % of the global emissions, and on the other hand because it is an essential part of the everyday life of people who work in the industry or travel thanks to it. In order to achieve these goals in the aviation sector, improvements must be introduced in the whole life cycle, from industrial production to flight management and organisation. Moreover, the sustainability concept must be extended in the design phases too, through a collaborative and multi-disciplinary design. Major successes can be achieved in the design of new vehicles or parts of them. In this work, we will focus on the aircraft design. In this field, the concept of sustainability can be split into environmental and economic aspects. Both aspects must be considered in aircraft design, in order to produce a "successful" model. As a part of the economic aspect, we include the cabin comfort. Airliners could attract more passenger with more comfortable aircraft, and those passengers might accept to bear an extra-cost for a more comfortable flight, especially for long-haul journeys. Therefore, the dual sustainability concept can be declined in:

- emissions reduction, as pollution and noise, produced by the aircraft operations;
- passengers, crew and pilots' comfort increase during the flight.

Hence, the basic concept of this work is the combination between environmental sustainability and economic one: an aircraft must be "green" and suitable, in terms of cost and travel experience.

The production of emissions during flight and in the airport phases can be reduced in several ways, either by optimising the engines, lightening the aircraft structure or improving its aerodynamic efficiency. It is a general belief in the aviation industry that the traditional cylindrical aircraft windowed configuration, which has dominated the

skies since the dawn of aviation, can no longer lead to significant improvements, having already been exhaustively optimised. For this reason, several researches, and thus investments, are exploring new aircraft configurations for the aviation of the future. These new configurations are often extremely innovative, leading to a complete revamp even in the production and airport phases. On one hand, this brings great benefits, on the other hand it can generate new problems, as well as a certain mistrust of these configurations on the side of the various users. The configuration, proposed by the author in this work, is a windowless fuselage where the windows are replaced by monitors connected to external cameras. This configuration still exploits the classical aircraft shape, although the windows removal has several benefits, first of all, a significant reduction in structural weight, which leads to a decrease in the emissions. The reduction in weight is due to the removal of the windows reinforcements and frames. In order to consider the dual sustainability concept, monitors avoid any claustrophobia problem, enriching the cabin design. Moreover, this configuration can be extended to other more disruptive aircraft design, as geodesic fuselage, blended wing body aircraft or sub-orbital vessel, where windows can not be placed. The study is carried on in the preliminary design field.

The sustainability in terms of comfort is subject to many factors in an aircraft. However, there is no doubt that the centre of influence is the passenger cabin and, in the case of pilots, the cockpit. In this work, we focus on a rather neglected aspect, particularly until the 1990s, the internal noise. The current medium-to-high noise level in aircraft are one of the factors that most affect comfort, in addition it can rarely lead to health problems. In order to achieve a reliable noise reduction in the passenger cabin, two main steps must be followed:

- to create and exploit an accurate numerical model of the aircraft or of part of it. The main issue when studying noise spread in the aircraft is the absence of reliable preliminary tools, as those applied for the weight and emissions estimation. Therefore, in order to obtain reliable results, a more detailed analysis has to be carried on with numerical tools;
- to find and apply a noise reduction solution considering the acoustic sources and the frequency spectrum. Moreover, this solution must be evaluated in terms of weight and volume too.

The first step is assessed exploiting two different aircraft models, which have been previously and partially validated:

- a turboprop aircraft fuselage, the baseline of this model has been developed in the CASTLE (CAbin Systems design Toward passenger welLbEing), an EU-funded project in the Clean Sky 2 program. In this work, we enhance and study the model under different boundary conditions. The main limits of this model are the

low accuracy in the component connection description and the low flexibility in the design;

- a fuselage barrel of a turbofan aircraft, the baseline of this model has been developed by DLR (*Deutsches Zentrum für Luft- und Raumfahrt*) and it is referred to as CPACS based model. The numerical model has a high degree of accuracy in the components and connections description. Moreover, the whole structure is stored in a standardized language for Multi-Disciplinary Design Optimization (MDO), CPACS.

The second step follows the development of new noise reduction solutions. A very promising field is the study of Acoustic Metamaterials (AMMs). The concept is similar to those of electromagnetic or mechanical metamaterials, but the target are the acoustic waves. In particular we focus on low frequency noise, and so the tool is the Finite Element Method (FEM). At low frequencies traditional solutions struggle to achieve high performances without increasing weight.

During this research, it is noted that the analysis to the noise problem is often limited by the computational cost and accuracy of the structural models, in particular when dealing with sandwich or multi-layer materials, as composite or AMMs. Other limitations to the accuracy are given by the boundary conditions or by the simplification made during modelling of complex structures. Therefore, we choose to apply and develop a powerful approach, the Carrera's Unified Formulation (CUF), which enhances a wide class of shell and beam theories, allowing to reduce the computational cost of the problem and increasing the accuracy. In order to apply the CUF to the noise problem, several updates in the formulation and in the related software, MUL2, are done and validated. The purpose of this development is not limited to preliminary researches, as very simple models (e.g., plate-cavity system), but aims to lay the foundations for the future use of CUF in the study of the complete aircraft/fuselage, significantly reducing the computational cost of the problem without affecting the accuracy of the solution. Nowadays, this is one of the major limitations in studying low-frequency noise with FE methods.

The work is organized in four main chapters. The sustainability concept is outlined in Chapter 1 in terms of pollution and comfort assessment, with a focus on the discomfort due to the noise. Then, the preliminary design methods and tools to estimate the aircraft weight for a windowless configuration are described in Chapter 2. Moreover, the CPACS concept and standard language is defined in a MDO framework. The internal noise problem in aircraft is described in terms of equations and state of art in Chapter 3, that introduces the next one. The next two chapters assess the main part of this work. In Chapter 4, the CUF is depicted and the related progresses performed in this work are reported with their validations. In Chapter 5, the case study description and results are reported, the reduction in weight of the windowless configuration is calculated within

its acoustic behavior, then a noise reduction solution is proposed and studied. The sustainability of the configuration is estimated in terms of emissions reduction and operating costs saving.

Chapter 1

New challenges for commercial aircraft

1.1 New design demands for the 21st century aircraft

Traditionally, aircraft design demands have to meet the mission requirements at minimum cost, satisfying requirements for passengers safety, reliability and minimum comfort standard. These requirements are still important, but new demands and standard are emerging in the last years. In fact, the effect of aircraft operations on environment, both on global climate and local air quality described in Section 1.2.1, has become an important aspect in aircraft design, for both the general public and the governments. Moreover, comfort standards are becoming higher than before, in particular because the competition from other more comfortable and smart means of transport, as high-speed train or road transport, as described by Alabalte et al. [1], in particular in regional and medium range routes.

The green aircraft new demand is led by the concern of general public, and therefore of the governments, about the rise of global warming and about noise and pollution near airports, in particular for residential area. Several regulations, issued by governments and civil aviation organizations as ICAO (International Civil Aviation Organization), exist to limit aircraft impact on climate, both global and local. Several projects aim to reduce the aviation emissions and noise in next years. In the European Union, Clean Sky 1-2 and Clean Aviation projects aim at the reduction of CO_2, gas emissions and noise levels produced by aircraft. The ACARE (Advisory Council for Aeronautics Research in Europe) vision "Flightpath 2050" is:

- to reduce CO_2 emissions of 75%, NO_x (nitrogen oxide) emissions of 90%, and 65% reduction in perceived noise (relative to new aircraft delivered in 2000);
- to free emissions from aircraft when taxiing;

- to design and manufacture air vehicles to be recyclable;
- to lead Europe on becoming a centre of excellence for sustainable alternative fuels including for aviation;
- to allow Europe to lead atmospheric research and establishment of global environmental standards.

Similar goals are shared by NASA in the United States "for a 2030 era aircraft" relative to new aircraft delivered after 2013:

- a 71-decibel reduction below current Federal Aviation Administration noise standards, aimed to contain objectionable noise within airport boundaries;
- a greater than 75% reduction on the ICAO CAEP/6 standard for NO_x emissions, to improve air quality around airports;
- a greater than 70% reduction in fuel burn to reduce greenhouse gas emissions and the cost of air travel.

Finally, the increase of jet fuel price is affecting the aircraft optimization, referring to the work by Jupp [2].[1] Hence, to prevent an increase in operating costs, new aircraft and jet fuel design must reduce the fuel consumption or change the fuel itself.

On the other hand, the increase in passenger comfort inside the aircraft cabin is becoming an important design demand, as described in Section 1.2.2. Customer requirements are recognized as a key motivation in business and design, as described in the work by Hall et al. [3]. Drivers are comfort and customer experience. In fact, airlines enhance passenger experience to attract and retain customers. The experience means also the quality of the flight and so the comfort of the aircraft cabin. Cabin comfort design involves many issues as aesthetics, space, safety, service efficiency and physical aspects (sound and vibrations transmission, heating and air-conditioning, ventilation, lighting and other ergonomic aspects). Nowadays, an aircraft to be competitive on the market must take in account a human centred cabin design.

In the last years, next to more traditional design demands, customers, passengers and therefore airlines, look to the aircraft impact on the environment and to the cabin comfort level. Moreover, the inevitable increase in jet fuel price leads to new design solutions to reduce fuel consumption. These new demands can only partially be achieved by the current cylindrical aircraft configuration and shape with low wings and a turbofan or turboprop engine. The aeronautical industry is increasingly moving towards

[1] This trend is further accentuated by the Covid-19 pandemic and the war in Ukraine, as reported in a IATA factsheet, `https://www.iata.org/en/iata-repository/publications/economic-reports/the-impact-of-the-conflict-between-russia-and-ukraine-on-aviation/`.

new aircraft concepts with completely or partially disruptive configurations and propulsion technologies within new design method.[2] Some of the most famous examples are the blended wing body aircraft, as experimented by Boeing with prototype X-48 , the Flying-V by *TU Delft*, the Prandtl plane by *Univeristà di Pisa* or the hydrogen powered aircraft, as studied by Airbus with ZEROe concepts. In this work, as a case study, we propose a windowless aircraft configuration, which presents an important reduction in the empty weight with a less disruptive configuration. The concept is described in Chapter 5 and can be extended as a benchmark for other windowless configurations.

1.2 Sustainability

1.2.1 Aircraft pollution

An aircraft needs a horizontal force to fly. This force is generated by the engine, converting thermal energy to mechanical energy and giving to the aircraft enough thrust to fly. The engine burns fuel to generate the thermal energy from a chemical reaction. In fact, inside the engine there is a reaction between air (composed of nitrogen N_2 and oxygen O_2), coming in from the outside atmosphere, and fuel (composed of gasoline C_nH_m and sulfur S*). After the combustion process, we obtain the following products:

$$CO_2 + NO_x + SO_x^* + HC + CO + H_2O + BC^* \tag{1.2.1}$$

The aircraft emissions are composed by carbon dioxide (CO_2), water vapor (H_2O), hydrocarbons (HC), carbon monoxide (CO), nitrogen oxides (NO_x or NO+NO_2), sulfur oxides (SO_x) and non volatile black carbon (BC or soot). The drawing in Fig. 1.1, from the introduction of the work by Sarkar [4], shows the greenhouse gases and other emissions from the aircraft engine. The aircraft emissions can be at low altitude or at the sea level, during take-off and landing phase, or, for most of the flight, at cruise altitudes within the upper troposphere and the lower stratosphere (UTLS).

Referring to high altitudes emissions and to the work by Guy et al. [5], we can describe the effect of combustion products on climate. Direct emissions of gases like CO_2, H_2O and soot particles, by-products like O_3 and stratospheric H_2O and perturbed methane CH_4 tend to have a positive radiative forcing RF and therefore a warming effect. The RF, expressed in Wm^{-2}, is a global index for instantaneous climate forcing that quantifies the mean net radiative energy per unit time at the top of the troposphere. Gaseous emissions of SO_x, NO_x and of gaseous HC partially evolve into volatile nitrate, sulfate aerosols and semi-volatile organic particles respectively, which also contributes to climate change. On the contrary, particles like sulfates generally have a negative RF and therefore a cooling effect, unless they coat soot particles, which exert warming

[2] From the Clean Aviation website `https://www.clean-aviation.eu/free-radical-innovative-configurations-and-propulsive-concepts-for-the-2030s`.

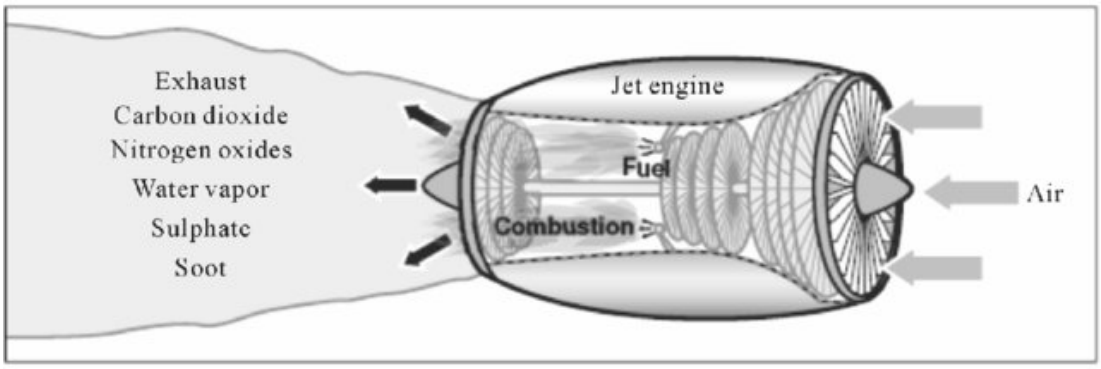

Source:GAO.

Figure 1.1: Selected greenhouse gases and other emissions from the aircraft at cruising altitude.

effects.

Another contribution to the climate warming at high altitude is given by persistent linear contrails produced in the wake of aircraft. Moreover, the contrail-induced cirrus cloud (AIC) are expected to contribute to RF, but the quantity of this contribution remain highly uncertain. In general the short period and long period RF of non-CO_2 aviation emissions is not the sum of various RF, there is a non-linear interaction between them, and therefore it is not possible to quantify this effect with RF metric.

During take-off and landing aircraft fly near residential areas and airports. Moreover, the fuel burnt during taxi phase and by the auxiliary power unit (APU) must be taken in account. Several studies, as those by Campagna et al. [6] and Hudda et al. [7], describe and point out the possible health issues, like cardiovascular disease, caused by aviation particulate matter (PM) and particularly by ultra-fine particles (UFP) on people who live or work near the airports.

Finally, the last undesired product from an operating aircraft is noise. The noise affects people and animal outside, in particular in near ground flight phases, and passengers and crew inside the aircraft. The sources are varied in number and kind. The principal sources are the engine (in the airport also the APU), the lifting surfaces (wing, tail and high-lift devices), the turbulent boundary layer around the fuselage and the flow around the landing gear during the take-off and landing. Moreover, for internal noise, cabin conditioning and pressurizing system noise, structure-born noise and other systems noise must be taken in account, a description of the cabin noise is given in Section 3.5.2. Noise exposure can lead to noise-induced hearing loss or to non-auditory effects (annoyance, cardiovascular disease, sleep disturbance, etc.) as described by Basner et al. [8]. This work focuses on the challenge that we cannot predict the structural and acoustic behavior of these new, sustainable configurations and how noise treatments can be considered in the design phase to fulfill future requirements. Therefore, we do not know how to accurately model the new sustainable layer-based sandwich materials or acoustic metamaterials (AMM) for noise treatments.

In order to summarize this section, we report the results from ICAO report,[3] aviation affects:

- global climate through engine greenhouse gas, ICAO estimates the aviation sector contributes from 3% to 5% to the global warming and approximately 65% of global aviation fuel consumption is from international aviation;
- local air quality through engine emission and aircraft noise.

1.2.2 Comfort

The factors, that affect the comfort level in an aircraft cabin, include visual comfort, interaction comfort (usability, ergonomics such as reachability, accessibility and visibility), postural comfort (including postural angle, sitting pressure distribution, surfaces of contact), living space comfort, acoustic comfort and thermal one. In the end, according to the work by De Looze et al. [9]:

- comfort is a construct with subjective and personal elements;
- various factors influence comfort (psychological, physiological and physical);
- comfort is a reaction to the environment (e.g., the passenger cabin).

Visual comfort and interaction comfort are usually studied in cabin interior design in particular referring to seats and aisle, or to the cockpit for the pilots. For a review on ergonomics in the aviation see the work by Neville et al. [10]. Visual comfort depends on the sense of sight and includes the look of the cabin interior and the illuminations. Moreover, thermal comfort and air quality, regulated by the air pressurization and conditioning system, must be taken in account.

In this work, we principally consider acoustic comfort as in important factor, which was not really considered in the dawn of aviation. In fact, only in the last few years, comfort in the cabin is becoming an important requirement, leading to the realization of future regulations and objectives, also at a global level, reversing the sentence in one of the first work in interior noise by Basset et al. [11]: "No attention has been paid to noise, however, until now. Pilots and early passengers took it for granted that the noise was just an unavoidable evil that went with flying and high speed." Noise has several negative effects on people, in particular caused by a one-time exposure to an intense impulse sound or by steady state long-term exposure with sound pressure level higher than 75-85 dBA, which are the average noise level in a turbofan aircraft cabin. In aircraft, the main effects is the decreasing of the comfort level as studied by Pennig et al. [12]. Moreover, the noise affects the thermal comfort and perception too, as reported in the work by Bourikas et al. [13].

[3] `https://www.icao.int/environmental-protection/Pages/envrep2022.aspx`

Finally, two secondary and indirect effects are related to the noise reduction in the cabin. The understanding of the noise propagation in the passenger cabin and in the aircraft structure, could lead to find solutions for the external noise reduction. Moreover, noise is usually associated to structural vibrations, and a decrease in noise transmission is connected to vibrations reduction.

1.2.3 Comfort assessment

The main problem when dealing with comfort is its assessment, in particular in the preliminary design phase, when a flexible design method is necessary and not all parameters have been defined yet. Generally, comfort is studied on existing aircraft in order to find the main issues for further aircraft design or cabin interior improvement. These researches are usually made through questionnaires to develop an assessment that identifies dissatisfaction indicators of cabin comfort, two examples are the works by Restuputri et al. [14] for a general overview on comfort indicators and by Pang et al. [15] for thermal comfort.

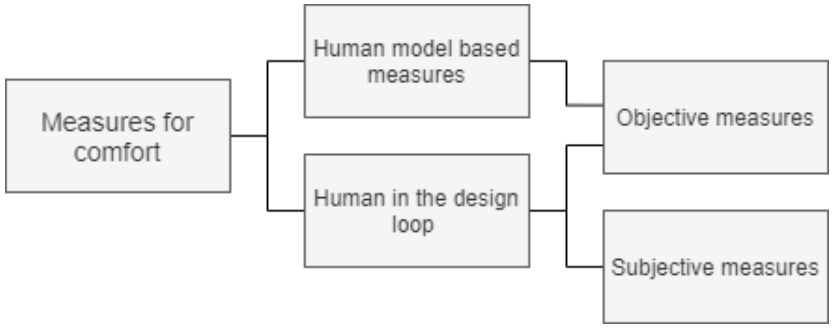

Figure 1.2: The two different approaches for comfort assessment depending on the user engagement in the design process.

In design phases comfort evaluation can follow two different paths to measure it as described by Bagassi et al. [16] in Fig. 1.2. A human model based measurement considers the human as a model, which generally has some maximum, minimum and average parameters. These can be obtained from physical and physiological laws (e.g., the size of a passenger for ergonomics or the maximum loud noise) or from statistical survey proposed to the users (the passengers, the crew and the pilots). The advantage of this approach is the simplicity, and the fact that it can be applied at any step of the design process. Although, these parameters do not take in account subjective measurements and are unable to capture user's perception in terms of emotional feelings. In order to improve comfort, it is important to have the user centred design process. This is possible through cabin or interior mock-up, where the user experience is evaluated with questionnaires survey using psychometric scales. In the preliminary design phases, the main issue is the availability of large and detailed mock-ups. Nevertheless, new technologies as virtual reality and augmented reality can create virtual mock-up in

a more flexible and cheaper way, allowing to switch and submit to the user several design concepts and possible improvements as studied in the work by De Crescenzio et al. [17]. A user centred design can also be applied to other aspects and disciplines of the preliminary aircraft design, in particular for the aircraft flight control in terms of stability and maneuverability, as described by Kiehn et al. [18] in the COAST project, where the users are pilots. They evaluate new aircraft configurations maneuverability through immersive flight simulators.

In noise evaluation the human model based measures are the standard practice based on the parameters described in Section 3.4. Usually a noise level above 85 dB must be avoided for health reasons (the level is lowered for long exposure, as in residential area). In this work a conceptual solution for a human centred design for the noise problem is described in Section 3.6.

Chapter 2

The preliminary design process

2.1 Introduction to preliminary design

The preliminary design constitutes a link between the conceptual design and the final design, establishing in particular the feasibility of the conceptual one. It is often used when the project has not yet reached such completeness to allow a final study and it gives the points and data where to start the final design. The preliminary design is a highly iterative process, very flexible and multidisciplinary, where initial requirements and data may vary over time and between iterations. The design process can be defined as: "The whats initiating conceptual design produce hows from the conceptual design evaluation effort applied to feasible conceptual design concepts. Next, the hows are taken into preliminary design through the means of allocated requirements. There they become whats and drive preliminary design to address hows at this lower level."[1] The preliminary design materialises the how into the what. In the aviation field, the question is whether an aircraft design in its conceptual state is capable of moving to a more advanced state of design from the point of view of feasibility and cost-effectiveness. Moreover, only six initial parameters are usually required to conduct this type of study on a civil aircraft: the type of aircraft, the engine, the number of passengers, the cruising speed (Mach of flight), the flight altitude and the maximum cruising range.

In this chapter, the preliminary design theory is briefly described referring to the classical works on aircraft design by Torenbeek, Raymer, Jekinson et al. and Sforza [19–22]. Moreover, a statistical survey based on this theory is performed in order to have a base for the development of the case study in Chapter 5 and to estimate any parameter needed, but not directly calculable, as for example the correlation between the number of windows and the aircraft geometry. Then, the multi-disciplinary optimization method is introduced within a driver for this kind of design, CPACS (Common Parametric Aircraft Configuration Schema).

[1] S. Blanchard and J. Fabrycky, Systems engineering and analysis, Prentice-Hall, 1981

2.2 Preliminary design theory

In this section, the focus is on the preliminary design principles and equations used to develop the study case in Chapter 5, in particular for the weight and fuel consumption estimation. The aim is to calculate the new fuel consumption of an existing aircraft, following a structural weight reduction, in order to estimate the emissions and operating costs savings. Therefore, the preliminary design models are used for the three following problems:

- the weight estimations of some subsystems, which can be calculated by equation in [19, 21, 22] in particular for wing, landing gear and control surfaces;
- the fuel consumption calculation from the Breguet's equation;
- the previous point needs at least a preliminary estimation of the aerodynamic efficiency and of the cruise fuel fraction.

The Breguet's equation is written as follow in order to calculate the cruise range R of an aircraft:

$$R = \frac{V}{SFC} E \cdot ln\left(1 + \frac{W_{cruise\ fuel}}{W_{flight}}\right) \tag{2.2.1}$$

where V is the cruise speed, SFC the specific fuel consumption and E the aerodynamic efficiency. The argument of the natural logarithm depends on the fuel used for the cruise $W_{cruise\ fuel}$ and by the remaining weight W_{flight}. The aircraft speed depends on the aircraft model and can be found in the aircraft data sheet. The SFC in first approximation is equal to 0.6 $lb/(lbf \cdot hr)$ in the imperial system. The other parameters must be calculated or estimated.

The aerodynamic efficiency is not always available for existing models. The standard definition is:

$$E = \frac{L}{D} = \frac{C_L}{C_D} \tag{2.2.2}$$

where L and D are the lift and drag, and C_L and C_D their dimensionless coefficients. The lift coefficient is defined as:

$$C_L = \frac{L}{0.5\rho S V^2} \tag{2.2.3}$$

in which ρ is the density of the air, S is the wing surface and V is the cruise speed. These three terms are known and easily retrievable. The lift in cruise condition is proportional to the aircraft weight. We can assume that the aircraft weight is equal to the take-off weight without the fuel used during engine start, warm up and taxi. These phases are the first two fractions in the fuel fraction method and they are equal to the 2% of the aircraft take-off weight $L = 0.98 \cdot W_{TO}$.

The drag coefficient can be written as the sum of zero-lift (or parasitic) drag coefficient and of induced drag, which depends on a constant terms k and of lift coefficient:

$$C_D = C_{D_0} + kC_L^2 \tag{2.2.4}$$

Moreover the effect of interference between wing, tail and fuselage must be taken into account, the interference drag, within the wave compressibility effects that rise exceeding the critical Mach number, the wave drag.

The zero-lift drag could be expressed as the sum of the zero-lift drag of each component of the aircraft. The zero-lift drag of each component derives from the skin friction coefficient C_f, the form factor FF, the interference factor Q and ratio between the wet surface area of the component S_{wet} and the reference surface area, the wing surface area, S:

$$C_{D_0} = \sum_{i=1}^{n} C_{f,i} FF_i Q_i \frac{S_{wet,i}}{S} \tag{2.2.5}$$

The first term, the skin friction coefficient, depends on the type of flow and so on the Reynolds' number, while the form factor, the interference factor and the wet area depend on the component. These parameters are calculated based on the already cited work [19,21,22]. The induced drag depends on the lift coefficient in Eq. 2.2.3. The term k depends on two factors, the wing aspect ratio and the Oswald's factor. The former depends on the wing geometry. The latter can be estimated either from the taper ratio, the swept angle and the fuselage size or from the zero-lift drag of the aircraft. The interference drag is calculated from the Horner's equation and the wave drag depends on the Mach number and on the wing swept angle according to the work by Ogur et al. [23]

The second problem is related to the weight estimation and the solution is based on the fuel fraction method. The fuel fraction method is described by Sforza [22] and it is defined by the following equation:

$$M_{fuel} = \frac{W_{fuel}}{W_{TO}} = 1 - \prod_{i=1}^{n} \frac{w_i}{w_{i-1}} \tag{2.2.6}$$

where the ratio w_i/w_{i-1} is the $i-th$ fuel fraction and n is the total number of fuel fractions. Each fraction describes a segment of the aircraft mission, as reported in Fig. 2.1. The fuel fractions include the consumed fuel during the mission and the reserve fuel, imposed by regulation.

The two weights in the Eq. 2.2.1 are the fuel for the cruise segment 5 and the aircraft weight without the fuel used from segment 1 to 4, corresponding to the engine start and warm-up, taxi, take-off and climb. The first two phases, according to the fuel fraction, are equal to the 4.5% of the take-off weight, therefore $W_{flight} = 0.955 \cdot W_{TO}$. The cruise

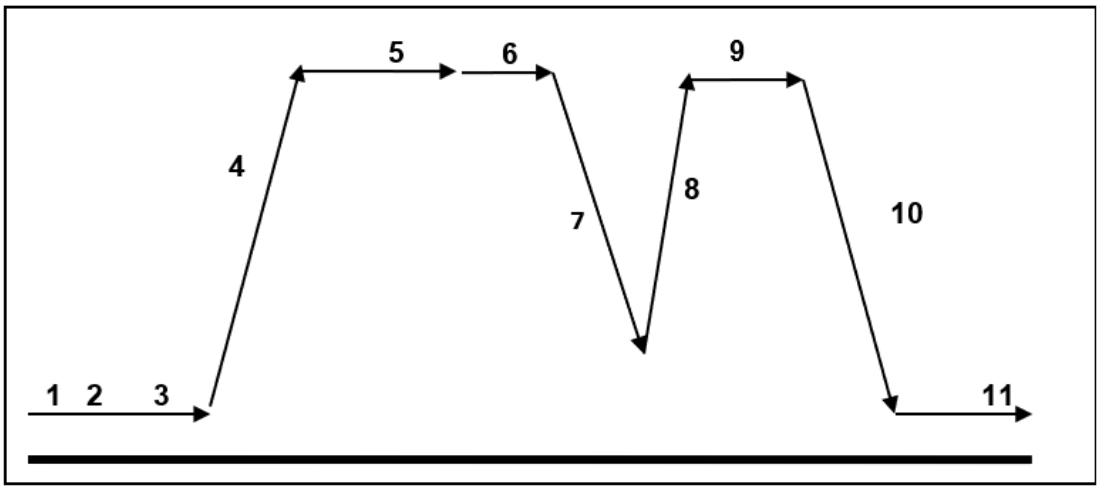

Figure 2.1: The fuel fraction mission of a medium range aircraft [22].

fuel weight can be obtained from the fuel weight W_F as:

$$W_{cruise} = W_5 = W_F - W_{1-4} - W_{6-11} \tag{2.2.7}$$

where the segments from 6 to 9 are imposed by the regulation and represent one additional hour of flight at cruise condition, descent to destination and refused landing, the climb and the diversion to a different airport 200 nm distant. The segments 10 and 11 are the descent and the landing phases.

Finally, all terms in the Eq. 2.2.1 are known and it is possible to calculate the range and the fuel consumption as the ratio between the cruise fuel volume (or mass) and the range.

2.3 Correlation between the number of windows and fuselage length

In order to understand the correlation between some aircraft parameters, a statistical survey on the existing aircraft model is performed. In particular, the aim is to integrate in the existing survey in [19–22], the number of windows (on one side of the aircraft) for preliminary calculation carried in Section 5.2. As it can be easily deduced, this parameter plays a primary role in the calculation of the weight reduction of a windowless configuration. The survey is performed and reported in author's work [24] on ten aircraft models in short-medium range. The number of windows $N_{w/2}$ is correlated to the fuselage length L, to the passenger cabin length L_c, and to the maximum take-off weight W_{TO}. Moreover, the correlation between the fuselage fitness ratio $F = L/d$ and cabin fitness ratio $F_c = L_c/d_c$ is derived in order to correlate the fuselage and the cabin size.

The four correlations are reported in Fig. 2.2. As expected, an increase in the fuselage length leads to a higher number of windows, as well as, an increase in the take-off weight. This can be easily explained, usually a longer aircraft is heavier. The relation between the two shape factors is quite scattered, because the cabin length linearly increases with the fuselage length as reported in Fig. 2.3(a), while the fuselage width has a step increase, usually depending on the manufacturers as reported in Fig. 2.3(b), the same is valid for the cabin width. For the windows size, there is no need to find a correlation, because the differences between the aircraft models are small and depend on the industry. Data are not available for windows reinforcements and so their size and weight must be directly calculated as described in Section 5.2.

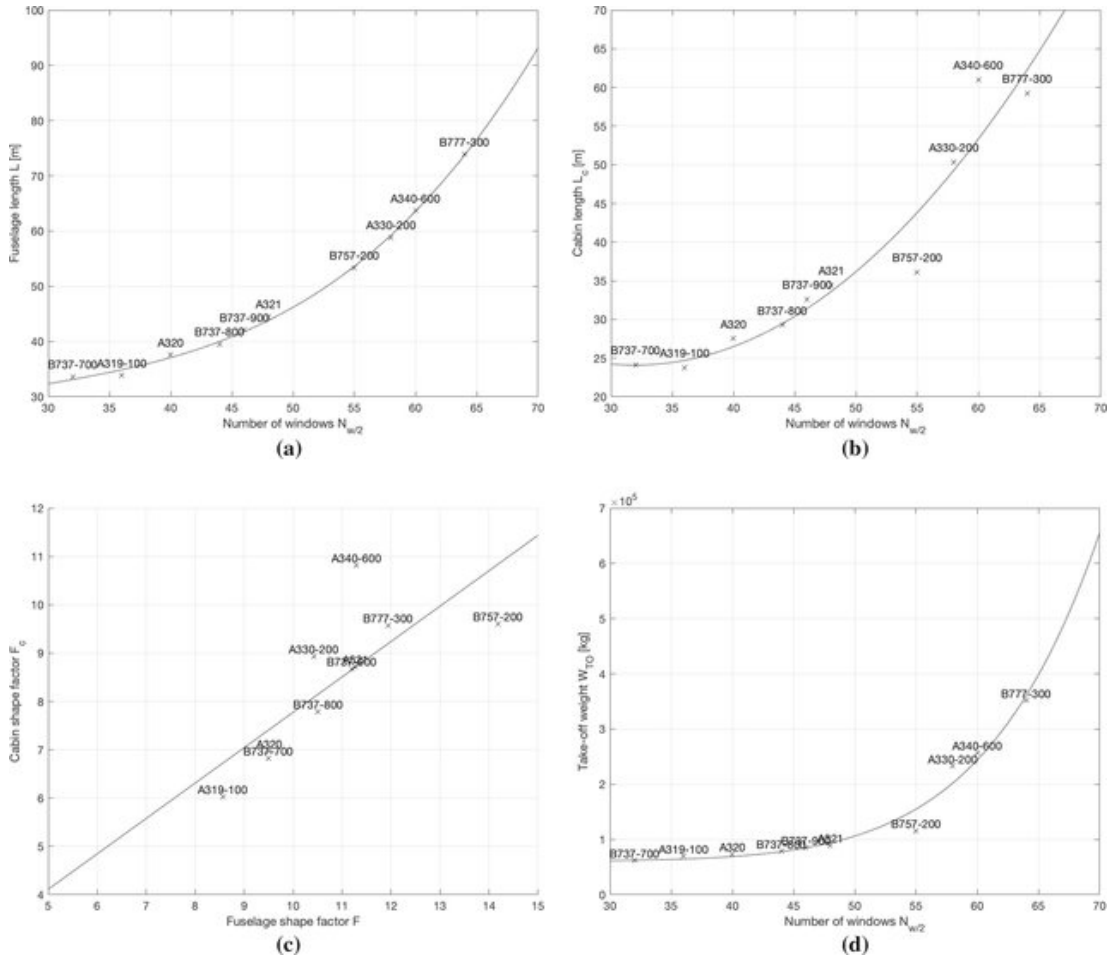

Figure 2.2: The correlations obtained from a sample of ten single-aisle aircraft. (a) Fuselage length L as a function of the number of windows $N_{w/2}$. (b) Cabin length L_c as a function of the number of windows $N_{w/2}$. (c) Cabin shape factor F_c as a function of the fuselage shape factor F. (d) Max take-off weight W_{TO} as a function of the number of windows $N_{w/2}$.

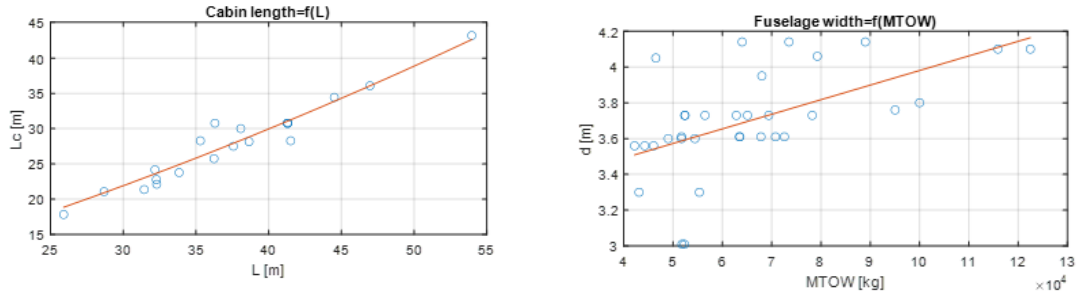

(a) **(b)**

Figure 2.3: The correlations for the fuselage and cabin geometry. (a) The fuselage length L and the cabin length L_c. (b) The maximum take-off weight $MTOW$ and the fuselage width d.

2.4 MDO and standardization

2.4.1 Introduction to MDO

Multi-disciplinary design optimization (MDO) is an engineering field which studies the optimization process of different integrated disciplines. In the aircraft design, MDO could lead to important results, in particular at early design phases, as in the conceptual and preliminary stages for structural and aerodynamic design [25]. It is not the aim of this small introduction to review the state of art of MDO in aircraft design. Nevertheless, the aircraft design new trend seems to move toward the exploitation of MDO process and platform, as demonstrated by the several projects involving MDO, as the Agile 4.0 project [26][2] or in the COAST project [18]. One of the main problem in MDO process is to manage the transmission and the conversion of data between research groups working on different disciplines. This issue can be solved using a standardised language for storing all data [27], as CPACS described in Section 2.4.2. For this reason part of this work is developed inside the CPACS framework, in order to provide a tool and data usable in a future MDO process.

2.4.2 CPACS

"The Common Parametric Aircraft Configuration Schema (CPACS) is a data definition for the air transportation system. CPACS enables engineers to exchange information between their tools. It is therefore a driver for multi-disciplinary and multi-fidelity design in distributed environments. CPACS describes the characteristics of aircraft, rotorcraft, engines, climate impact, fleets, and mission in a structured, hierarchical manner. Not only product but also process information is stored in CPACS. The process information helps in setting up workflows for analysis modules. Since CPACS follows a

[2] `https://www.agile4.eu/project/`

central model approach, the number of interfaces is reduced to a minimum."[3]

CPACS is XML (eXtensible Markup Language) based framework developed by DLR [27, 28]. Aircraft data come in XML files, that can be managed, modified, and used in several ways as reported in the works by Walther et al. [29,30]. CPACS is an open-source data definition system, which is becoming commonly used to solve multi-disciplinary issues in aircraft design and in MDO processes. The aircraft geometries, materials and properties are given in a hierarchical order in a top-down description of a system-of-systems which decomposes a generic concept into a more detailed description of its components as reported in Fig. 2.4.[4] The aircraft fuselage component are based on mathematical functions for the geometry and on material models for the structure. Any component in the fuselage and in the cabin is generally defined by:

- ID of the component;
- geometry profile (shell, beam, etc) and properties;
- material or composite;
- any interaction with other components (e.g., the frames at the edges for a panel).

Profiles for beams or sheet for plates are defined in the XML file, within materials and composite. In order to clarify the format concept, we report an example for a fuselage panel.

The panel of the fuselage skin named *Panel_1-1* is defined by:

- its ID (e.g. the name);
- the sheet ID *PanelElement_1*, so the geometrical shape and the material;
- the IDs of the right and left frames;
- the IDs of the top and bottom stringers.

From Fig. 2.5(a) it is possible to see the IDs of all these components. The frames as circular beams are defined by their position along the fuselage, while the stringer by the starting and ending point on the fuselage length, both are defined by a structural profile, for the geometry and the material. The panels size is defined by the stringers and frames position. The sheet of the panel, and similarly the profile of the stringers and the frames, has three properties as reported in Fig. 2.5(b):

- the ID, in this case *PanelElement_1*;

[3] `https://www.cpacs.de/`

[4] See CPACS documentation `https://www.cpacs.de/documentation/CPACS_systems/html/c0ba9e4f-907d-6cd2-42c4-d4ed9179a9dd.htm`

- the material ID, so *Aluminium2*;
- the sheet thickness.

Moreover, in Fig. 2.5(c) the material block is reported, for an isotropic material the properties are the name, the two Lamé parameters (the Young's modulus and the Poisson's ratio) and the density. For composite materials, each layer is described in terms of material, thickness and orientation. Finally, in Fig. 2.5(d), the definition of an attachment between two components is showed (e.g., a rivet). In this case the attachment is described by:

- the attachment element ID, which connects the component to the attachment elements library. In this library, as for profile of sheet, the different type of attachment are described in terms of stiffness and mass;
- the two components connected by the attachment, in this case the *sidewallPanel4* and the frame *C03*;
- the position of the attachment on the two components.

Other components are described in similar ways, depending on their properties and functions. Information on the numerical models or results can be added too.

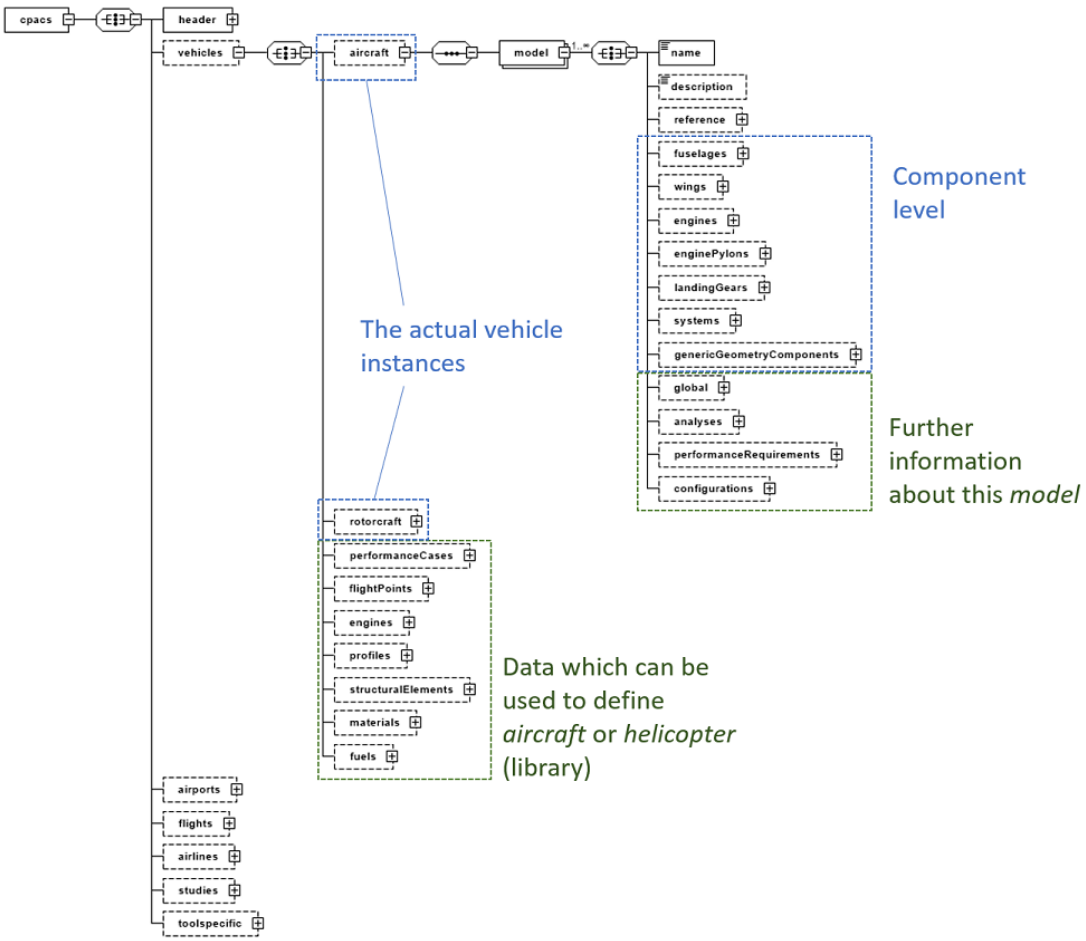

Figure 2.4: The top-down hierarchical order used by CPACS to describe system.

Figure 2.5: The CPACS description in a hierarchical order of a panel of the fuselage skin and of a structural attachment between a frame and a cabin sidewall panel. (a) The fuselage panel. (b) The sheet element of the panel. (c) The isotropic material of the sheet element. (d) The structural attachment, a rivet.

Chapter 3

The noise problem in the preliminary field

3.1 General overview

As pollution, noise is an undesired and potentially dangerous product of the aircraft. Its generation and physical phenomenon are directly linked with the structure vibrations, so we can refer to the noise and vibrations (N&V) problem. Before introducing the N&V problem in the aircraft, we need to deeply understand the mathematical and physical laws behind the acoustics. In this work, the N&V problem is related on one hand to the interaction of the acoustic waves with the structures of the aircraft and on the other hand to their diffusion in the acoustic cavities of the aircraft, in particular the passenger cabin. Therefore, in the following description we will refer to the acoustic and vibro-acoustic theories. The influence on the acoustic phenomenon of the aerodynamics and thermodynamic process, aero-acoustics and thermo-acoustics respectively, is not considered in this work. Their influence on the vibro-acoustic problem are managed as external boundary conditions.

In this chapter, the acoustic and vibro-acoustic problems are assessed in Section 3.2 and Section 3.3 within the main parameters used in the noise estimation in Section 3.4. Then, a literature review on the internal noise in commercial aircraft is presented in Section 3.5 in order to show the improvements and the limits in the understanding and modelling the noise generation and in the noise reduction solutions. Finally, a conceptual method to evaluate the acoustic comfort and noise perception in a passenger cabin, through a human centred approach, is proposed in Section 3.6.

3.2 The acoustic problem

3.2.1 Wave equation

Noise refers to the negative effect on comfort, the physical variable is the acoustic pressure, which is a periodic variation of pressure in time and space. Sound travels through a medium in acoustic wave with rarefaction and compression phases. In the following discussion we assume two hypotheses on the acoustic problem:

- the fluid is homogeneous, inviscid and irrotational compressible;
- the body forces, as the gravitational effects, are neglected.

In a free field, so without any boundary condition or other sources, the acoustic pressure is well described by the wave equation:

$$p_{,ii} = \frac{1}{c_f^2}\ddot{p} \tag{3.2.1}$$

in which p is the fluid pressure and, c_f the speed of sound. The subscript $_{,ii}$ represents the second derivative over the space coordinates (as the ∇^2 operator) and the $\ddot{}$ (*double dot*) the second derivative over time. In the wave equation, the derivative of the pressure in time and the one in the space are correlated through a constant: the speed of sound. This constant is defined by the density of the medium ρ_f and by compressible bulk modulus β:

$$c_f = \sqrt{\frac{\beta}{\rho_f}} \tag{3.2.2}$$

so it is a property of the material.

3.2.2 Boundary conditions

In addition on the free field, several boundary conditions can describe many physical problems, we will proceed with a brief description of those related to the problem in this work and commonly used:

- imposed pressure (Dirichlet boundary condition), this condition sets a pressure value on a location $p = p_0$. If the pressure is equal to zero, we obtain a free surface condition;
- imposed normal velocity (Neumann boundary condition), so the normal velocity is defined as:

$$p_{,i} \cdot n_f = -\rho_0 \ddot{u}_{f_n} \tag{3.2.3}$$

where n_f is the outward normal and $\ddot{u}_{f_n}$ is the fluid acceleration. On a rigid wall the normal velocity and so the acceleration are zero, therefore we obtain the following boundary condition $p_{,i} = 0$. In the numerical approximation in Section 4.2 this condition is automatically imposed;

- infinite or open boundary condition represents the disappearance of the pressure moving away from the source, avoiding any reflection of the waves. This condition is described by the Sommerfeld boundary condition

$$\lim_{r\to\infty}\left[r\left(\frac{\partial p}{\partial r}+\frac{1}{c}\frac{\partial p}{\partial t}\right)\right]=0 \tag{3.2.4}$$

where r is the distance from the source;

- acoustic impedance describes the opposition to the acoustic stream of a defined region of fluid (or a solid), it is described as the Robin boundary condition by the following relation (it suits admittance too)

$$p = \dot{u}_f \cdot n_f Z \tag{3.2.5}$$

where Z is the specific acoustic impedance (A for admittance).

3.2.3 Frequency domain

The time domain analysis provides information on the signal behaviour over time and on its temporal development. The frequency domain analysis provides information on the nature of the signal in the different frequency bands. In order to decompose the time dependant signal in its frequency dependant properties, we apply the Fourier transform.

The pressure field in the frequency domain is obtained by applying the Fourier transform:

$$p\left(x_i,\omega\right)=\int_{-\infty}^{+\infty} p\left(x_i,t\right)e^{-i\omega t}dt \tag{3.2.6}$$

where the frequency f is directly related to the pulsation $\omega = 2\pi f$.

In the frequency domain, Eq. 3.2.1 can be transformed in the Helmholtz equation:

$$p_{,ii} = -\frac{\omega^2}{c_f^2}p \tag{3.2.7}$$

where $p = p\left(x,y,z,t\right)$. In a similar way, the boundary conditions are expressed in the frequency domain.

3.2.4 Acoustic excitations

Several acoustic loads or sources can be exploited to reproduce real acoustic phenomena. The simplest pressure field is generated by a pulsating sphere, which radiates equally in all directions, the monopole. The pressure field generated by a monopole at a distance r is expressed by the following equation:

$$p\left(r,\omega\right) = A(\omega)\frac{e^{-ikr}}{r} \tag{3.2.8}$$

where A is the monopole amplitude, and k the wave number.

Other acoustic loads are the dipole, an oscillating sphere with no deformation, and the plane wave.

When dealing with a dipole, unlike the monopole source, the sound does not radiate equally in all directions. The dipole source can be visualized as two out-of-phase monopole sources separated by a distance, the former contracts and the latter expands. The plane wave is represented by an incident pressure field. The descriptions of these sources is not given, cause it is not exploited in this work.

A typical acoustic loading, is that of an acoustic diffuse field, which can be represented with a number of acoustic plane wave source. In order to define a random diffuse acoustic field, the orientation and the intensity of each source can be defined as a random uncorrelated value.

3.2.5 Governing equations: closed cavity

A classical simple acoustic model is the closed cavity. The mathematical representation of a volume domain Ω_f filled with a fluid and surrounded by rigid walls on Γ_N^f, so a Neumann boundary conditions, is given by a system composed by Eq. 3.2.1 and Eq. 3.2.3:

$$\begin{cases} p_{,ii} = \frac{1}{c_f^2} p & \text{in } \Omega_f \\ p_{,i} \cdot n_f = 0 & \text{in } \Gamma_N^f \end{cases} \tag{3.2.9}$$

in which p is the fluid pressure and n_f the outward normal. The system is in the time domain and written in the *strong* formulation where the unknown is the acoustic pressure p. For the further discussion on the numerical approximation of the system it is useful to have *weak* formulation. In order to obtain the variational formulation associated with the system in Eq. 3.2.9, the test function method is applied. The *weak* formulation introduces arbitrary weighting functions, which represent the principal field variables that describe the evolution of the system. This *weak* formulation is equivalent to the Principle of Virtual Displacement (PVD) applied on the same system. The

acoustic system, can be written as:

$$\int_{\Omega_f} \delta p_{,i} p_{,i} dV + \int_{\Omega_f} \frac{1}{c_f^2} \delta p \ddot{p} dV = 0. \tag{3.2.10}$$

in which δp is the virtual pressure.

3.3 The vibro-acoustic problem

3.3.1 Overview

The vibro-acoustic field studies the interaction between an acoustic cavity and a structure. An excitation on the structure produces vibrations, which affect the acoustic cavity. A periodic pressure fields spread in the cavity. If the vibrations are small, the fluid-dynamic effect on the fluid can be neglected. Vice versa, an acoustic pressure on the fluid generates vibrations on the structure. This phenomenon is called vibro-acoustic coupling. The effect of the structure on the fluid (structure-fluid coupling) is usually greater than the effect of fluid on structure (fluid-structure coupling), which can be neglected in several problems. If the fluid-structure coupling is neglected, the model exploits a one way coupling or a weak coupling. Otherwise, for a fully coupled system, the problem exploits a two way coupling or strong coupling. In a plate-cavity system, the vibro-acoustic coupling can be estimated by the coefficient β_c with the following equation:

$$\beta_c = \frac{\rho_f c_f}{\rho_s h_s \omega_s} \tag{3.3.1}$$

in which ρ_s and ρ_f refer to the density of the structure and of the fluid respectively, c_f is the fluid speed of sound, h_s the plate thickness and ω_s the first natural frequency of the structure, which is linked to the structural stiffness. For a strong coupling, the coefficient is greater than one, $\beta_c >> 1$, that it usually happens for high density fluid (as water) or very thin plates. If $\beta_c << 1$, the coupling is weak, for example we obtain this case for low density fluid (as air) and for structures with high stiffness.

In the following sections, the governing equations of the a vibro-acoustic system, a cavity surrounded by a structure, are described, combining the acoustic system in Eq. 3.2.9 and the structural model.

3.3.2 Governing equations: plate baked to a cavity

The plate-cavity system is a reference vibro-acoustic system and several more complex problems can be brought back to this model. Therefore, the model is made up of by three components:

- the fluid cavity (subscript f) is defined by the domain Ω_f. The cavity is filled by

a fluid, whose properties are the density ρ_f and speed of sound c_f. The cavity is closed by rigid walls applied on the domain Γ_N^f;

- the plate (subscript s), the elastic structure, is defined by the domain Ω_s and made by a material defined by the density ρ_s and the matrix of the elasticity coefficient $\boldsymbol{C}$. On the plate domain there are regions where loads can be applied Γ_N^s and displacements can be set Γ_D^s;
- the structural and acoustic regions have a common interface defined by Γ_{fs}. On this interface the fluid-structure coupling happens.

The model is built under the following hypotheses:

- the fluid–structure system has a linear behavior;
- the deformations for the structure are small, in order to fulfil the continuum body hypothesis;
- the fluid is homogeneous, inviscid and irrotational compressible;
- the body forces, as the gravitational effects, are neglected.

The unknowns of the problem are the fluid pressure p and structural displacement s_i. The acoustic system is described by Eq. 3.2.9, while the structural one as a relation between the stress tensor σ_{ij} and the displacement second derivative over time. The stress tensor is directly linked to the deformation tensor ε_{ij} by the constitutive equation:

$$\sigma_{ij} = \boldsymbol{C}_{ijkl}\varepsilon_{kl} \tag{3.3.2}$$

Moreover, the structural boundary conditions depend on a constant: a surface force f_i and the assigned displacement $\bar{u}_i$, for the Neumann and Dirichlet boundary conditions respectively.

In view of above, the following structural and acoustic systems are derived:

$$\begin{cases} \sigma_{ij,i} = \rho_s \ddot{u}_i & \text{in } \Omega_s \\ \sigma_{ij} n_j^s = f_i & \text{in } \Gamma_N^s \\ u_i = \bar{u}_i & \text{in } \Gamma_D^s \\ \sigma_{ij} n_j^s = p n_i^f & \text{in } \Gamma_{fs} \end{cases} \tag{3.3.3}$$

$$\begin{cases} p_{,ii} = \frac{1}{c_f^2} p & \text{in } \Omega_f \\ p_{,i} n_i^f = -\rho_f \ddot{u}_i n_i^f & \text{in } \Gamma_{fs} \\ p_{,i} \cdot n_f = 0 & \text{in } \Gamma_N^f \end{cases} \tag{3.3.4}$$

where n_i^s and n_i^f are the normal vectors of the structural domain and of the fluid domain respectively.

Through the same process applied for the acoustic system in Eq. 3.2.9, the variational formulation for the coupled system is obtained in terms of virtual displacement δu_i and virtual pressure δp:

$$\begin{cases} \int_{\Omega_s} \delta u_i \sigma_{ij} dV + \int_{\Omega_s} \delta u_i \rho_s \ddot{u}_i dV = \int_{\Gamma_N^s} \delta u_i f_i ds + \int_{\Gamma_{fs}} \delta u_i p n_i ds \\ \int_{\Omega_f} \delta p_{,i} p_{,i} dV + \frac{1}{c_f^2} \int_{\Omega_f} \delta p \ddot{p} dV = -\rho_f \int_{\Gamma_{fs}} \delta p \ddot{u} n_i ds \end{cases} \tag{3.3.5}$$

where the normal of the fluid is opposite to that of structure on the interface $n_i^f = -n_i^s$ in Γ_{fs}. The structural equation in the system is composed by a stiffness term, a mass term, an external load and, a coupling term. Likewise, the fluid equation has a stiffness term, a mass one and, a coupling term. The fluid external loads are neglected in this model, but they can be added later.

3.3.3 The structural model

The stress tensor definition given by Eq. 3.3.2 can be expressed thank to the Voigt formulation to lighten the notation:

$$\sigma = \boldsymbol{C}\varepsilon \tag{3.3.6}$$

with:

- $\sigma = \begin{bmatrix} \sigma_{xx} & \sigma_{yy} & \sigma_{zz} & \sigma_{yz} & \sigma_{xz} & \sigma_{xy} \end{bmatrix}^T$
- $\varepsilon = \begin{bmatrix} \varepsilon_{xx} & \varepsilon_{yy} & \varepsilon_{zz} & \varepsilon_{yz} & \varepsilon_{xz} & \varepsilon_{xy} \end{bmatrix}^T$

The elasticity matrix $\boldsymbol{C}$ is derived in the global reference system (x, y, z) from the local matrix $\boldsymbol{C}^*$ in the material reference system (1, 2, 3) through the rotation matrix $\boldsymbol{R}$:

$$\boldsymbol{C} = \boldsymbol{R}^T \boldsymbol{C}^* \boldsymbol{T} \tag{3.3.7}$$

The unknowns of the structural problem are the displacements u_i or $\mathcal{U}$, the vector of the three components of the displacements in the three directions. The strain vector has a correlation with the displacements, according to the following equation:

$$\varepsilon = \boldsymbol{b}\mathcal{U} \tag{3.3.8}$$

where $\boldsymbol{b}$ is the matrix of the differential operators.

3.4 Noise parameters and scales

In acoustic and in noise reduction we refer to several parameters and scales. In this section we will briefly describe those used in this work.

The acoustic pressure is the physical parameter that we use to quantify the noise. In this field, this parameter is usually defined as a Sound Pressure Level SPL in the logarithmic decibel scale dB:

$$SPL = 10 \cdot \log_{10} \left(\frac{p^2}{p_{ref}^2} \right) \tag{3.4.1}$$

where p_{ref} is the standard reference sound pressure equal to 20 μPa.

In a direct frequency response analysis, the results are function of the frequency. In order to have an average value in the frequency range of the analysis (from f_{min} to f_{max}), we introduce the Overall Sound Pressure Level $OASPL$ in dB:

$$OASPL = 20 \cdot \log_{10} \left(\frac{\sqrt{\int_{f_{min}}^{f_{max}} p^2 dp}}{p_{ref}} \right) \tag{3.4.2}$$

The human ear has a different sensitivity in the frequency range, for example it strongly attenuates sound below 1000 Hz. In order to take in account this effect, a filter is added to the SPL value according to the frequency. In literature there are four filters, from A to D, calculated through experiments. In this work we will use the most common one, the A filter, and so the dBA.

When we study the noise reduction solution, we want to quantify the effectiveness of this solution. Therefore, the introduction of the Transmission Loss TL, in dB, estimates the amount of energy (and so noise) lost or stopped through a chosen region. The TL is defined as the ratio between incident W_i and transmitted power W_t of a wave:

$$TL = 10 \cdot \log_{10} \left| \frac{W_i}{W_t} \right| \tag{3.4.3}$$

3.5 Noise in aircraft

3.5.1 Sources

The traditional commercial aircraft is a cylindrical body hold by lifting wing. The lift is generated by the engines thrust and by the flow around the wing. Moreover, inside the aircraft there are several systems and processes to guarantee safety and comfort to the crew and the passenger. The sources of noise are deeply inherent to these processes. Though, it is not the aim of this work to describe and estimate the sources of noise, a brief description is necessary. In this work we refer the acoustic behaviour of the aircraft fuselage and the spread of the acoustic waves inside the passenger cabin. Therefore, the following brief description will be focused on the passenger cabin [31, 32].

A very first classification of these sources could follow the aircraft definition as cyl-

indrical body hold by lifting wing for a cruise phase:

- the turbulent flow around the fuselage, so the acoustic pressure generated around the fuselage skin;
- the flow around the aerodynamic surfaces, as well as the aero-elastic effects. These loads follow a structure-born path from the wing or an air-born through the fuselage skin;
- the engine noise generation process is quite complex due to the number of subsystem. It is one of the most important sources and it affects the acoustic behaviour from low to high frequencies;
- internal systems, as air and pressurization system, actuators or the electrical system play and important role in noise spread through the cabin. Although, the influence of this sources and their acoustic models are not completely understood;
- other acoustic sources can rise from the human noise in the cabin to the flow around the landing gear during landing and take-off.

The sketch in Fig. 3.1 shows the previous classification of noise sources within the path followed by acoustic wave in the direction of the passenger cabin. The complexity of the system requires a simplification. A more detailed study of the noise source from a component point of view analyze the contribution of each aircraft component: from the engine sub-system (the turbine and the combustive chamber, the fan exhaust and inlet and the jet or for a turboprop the propeller wake) to the wing and high-lift devices, including tail and landing gear. These sources play an important role both for external and internal noise. Other sources, as the air conditioning and pressurization system, are relevant for cabin noise only.

In this work the study of the sources is kept at a literature survey level. Therefore, the purpose is not to study and quantify the intensity of the acoustic sources, but to validate new solutions through an understanding of the vibro-acoustic behaviour of the aircraft structure. In order to estimate the cabin noise, a full comprehension of the structural path followed by the acoustic wave of the vibro-acoustic coupling is necessary. The structural path includes not only the wing structure as shown in Fig. 3.1, but also the structural behaviour of the entire fuselage.

3.5.2 Cabin noise

In this work we will focus on the noise spread inside the passenger cabins. In order to have a complete understanding of the vibro-acoustic behaviour and the structural coupling between the various components, we study the fuselage system around the cabin. The system is geometrically and physically complex. In the first paragraph the

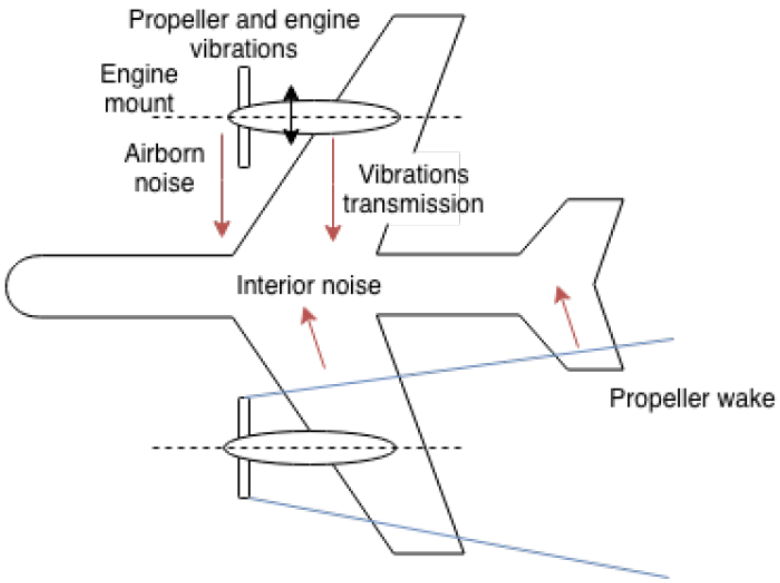

Figure 3.1: The acoustic waves propagation in a turboprop aircraft focusing on the engine and on the propeller.

fuselage structure and the cabin components are briefly described. Then, the cabin acoustic problem is defined and, in the last paragraph, the state of art of the subject is summarized in order to give to the reader a full description of the physical and numerical problem.

The fuselage system is the core of the aircraft, carrying the payload, the cockpit, the wing box, that transmits the wing loads to the fuselage structure, and the tail. In a commercial aircraft the payload refers to the passengers; therefore the cabin includes several system for their safety and comfort, within other subsystems, that run across the fuselage. In this work, aiming at the study of the passenger cabin noise, we will refer to the fuselage without considering nose (the cockpit) and tail. The fuselage has a quasi-cylindrical shape. A deep description of the fuselage, already done by several works, is not necessary for the purpose of this thesis. The fuselage can be divided into several subsystems and parts, here a first classification:

- the primary structure includes the aircraft skeleton, so the stringers, the frames and panels of the fuselage, the passenger and cargo decks supports and their panels on which the floor is placed, the bulkhead and wing box. Moreover windows frames, first glass pane and reinforcements are included in this subsystem. These components are of vital importance for the safety of the aircraft;

- the secondary structure includes all the non-vital structural components of the aircraft. Within fuselage these components are seats with their supports, lining, ceiling and dado panels of the cabin, overhead luggage compartment and luggage compartment in the cargo hold;

- cabin interiors, as the floor carpet, the galleys and the toilets;
- several subsystems, as the air conditioning and pressurisation system, the electrical system, the thermal insulation system, etc;
- passengers, crew and luggage;
- acoustic cavities, in the fuselage there are several cavities filled by air, as the passenger cabin, the cargo hold, the gap between the lining panel and the fuselage, the small air gap in the windows. Inherent to the presence of a cavity, we have to consider the relative interface with the structure.

From an acoustic point of view, we have to understand the contribution of each subsystem. Nevertheless, the high complexity of the system require some degrees of simplification. In particular in the further literature survey we can obverse how, due to their complexity, the non structural subsystems are usually neglected, or must included as boundary conditions if they generate any acoustic excitation. Moreover, we have to consider an important lack of specific and technical information on these subsystems.

A classical cabin model is reported in Fig. 3.2. Several subsystem are neither considered nor inserted as boundary conditions. The components in this model are the structures, the cabin interiors and the acoustic cavities. Even if, the model is simplified, it still exploits different subsystems and structures. We will try to describe each component in the model.

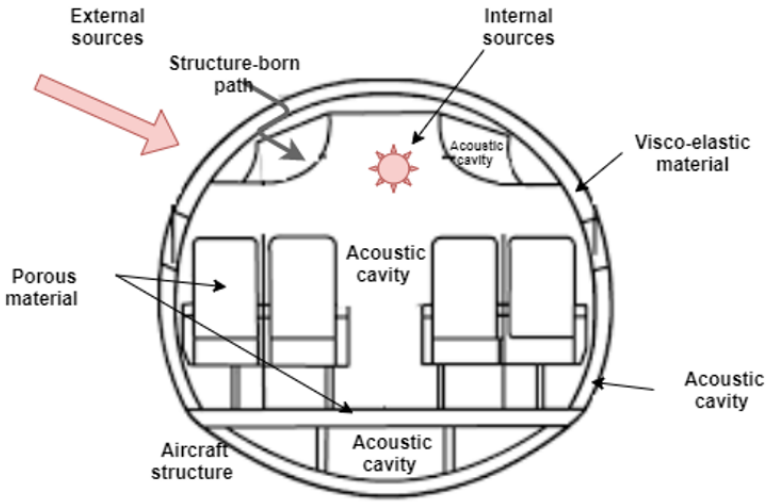

Figure 3.2: The sketch of a section of the fuselage and passenger cabin from an acoustic point of view. The different vibro-acoustic components and phenomena are underlined in order to show the complexity of the problem.

The first component is the fuselage structure, made by stringers, frames and panels. These structural components are linked altogether by joints. In this structure we include the supports and the panels of the two decks, the windows panels and their reinforcements. These components are made of aluminum or CFRP (Carbon Fiber

Reinforced Polymer), with a high stiffness. The system interfaces with the secondary structure of the passenger cabin through joints and shock absorbers. Moreover, there is a vibro-acoustic interface between the structure and air gap surrounded by the cabin and the fuselage, and with the cargo hold cavity. These two cavities are usually merged together in the secondary cavity. The windows can have an interface with the passenger cavity, but in some aircraft, there is a dust cover on the passenger cabin side. Several subsystems, such as cables and pipes, are housed in the gap between the fuselage and cabin. Moreover, a foam is placed on the cabin lining panels to thermally insulate the passenger cabin. This layer of foam usually presents a thermal and acoustic insulation.

The passenger cabin is bounded by several panels connected to the primary structure. All these panels make up the lining panel of the cabin as sketched in Fig. 3.3:

- the sidewall panels, with an hole for the windows, are those aside the passenger, usually with recess for the passenger's shoulder;
- the dado panels, at foot height, are separated from the lining panels for maintenance reason and can be carpeted;
- the cowl panels, above the lining panels and below the overheads, create the slope where the above-head systems (the lights, the conditioning fans, the oxygen mask, etc.) are placed;
- the ceiling panels, on the top of the cabin, where are installed the cabin lights;
- the overheads above the passenger seats, where passengers store their luggage and coats.

All these panels are usually made by fiberglass or plastic materials with an honeycomb core in order to absorb the vibrations from the primary structure. The floor is covered by the cabin carpet. In the passenger cabin there are the seats, usually made of aluminum or CFRP for the structural part, and with a porous material covered by leather or fabric. The cabin environment is the final stop of several subsystems, that can affect the acoustic behaviour of the cabin itself.

Passengers are obviously part of the cabin environment. From an acoustic point of view, they generate noise and they are the receiver of the noise. Therefore, any acoustic analysis has to consider their peculiarities, as the passengers position in the cabin and the sensitivity of the human ear to different frequency bands (see Section 3.4). Finally, the cabin is closed by the bulkheads on the two sides covered by lining panels. In first approximation the bulkhead can be approximated by a rigid wall boundary condition due to the high stiffness, which is automatically imposed in a FEM model.

The boundary conditions and the loads define the interaction of the system with the external environment or they simplify some complex system in a simple condition. The

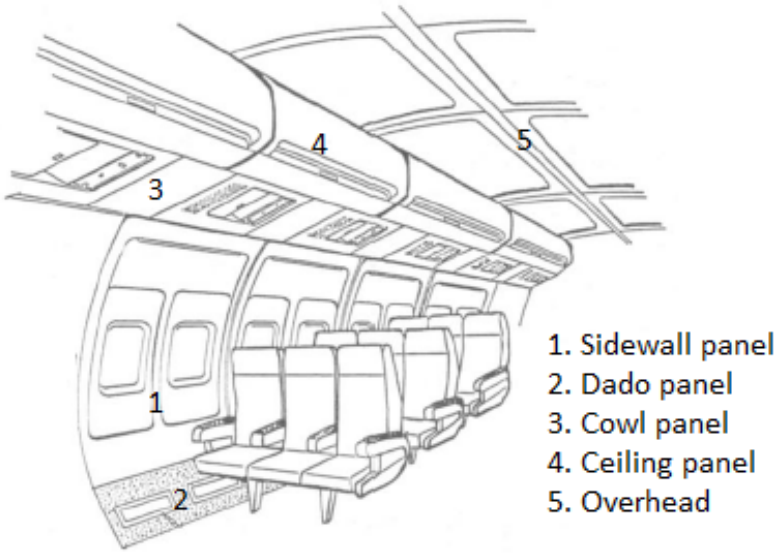

Figure 3.3: The lining panels in the passenger cabin are made up by different separated components. Together with the carpet, they bound and isolate the passenger cabin from the fuselage structure.

acoustic boundary conditions are described in Section 3.2.2, while the structural one are usually the clamped and simply supported conditions. The loads (or sources) are split in internal and external sources. As previously described, the external sources represent all the phenomena outside the fuselage and are applied on the fuselage panel, usually as a complex pressure. In this way is possible to simplify the problem and separately compute the sources contribution and their interaction with the fuselage structure. The internal sources are all those phenomena inside the fuselage which generate a significant amount of noise or vibrations. These sources are more difficult to compute because on one hand it is not always possible to decouple their description from the fuselage system and, on the other hand there is an important lack of information and knowledge of the acoustic behaviour of these systems. In absence of information, theoretical sources can be exploited to simulate an acoustic excitation.

Once noise is defined inside the aircraft, different solutions can be exploited, a general overview is given in [33, 34]. A first solution is the acoustic (vibro, aero, thermo, etc.) optimization of the possible acoustic sources of the aircraft in order to decrease their intensity. Then we can apply other solutions on the aircraft. A first classification of noise reduction solutions is between passive and active. The former are usually the simplest, as visco-elastic materials, that absorb noise or vibrations, as those applied around the passenger cabin or near the engine. The latter need energy and increase weight and complexity, but they can obtain better performances and increase the operating frequency range, controlling for example the structural vibrations. Both these solutions can be applied to the acoustic source, on the path of N&V or near the receiver (e.g., the

passenger or the crew). The main parameters to evaluate a solution are the transmission loss in terms of energy, the OASPL inside the cabin, possibly the impedance, but also the weight, the volume and installation problem within the aircraft regulations. For shell (as a fuselage panel) a simple law for TL can be used:

$$TL \propto \rho df \tag{3.5.1}$$

so the amount of energy absorbed depends on the thickness of the plate/shell d, on the material density ρ and on the frequency of signal f. It is quite simple to reach the following considerations:

- to stop high frequency noise, some materials (e.g., aluminum or composite) work well, compensating the low thicknesses (as those of a fuselage skin) with a quite high density and high frequency signal, on the other hand material with low density can be thicker without increasing the weight, such as foam. Therefore, with traditional material high frequency can be stopped;
- to absorb low frequency or to obtain an high TL for a low frequency signal the material must be thick and/or heavy (high density), increasing the weight, which must be avoided on an aircraft. Therefore, conventional materials are not suitable to stop low frequency noise.

From the last consideration, this work focuses on low frequency noise and on "unconventional" material for the absorption. In particular, a new class of low density materials, the acoustic metamaterials (AMM), can present very high absorption properties in the low frequency range. This kind of materials will be better explained in the Section 3.5.3 on the development of the CASTLE project, as part of the Clean Sky 2 program, and in the Section 5.3. A general review of AMM can be found in [35].

In the following paragraphs the state of art on the internal cabin noise in commercial aircraft, at author's knowledge, will be summarized in order to give a description of the problem though several reliable works. The stream starts from the physical problem addressed by field tests and measurements, then the focus switches to the numerical tools and methods in order to study the noise spread in the aircraft, defining the sources and the cabin components. In this survey we focus on the FEM solutions, and only a few mentions will be reported on other methods such as SEA. Finally, the design process in the CASTLE project is described in Section 3.5.3 in order to show for a detailed study of the noise problem in a turboprop aircraft both at low and high frequency.

Experimental studies

Few works comprehensively measure and study the noise propagation inside the aircraft cabin. This limit is caused by the cost and the complexity in taking these measurements.

Moreover, the on field results give a general view of the aircraft noise in a selected flight phase, but the quality of the results strongly depends on several uncontrollable factors, that lead to unusable results for the validations of numerical models. In general, a measurement depends on the commercial aircraft model, the flight phase and conditions (speed, altitude, etc.), the life cycle of the aircraft itself and on other factors.

The study of the state of the art starts with the following two works, where the authors perform a series of flight tests with DLR's A320-232 in order to study the noise and vibrations spread through the passenger cabin and the aircraft structure. In the work by Hu et al. [36] the contribution to the internal noise of the different aircraft components is investigated. In particular, the authors focus on the air conditioning system (ACS), on the turbulent boundary layer (TBL) and on the jet noise. Three different engine working conditions are considered. The noise is measured by microphones inside the passenger cabin, installed at the height of the seat headrests, in the middle of every second seat row on the left and in the aisle, respectively. The conclusions of this work can be very useful to understand the contribution of the three sources taken in account, although they do not give any help in modelling these sources for simulation purpose. In order to summarize the results:

- ACS noise plays a minor role. Noise increases of about 1–2 dBA in OASPL in the bow of the aircraft. The importance of the ACS noise is further reduced with an increasing flight speed. The engine working conditions also impact the measured ACS noise;
- the TBL increases of about 3–4 dBA when moving from the bow (close to the wing root leading-edge) towards the aft of the aircraft. Moreover, it rises with a decreasing flight level and with an increasing flight speed. TBL-induced noise is the dominant contributor in cruise phase;
- the jet noise, caused by the jet exhaust stream, affects mostly the aft part. Its relative importance, in particular in the cruise condition, grows with the increase of flight level and speed.

During the same experiment campaign, Norambuena et al. [37] study the energy transfer mechanisms. They compare the vibrational behavior of the fuselage structure with the existing sound field inside the cabin in order to identify the potential driving sources for different flight conditions. They conclude that there is a major role played by the engines as a structure-borne sound source responsible for the cabin noise.

In the work by Ozcan et al. [38] a test campaign has been carried on in the cabins of two similar single-aisle Airbus A321 jet passenger aircraft. The aim is to quantify and define the noise level, split in continuous and discontinuous types. The former is the noise caused by TBL, ACS, engine, etc. The latter is caused by passenger activities such as conversations and luggage-related rearrangements as well as those caused by

flight-crew such as flight attendant-related speaking activities, announcements from pilot and flight attendants, mechanical noises during food/beverage services and flight security demonstrations, and other announcement signals. Therefore they consider non-aircraft-originating noise sources. The results given by the continuous noise level are quite conventional, while the ones related to the instantaneous noise level are interesting, showing the different sources in different flight phases. From the predominance of noise caused by the the closing of the luggage compartment and the passenger conversations during the parking and taxiing to the live announcements by flight crew in the cruise phase and eventually to the mechanical noise in the final ground phase.

A very extensive work is the one by Lee et al. [39] where a test campaign on several Airbus models has been performed using a calibrated in-house developed smartphone application. The study highlights the significant presence of low-frequency noise which is the leading cause for the increase in sound pressure level in terms of dBC with respect to the SPL in dBA. This high level of SPL in dBC could have negative effects on the health of the passengers and of the crew. For a similar work on over 200 flights, we refer also to the work by Zevitas et al. [40], they calculate a sound levels across all flight phases and aircraft groups ranged from 37.6 to 110 dBA with a median of 83.5 dBA.

FEM model

In the first work of this review, presented by Hesse [41] an active structural–acoustic control (ASAC) system for a composite fuselage type structure is developed. For ASAC applications the structural contributions to the interior sound field are usually described in terms of the acoustic radiation modes (ARMs). The author considers a cylindrical shell coupled to an interior cylindrical cavity, where the stringers and the frames are disregarded. The differential equation in cylindrical coordinates of interior sound radiation is solved through Bessel's function. The ARMs developed by this new formulation will be used for the ASAC since they are simple to be implemented because they are frequency independent. The author validates a coupled FEM model, that will be used to test the active control system based on structure-integrated sensors and actuators. Finally, using an optimal control law and considering different subsets of ARMs, it is possible to correctly estimate the dominant contribution to the acoustic potential energy (APE).

A quite different work is developed by Herdic et al. [42]. This research compares and validates numerical results with experimental one for an aircraft fuselage, which is quite rare in the vibro-acoustic field. The authors evaluate the frequency response of a Cessna Citation fuselage section under three different forcing functions (10–1000 Hz) through spatially dense scanning measurement. The fuselage does not have any cabin element (panels, luggage compartment, seats, etc.). From this research they develop a FEM model of the fuselage as a predictive tool. In particular the validation for

the numerical model is performed considering a one point excitation applied to the stiffener intersection in a low frequency range (30-250 Hz). The comparison shows a good accuracy except for a small difference due to the loss factor formulation. Further validations are performed comparing the modal shapes and frequencies with an excellent agreement. The FEM model accuracy depends on several factors:

- structure non-axial symmetry (they only consider half of the fuselage);
- mesh resolution;
- mass distribution;
- window material properties;
- structural damping;
- rivets.

A similar work is performed by Grewal et al. [43] for a fuselage shell with stringers of regional commercial aircraft De Havilland Dash-8 S100/200, a validation of the numerical approach and of the FEM model is carried on based on literature and experimental data. The maximum frequency of the validation is 400 Hz.

Other works focus on a component of the aircraft trying to define its contribution in the cabin noise, in particular the components are:

- seats [44];
- windows [45];
- fuselage panels [46].

Blech et al. [44] start from a simple three-seats row FEM model of an aircraft fuselage and cabin coupled to internal fluid in Fig. 3.4 to study the contribution of the seats on the noise spread inside the cabin. This work show how accurate FEM models are built with a traditional numerical approach:

- the cabin sidewalls made of a sandwich material are composed by shell elements on the faces and solid hexahedral element in the core;
- the inner insulation glass wool between the cabin and the fuselage panel is modeled as an homogeneous fluid;
- the fluid is air, modelled by solid elements;
- an artificial TBL load is applied on the outer skin.

In order to understand the seats influence on the noise, experimental data for the damping characteristics are applied to reproduce the seats behaviour in the FEM model, exploiting two possible ways:

- applying a frequency dependant loss factor η_f for the cabin, so a complex speed of sound $\bar{c}^2 = c\,(1 + i\eta_f)$ where c is the real part of the speed of sound. Therefore, the cabin has an homogenized damping;
- creating an acoustic surface impedance on the area occupied by the seats.

The results are similar, but with a low computational effort on the frequency dependant loss factor. The comparison shows a better understanding of the influence of seats on the pressure map shape with impedance surfaces. In particular the contribution of the seats backrest is underlined.

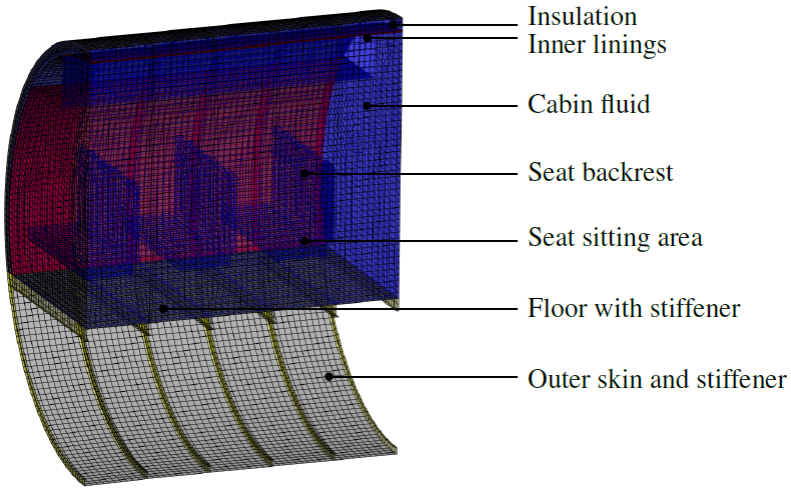

Figure 3.4: The FEM model of three-seats row fuselage barrel created by [44] for the evaluation of the seats contribution in the cabin noise.

In the work by Aloufi et al. [45] a fully vibro-acoustic model for sound transmission across a multi-pane aircraft window is developed. The aircraft windows geometry is reported in Fig 3.5. The FEM model validation is performed for a double aluminum plate, comparing results with literature. Several designs of windows are compared changing materials and number of panes. This work shows a very accurate way to model windows in an aircraft. Although, the application of this model in a full aircraft FEM mesh, could be quite difficult for computational reason. In particular the coupling between the windows panes and the air gap will increase the computational cost.

Finally, the work by Henry et al. [46] studies a method to reduce sound radiation from individual panels into an acoustic space through feedback control systems for the control of stochastic inputs, such as TBL excitation. While Hesse [41] consider the whole fuselage, the authors develop a method for a single fuselage panel. It has been

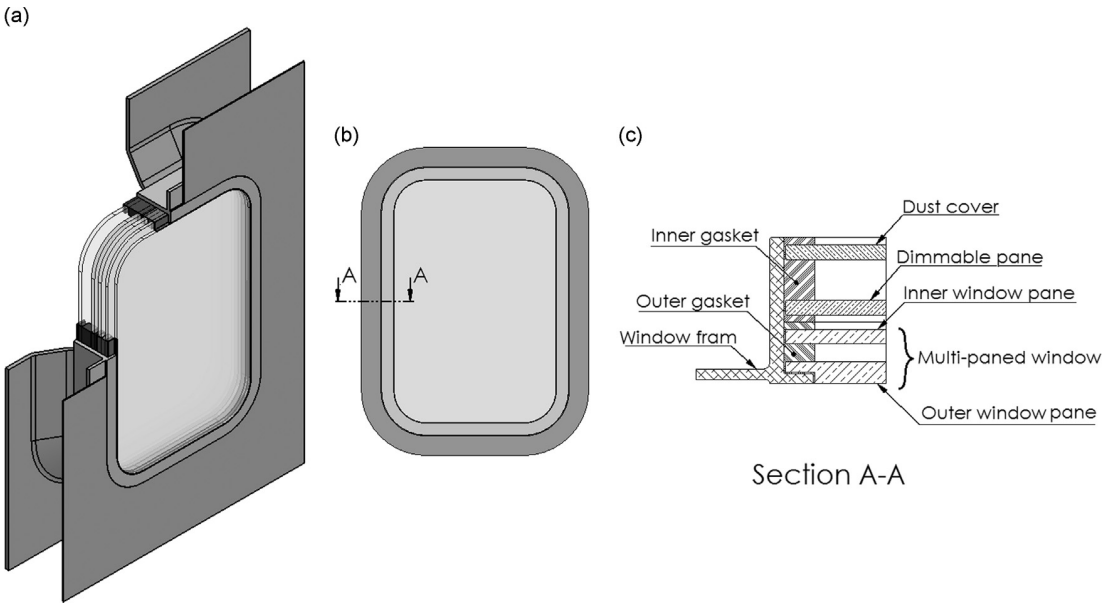

Figure 3.5: The sketch of an aircraft window presented in [45] to study the noise transmission through it. (a) Isometric view. (b) Front view. (c) Side cross section view.

found that, for a typical aircraft panel, predominantly axial structural modes couple more efficiently with the acoustic modes of the enclosure. Therefore, the design of structural acoustic control should focus on low-order axial structural modes to reduce sound transmission in the cabin. Moreover, the position of the panel on the cylinder does not significantly affect the structural acoustic coupling and so a similar control strategy can be applied to each panel of the cylindrical fuselage.

Other numerical methods

In this work the focus is on the low frequency range vibro-acoustic problem, which is usually studied and solved through FEM. Nevertheless, for large fluid domain, the Boundary Element Method (BEM) can be applied, otherwise a large FEM-based 3D mesh would be required. BEM is more computationally expansive than FEM for an equal amount of DoF, but it usually requires fewer DoF than FEM to obtain the same accuracy. A FEM-based model is usually faster for solving small and medium-sized acoustics models than BEM. FEM-BEM hybrid model are used to exploit the advantages of the two formulations. BEM solves equation formulated in an integral form (e.g., boundary integral equation BIE), for a review on BEM see the work by Liu [47].

FEM is not suitable for high frequency problem, Statistical Energy Analysis (SEA) is preferred [48]. SEA method represents a system with several coupled subsystems and therefore a set of linear equations is derived. In order to describe the input, storage, transmission and dissipation of energy within each subsystem, their parameter are derived from statistical assumption, simplifying the building of the model if compared

to FEM and BEM. The main limit of this method is the form of the results, that is not deterministic as in the other methods and local results (e.g., pressure values) are difficult to be obtained. SEA predicts the average response of the subsystems. Moreover, SEA subsystems size must be large if compared to the wavelength of the problem.

Mid frequencies problems represent a limit for understanding the vibro-acoustic behaviour of the aircraft, because neither FEM/BEM and SEA model can accurately understand the frequency response of the system. Several hybrid models have been proposed [49].

3.5.3 CASTLE project

Inside the Clean Sky 2[1] framework, the CASTLE (CAbin Systems design Toward passenger welLbEing) consortium is developing a new aircraft design for a commercial regional turboprop aircraft and a business jet. Focusing on the regional aircraft, one important aspect in the user centred design is the comfort, which includes the acoustic comfort [50]. This project is particular important because it shows the whole process in the aircraft acoustic design: the assessment of the acoustic behavior of the aircraft structure, the experimental and numerical design of noise reduction solution and their application in the aircraft through numerical methods, FEM for low frequencies and SEA for high frequencies. Following this simple consideration, several works have been produced within the project itself or in the surrounding, including part of this thesis. The acoustic characterization of the aircraft is performed through numerical analyses, FEM for low frequencies and SEA for medium and high, and experimental test to study the materials.

A baseline configuration is defined and several solutions are proposed for N&V reduction in the cabin. In particular, they proposed the following solutions applied around the passenger cabin:

- passive solution applied on the lining panel of the cabin, several materials and metamaterials are exploited;
- an active solution, a dynamic vibration absorber (DVA), applied on the fuselage to reduce the vibrations;
- application of nanofibers and optimization of the shape of seats headrest;
- an active noise control (ANC) placed on the headrest of a passenger seat on both sides of the passenger's head to create a local zone of quiet (comfort area) around the ears.

[1] `https://www.clean-aviation.eu/clean-sky-2`

This project and the several works published show the complexity of the problem and the simplification necessary to study the it. A non-exhaustive overview of the publications on the project and its surroundings is reported in the following paragraph:

- studies on possible solutions through acoustic metamaterials [51, 52], nanofibers on the headrest of the seats [53] and active solutions [54];
- vibro-acoustic studies on simplified model and on fully developed fuselage model (with some simplifications) for FEM analysis [55] and SEA [56, 57].

It is not the aim of this review to accurately describe the CASTLE project and for any further information see the report [50]. Moreover, in other sections of this work we will refer to the baseline FEM model and on the proposed solutions.

In order to summarize the results from a vibro-acoustic modelling point of view a FEM model and a SEA model are created to study the new acoustic solutions. The FEM in Fig. 3.6 is used for the low frequency range and the components of the model are:

- the fuselage structure (panels, stringers, frame and simplified windows). The fuselage is defined as monolithic cylindrical panel and stringer and frames as beam elements;
- a lining panel around the cabin built with a sandwich material (shell elements for the faces and solid elements for the core);
- the deck and its supports (panels and beams);
- the acoustic cavities (the passenger cabin cavity, the cargo hold cavity and the gap between the fuselage and the lining panel).

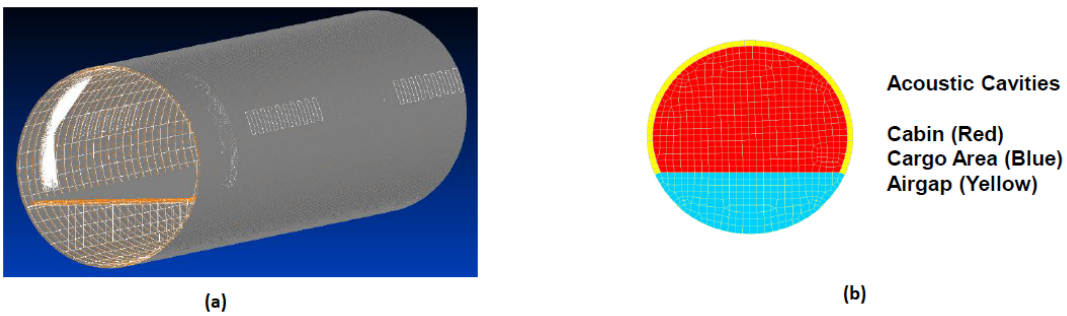

Figure 3.6: The FEM model developed in the CASTLE project [50]. (a) The structure rendering. (b) A sketch of the coupled system composed by the fuselage, the cabin structure and by the three acoustic cavities.

In the first FEM model the seats are not considered, while they are included in the SEA one. In a later work by Cinefra et al. [55], the authors investigate the influence of the several cabin components, such as seats and carpet, in the noise diffusion. The

components are modelled with the porous material formulations in a simplified fuselage model (considering a small half barrel for only one row of seats and spherical external source, see Fig. 3.7). This leads to the definition of the seats in the FEM model through a volume impedance condition, similar to the second solution proposed by [44]. The FEM model main issue is the absence of internal elements of the fuselage, as seats and luggage compartment, within the neglect of the rivets or connections (e.g., shock absorbers) between the fuselage structures and the lining panels. Moreover, the assumption of a monolithic lining panel leads to loose the partially uncoupled modes of the panels themselves. On the other hand, the exploitation of solid elements in the sandwich material core avoids a loose in accuracy in understanding the kinematic behaviour of this material, which is a limit of shell structural model. The solid elements are paid in terms of computational cost, increasing the degrees of freedom. Finally, in the FEM model the structure is excited by a complex pressure calculated by *Centro di Ricerca Aerospaziale* (CIRA) from engine information and defined as pressure on the fuselage panels.

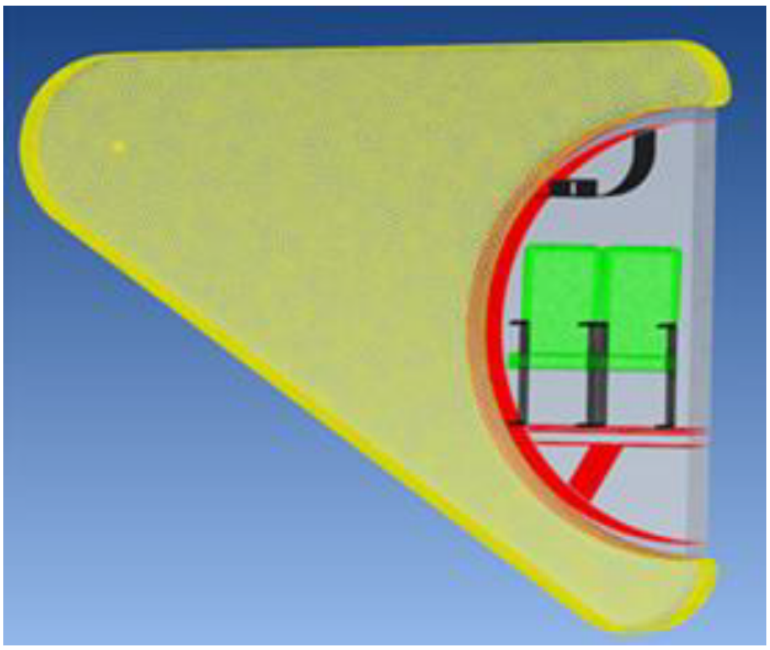

Figure 3.7: The FEM model proposed by Cinefra et al. [55] to study the seats and carpet influences on the cabin noise with a full porous material approach. In the rendering there are the cabin structure and internal components, as the seats and overhead compartments, and the external monopolar source.

The CASTLE project is one of the few published example of a comprehensive study of the aircraft noise with numerical analysis (partially validated) and tests. The aircraft noise footprint is derived taking into account the structures, the cabin elements (the lining panels for the FEM model, the seats and the overheads for the SEA one), the acoustic sources calculated for that particular aircraft model and finally several possible solutions compared to a baseline configuration, from classical foams or visco-elastic

materials to AMMs or active control systems.

3.5.4 Limits in actual solutions and approaches

In the previous reviews and chapters it is possible to derive three main issues in aircraft noise design, in particular at preliminary stage level, where an high flexibility is required and also exploratory researches on different noise solutions are carried out:

- the high computational cost in the FEM framework to solve the full aircraft noise problem (at least for the fuselage barrel) without losing accuracy and for a relevant frequency range;
- the need to study new unconventional solutions to reduce the N&V inside the aircraft without adding weight and complexity to the system, in particular at low frequency;
- until now the users is not placed at the centre of the design process for the noise problem. We have human based parameters, as A, C, B and D filters, the maximum admitted noise level or in general the possible positions of the users in the aircraft. Nevertheless, we do not have subjective measurements on the users experience.

The first issue depends on the complexity of the FEM model, as reported in Fig 3.8. there is a trade-off between the number of degrees of freedom and the computational cost. In model similar to those in Fig 3.6 the DoF depend on the coupling, which is an unavoidable problem for coupled vibro-acoustics models, on the elements size and interpolation, which affects the maximum frequency of the model (see Appendix A) and on the elements dimensions, so how many beam, shell and solid elements are used. In particular, an important number of DoF must be used for sandwich plate, as those of the lining panel in the cabin.

In order to reduce the DoF we can:

- use shell elements and accept a reduction in the accuracy increasing the frequency of problem;
- use a new formulation for shell elements which allow to still use shell elements without a decreasing in the accuracy: the Carrera's Unified Formulation (CUF) enhances several shell theories that can achieve this goal [58], as described in Chapter 4.

The second issue can be solved with the solution proposed in the CASTLE project [50, 51]: an acoustic metamaterial, a material that allows to manipulate and tailor the wave properties in order to achieve high acoustic characteristics without increasing the

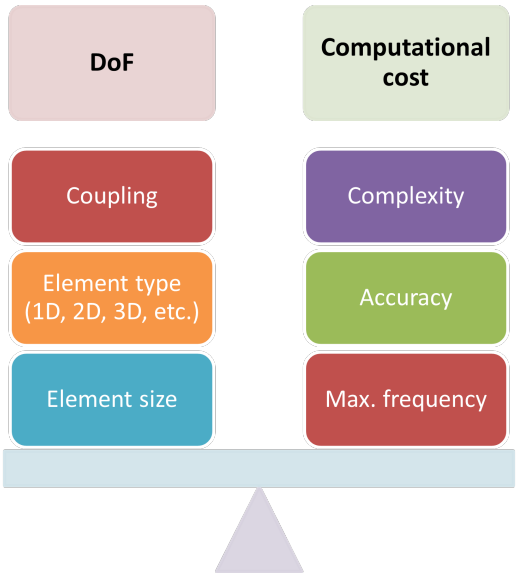

Figure 3.8: The trade-off between the number of DoF, to have an accurate analysis with a wide frequency range, and the computational cost of the model.

weight of the system. This solution will be presented in the case study of this work in Chapter 5.

Lastly, in order to solve the ”human centred design issue”, we take inspiration from the CASTLE project, where the cabin design part was evaluated with virtual and augmented reality tools as described by De Crescenzio et al. [17] for aesthetics and ergonomics issues. The concepts want to integrate inside the VR/AR model the aircraft noise and to study the users response in a visual and sound environment, the description of this new design tool is described in Section 3.6.

3.6 Auralization

In the previous sections N&V are being addressed in numerical and computational terms. Although, noise is principally a comfort problem inside the aircraft, which affects the passenger, the crew and the pilots. Traditional tools to evaluate the effects of noise on comfort levels are the A, B, C and D filters applied on the acoustic pressure to take in account the human’s ear sensibility to different frequencies; moreover, usually noise is measured in significant positions, occupied by passengers; finally maximum comfortable or dangerous value of noise are known. All these measurements and in general parameters are called human based factors. The users are not at the centre the design process, but only considered through human based parameters, regulations and general knowledge. As described in Section 1.2.3, the target in aircraft design and in particular in the cabin design, is to include the users in the design process. In this section a concept design for human in the loop process of the acoustic comfort assessment is proposed.

Traditional tools, exploited when dealing with noise or more in general for comfort evaluation, to study the users direct response to comfort innovations, are the physical mock-ups. The main disadvantages of this solution is the cost linked to the low flexibility of the tool: changing different interior designs or even different cabin configurations is time-consuming and expensive. This situation is aggravated if the mock-up has the noise integrated in the physical cabin through loudspeakers or other acoustic sources. As demonstrated in [17], VR/AR tools can enhance the human centred design removing the physical mock-up limitations. These tools allow to generate virtual mock-ups in a cheaper and flexible environment and their validity is already demonstrated to study ergonomics, aesthetics and visibility in the cabin. Following the author's works in collaboration with *Università di Bologna*'s Virtual Reality and Simulation Laboratory [59, 60], a concept design for the integration of acoustic sources (e.g., noise) in a virtual mock-up is developed: the so-called auralization. The concept idea is to introduce/integrate a spatial sound in the VR/AR environment, as presented by Cohen et al. [61]. Therefore, it will be possible to improve user engagement and confidence by providing realism to the virtual environment. Therefore, the user will provide a full range of subjective measurements from the virtual coupling of visual and acoustic experience. Several configurations can be evaluate in terms of visual and acoustic comfort through auditory experiments [62]. Moreover, the effectiveness of noise reduction solution on passengers will be studied in a user centred design. Finally, this concept will help a cooperative design process between acoustic engineering and other designers or stakeholders.

From an exploratory research in [59], three possible steps are developed to integrate sound in a virtual mock-up:

- the "simplest" way is far from the auralization concept and it fits for designers collaboration and visualization of the results. The idea is to reproduce pressure, displacements maps or modal shapes on the virtual mock-up structure, in order to visualize in a more intuitive way the cabin vibro-acoustic properties;
- inside the auralization field, it is possible to create acoustic sources in virtual environments. The accuracy of this internal simulation is given by the virtual material properties and the source definitions. Although, it will never achieve the accuracy of FEM or SEA numerical analysis. This choice is a preliminary way to study the acoustic comfort, characterizing only the materials and the sources;
- the full auralization would be the integration of numerical analyses in the virtual environment, importing the acoustic pressure results in the time domain.

At the concept design stage, a virtual mock-up of a passenger aircraft is developed at the second step level, so simulating the noise/sound spread directly in the virtual environment pre-processing phase with two internal sources as shown in Fig. 3.9 and

as described in [60].

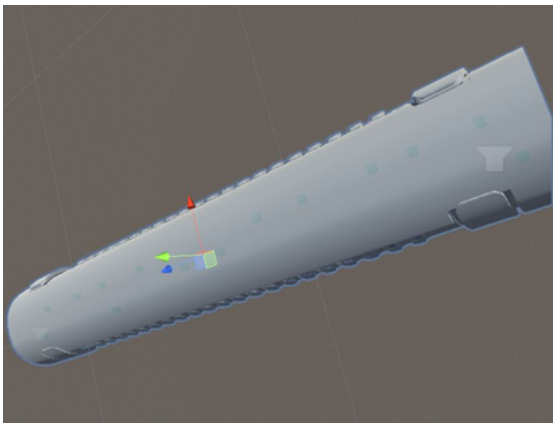

Figure 3.9: The virtual mock-up integrates a spatial sound through two acoustic sources (the two loudspeaker icons).

Chapter 4

Carrera's Unified Formulation for vibro-acoustic problems

4.1 Carrera's Unified Formulation

In this work, the structural part of the model is principally composed by shells, which mean solid components where one dimension is much smaller than the other two ones. It is common for aircraft structure to exploit multi-layer materials with important differences between the thickness of each layer (e.g., composite plates or sandwich panels). In order to obtain a flexible description of the structural model for different kind of plates, which is able to understand the complex kinematic behaviour of multi-layer materials, we decide to exploit an advanced mathematical model for the description of the displacements: the Carrera's Unified Formulation (CUF) [58]. This formulation is exploited to enhance a wide range of shell models, which allow to obtain a high accuracy to describe the kinetic behaviour of advanced structures.

A generic shell lays on the $x - y$ plane and perpendicular to z axis, on this axis the thickness h (from $-h/2$ to $h/2$) develops on different layers, pointed by the index k and so the thickness of each layer is h_k. According to the CUF the three-dimensional field of the displacement of a shell can be split in a two-dimensional field on the shell plane and an expansion on the thickness. The in-plane field is described by the chosen shell model $\mathcal{U}(x,\ y)$, while the expansion on the thickness by the function F_τ, called the thickness function:

$$\mathcal{U}(x,\ y,\ z) = F_\tau(z)\,\mathcal{U}(x,\ y) \tag{4.1.1}$$

The repeated index τ implies the application of Einstein's summation convention. In Equivalent Single Layer models the thickness functions are expressed on the through-the-thickness domain of the multilayered shells. Usually, these theories are accurate to estimate the global laminate response, but they became unsuitable if stresses at ply level are required. Moreover they can be inaccurate when there are localized loads

or in case of high anisotropy. These inaccuracies are amplified for sandwich structure, where the central layer (e.g., the core) is much thicker than the outer layers (e.g., the faces) [63]. Hence, we need to use more accurate model to understand the behaviour of cabin structures, which are usually made of sandwich shells with visco-elastic core. In order to correctly estimate the vibro-acoustic response of a vibrating shell, the thickness functions change according to the layer k:

$$\mathcal{U}^k\left(x,\ y,\ z\right) = F_\tau^k\left(z_k\right)\mathcal{U}^k\left(x,\ y\right) \tag{4.1.2}$$

where $z_k \in h_k$. In this case, the displacement continuity conditions have to be enforced at the layer interfaces.

In an Equivalent Single Layer (ESL) model, the thickness functions are based on Taylor expansion $F_\tau = z^\tau$ where in a finite expansion the highest order is N and so $\tau = 0, ..., N$ with $N + 1$ functions.

In a Layer Wise (LW) model the thickness functions are expressed by Lagrange interpolation polynomials through the thickness of layer k:

$$F_\tau^k\left(\zeta_k\right) = \prod_{i=0, i\neq\tau}^{N} \frac{\zeta_k - \zeta_{k_i}}{\zeta_{k_\tau} - \zeta_{k_i}} \tag{4.1.3}$$

in which ζ_k is the adimensional thickness coordinate within layer k (the bottom for $\zeta_k = -1$ and the top for $\zeta_k = 1$). The interpolation points are usually equally spaced in the layer k. In order to guarantee the displacement continuity at the interfaces between the layers, the following condition is imposed:

$$u_t^k = u_b^{k+1},\ k = 1, ..., N_l - 1 \tag{4.1.4}$$

so the displacement at the top of a layer must be equal to the one at bottom of the following layer, for the total number of layers N_l. The stress continuity can be obtained if enough Lagrange expansion term are used.

In a vibration analysis, the displacement field is time-dependent and Eq. 4.1.2 has the following formulation:

$$\mathcal{U}^k\left(x,\ y,\ z,\ t\right) = F_\tau^k\left(z_k\right)\mathcal{U}^k\left(x,\ y,\ t\right) \tag{4.1.5}$$

4.2 Numerical approximation

In order to solve the problem, a numerical approximation is exploited. The FEM has been already applied and validated in the vibro-acoustic field both on theoretical models and on study cases. In the FEM approximation the physical domain is divided in

elements defined by nodes. In order to build the continuous field for the unknowns from the discrete nodal unknowns, the shape functions N_i are introduced. In the plate-cavity system, the structural shell elements interface with the three-dimensional elements of the cavity. For the shell elements, the displacement field obtained in Eq. 4.1.2 is two-dimensional. The continuous variables of the vibro-acoustic problem, displacement $\mathcal{U}^k$ and pressure p, are calculated from the nodal displacement vector $U^k_{\tau i}$ and pressure vector P_i:

$$\begin{aligned} &\mathcal{U}^k_\tau (x,\ y,\ t) = N_i (x,\ y)\, U^k_{\tau i}(t) \\ &i = 1, ..., m_u\ \tau = 1, ..., n^k_i \end{aligned} \tag{4.2.1}$$

$$\begin{aligned} &p (x,\ y,\ z,\ t) = N_i (x,\ y,\ z)\, P_i(t) \\ &i = 1, ..., m_p \end{aligned} \tag{4.2.2}$$

in which i is nodal index inside the element, m_u and m_p the number of structural and fluid nodes respectively, n^k_i is the number of adopted LW expansions in layer k on the corresponding node i. On Eq. 4.2.1, we apply the CUF:

$$\mathcal{U}^k (x,\ y,\ z,\ t) = N_i (x,\ y)\, F^{ki}_\tau (z_k)\, U^k_{\tau i}(t) \tag{4.2.3}$$

where the i superscript on the thickness functions introduces the coupling between the shape and thickness functions, the so-called Node-Dependent Kinematics (NDK). In a similar way it is possible to obtain $\delta\mathcal{U}$ and δp:

$$\delta\mathcal{U}^k (x,\ y,\ z,\ t) = N_j (x,\ y)\, F^{kj}_s (z_k)\, \delta U^k_{sj}(t) \tag{4.2.4}$$

$$\delta p (x,\ y,\ z,\ t) = N_j (x,\ y,\ z)\, \delta P_j(t) \tag{4.2.5}$$

where indices j and s have the same meaning of i and τ respectively.

4.3 Fundamental matrices

The continuous system in Eq. 3.3.5 can be transposed in a numerical domain, from continuous unknowns to nodal one. The system is studied in its different terms in order to obtain the fundamental matrices. The aim is to obtain for each matrix a fundamental nucleus, which is only a function of the shape and thickness functions, of the material properties and of the differential operators.

For the stiffness structural term we apply the Eq. 3.3.6, Eq. 3.3.8 and Eq. 4.2.4 in order to obtain the stiffness structural matrix:

$$\int_{\Omega^k_s} \delta\mathcal{U}^{kT} \boldsymbol{b}^T \boldsymbol{C}^k \boldsymbol{b} \mathcal{U}^k dV = \delta U^{kT}_{js} \boldsymbol{K}^k_{ij\tau s} U^k_{i\tau} \tag{4.3.1}$$

where the fundamental nucleus $\boldsymbol{K}^k_{ij\tau s}$ is a 3×3 matrix, which includes the shape and thickness functions, the differential operator matrix and the elasticity matrix:

$$\boldsymbol{K}^k_{ij\tau s} = \int_{\Omega^k_s} \left(N_j F^{kj}_s \boldsymbol{b} \right)^T \boldsymbol{C}^k \left(N_i F^{ki}_\tau \boldsymbol{b} \right) dV \tag{4.3.2}$$

In a similar way the other structural matrices can be obtained with their fundamental nuclei, so we build the external load nucleus, a 3×1 vector, F^k_{js} and the structural mass nucleus, which include also the material density ρ_s, the 3×3 matrix $M^k_{ij\tau s}$.

The fluid-structure coupling term is expressed as follow:

$$\int_{\Gamma_{fs}} \delta \mathcal{U}^{kT} p \boldsymbol{n} ds = \delta U^{kT}_{js} \boldsymbol{S}^k_{ijs} P_i \tag{4.3.3}$$

in which the fundamental nucleus is a 3×1 vector:

$$\boldsymbol{S}^k_{ijs} = F_s \left(z_{fs} \right) \int_{\Gamma_{fs}} N_j N_i \boldsymbol{n} ds \tag{4.3.4}$$

in the nucleus we find the fluid-interface normal $\boldsymbol{n}$, the shape functions of the two-dimensional displacement field $N_j(x,\ y)$ and of the three-dimensional pressure field $N_i(x,\ y,\ z)$ and the thickness function on the interface F_s.

As done for the other nuclei, the acoustic stiffness nucleus is derived from the fluid internal work:

$$\int_{\Omega_f} \delta p_{,l} p_{,l} dV = \delta P^T_j \boldsymbol{H}_{ij} P_i \tag{4.3.5}$$

in which we introduced the summation index l. The fundamental nucleus is defined from the three-dimensional shape functions:

$$\boldsymbol{H}_{ij} = \int_{\Omega_f} N_{j,l} N_{i,l} dV \tag{4.3.6}$$

In a similar way the mass acoustic matrix can be obtained with its fundamental nucleus $\boldsymbol{Q}_{ij}$. In this case, the speed of sound term $1/c^2_f$ is conventionally written inside the nucleus.

The fundamental nuclei are expanded on the indices τ, s, i and j, we obtain the final equations for the coupled problem that include the FE approximation and the CUF. The system in Eq. 3.2.9 can be written in a matricial form with the fundamental nuclei formulation:

$$\begin{bmatrix} \boldsymbol{M} & 0 \\ -\rho_f \boldsymbol{S}^T & \boldsymbol{Q} \end{bmatrix} \cdot \begin{Bmatrix} \ddot{U} \\ \ddot{P} \end{Bmatrix} + \begin{bmatrix} \boldsymbol{K} & \boldsymbol{S} \\ 0 & \boldsymbol{H} \end{bmatrix} \cdot \begin{Bmatrix} U \\ P \end{Bmatrix} = \begin{Bmatrix} \boldsymbol{F} \\ 0 \end{Bmatrix} \tag{4.3.7}$$

This system has as unknowns the displacement and the pressure, the first term represents the mass matrix of the system, while the second the stiffness matrix. The mass matrix is not diagonal due to the coupling term, which can be neglected for low density

fluid, simplifying the resolution of the system. Therefore, the system exploits a weak coupling and, referring to Eq. 3.3.1, a $\beta_c << 1$. The stiffness term is non-diagonal too. The third term is the load vector, in particular $\boldsymbol{F}_{sj}$ represents the structural external load, defined by a 3×1 fundamental nucleus:

$$\boldsymbol{F}_{sj}^{k} = F_s(z_l) \int_{\Sigma^k} N_j(x,y)\, f_m^k(x,y)\, ds \tag{4.3.8}$$

where the external load is $f_m^k(x,y) = [f_u(x,y) f_v(x,y) f_w(x,y)]^T$ applied at the coordinate z_l, Σ^k is the reference area for the layer k which could coincide with the area of the interface between the plate and the fluid volume Σ_{fs}. The second row of the external load matrix is known if there is not any acoustic load, otherwise we will have the matrix F_p, which formulation is inserted in the CUF in Section 4.4.3.

The system can be transformed in the frequency domain through the Fourier transform, as done for the wave equation in Eq. 3.2.6:

$$\begin{bmatrix} -\omega^2 \boldsymbol{M} + \boldsymbol{K} & \boldsymbol{S} \\ -\rho_f \omega^2 \boldsymbol{S} & -\omega^2 \boldsymbol{Q} + \boldsymbol{H} \end{bmatrix} \cdot \begin{Bmatrix} U \\ P \end{Bmatrix} = \begin{Bmatrix} \boldsymbol{F} \\ 0 \end{Bmatrix} \tag{4.3.9}$$

The damping terms is absent, but can be included as the imaginary part of the stiffness matrix, multiplied by ω (see Section 4.4.4)

4.4 MUL2 integration and validation

4.4.1 MUL2 and commercial software

The CUF is applied in the MUL2[1] software developed by *Politecnico di Torino*. The software is written in Fortran 95 and includes several types of analyses (called procedures) and structural formulations (as ESL and LW approaches). In this work the focus will be on the vibro-acoustic analysis and modal extraction.

On the other hand, to validate the results and show the accuracy of the LW approach, ESL based commercial software are used as Ansys[2] and Actran.[3] Moreover, a home-made tool for a fast calculation of the analytical solution of the eigenvalue problem for simple geometries is developed (see Appendix B). Finally, comparisons with literature results are taken in account and cited in the text.

In this section the validations are performed comparing the obtained results to reference one, from literature or from analytical solutions. Nevertheless, literature data or analytical models are not always available for the problem presented in this section.

[1] `http://www.mul2.polito.it/`
[2] `https://www.ansys.com/`
[3] `https://www.mscsoftware.com/product/actran`

Therefore, the results from MUL2 are compared to those obtained well-known commercial software, as Actran and Ansys, whose reliability is proven for ESL approach and solid model and the author refers to the respective handbooks. This validation approach is preferred to obtain and use experimental data, because the former is less prone to environmental errors, such as boundary conditions that are not easily predictable.

4.4.2 Vibro-acoustic validation

Geometry and FEM model

The CUF formulation and the MUL2 software were developed for aeroelastic and structural problems. Only in the last years the CUF have been extended to the vibro-acoustic problem within the formulation based on fundamental nuclei in Eq. 4.3.9 came into being. In this section we will refer to the author's work [64], where the vibro-acoustic formulation in the CUF framework is validated. The MUL2 results are compared to those obtained by Actran.

The test case is the classical plate coupled to a cube cavity, as shown in Fig. 4.1. The square plate size is $1{\times}1\ m^2$ with a thickness equal to $0.01\ m$. The mesh is composed by 20×20 linear shell elements Quad4 in Actran and 10×10 nine-nodes plate elements Quad9 in MUL2. Two plate materials are selected:

- an isotropic material (aluminium) with the following properties: Young's modulus $E_s = 70\ GPa$, mass density $\rho_s = 2700\ kg/m^3$ and Poisson's ratio $\nu = 0.35$;
- an orthotropic material (Young's modulus $E_1 = 25\ GPa$; $E_2 = E_3 = 1\ GPa$, shear modulus $G_{13} = G_{23} = 0.5\ GPa$; $G_{12} = 0.2\ GPa$, Poisson's ratio $\nu_{13} = \nu_{23} = \nu_{12} = 0.25$ and a mass density $\rho_s = 1000\ kg/m^3$) composed by three layers with the following lamination $0 \times 90 \times 0$.

The cavity is a cube of $1 \times 1 \times 1\ m^3$ composed by $20 \times 20 \times 20$ linear elements Hexa8 in Actran and $10 \times 10 \times 10$ quadratic elements Hexa27 in MUL2. Two fluids are used for the validation:

- air (weak coupling) with the following properties: speed of sound $c_f = 343\ m/s$ and mass density $\rho_f = 1.225\ kg/m^3$;
- water (strong coupling) with the following properties: speed of sound $c_f = 1500\ m/s$ and mass density $\rho_f = 1000\ kg/m^3$.

The plate is placed on the top of the cavity and its edges are simply supported and an interface between the plate (structure) and the cavity (fluid) is created. A constant amplitude force excitation of $1\ N$ is applied on the plate at the point $A = (0.25,\ 0.35,\ 1.0)\ m$.

The analyses are performed at low frequency range 0–300 Hz. The measurement locations of the pressure are the points $B = (0.75,\ 0.75,\ 0.75)\ m$ and $C = (0.35,\ 0.70,\ 0.65)\ m$ inside the cavity (virtual microphones).

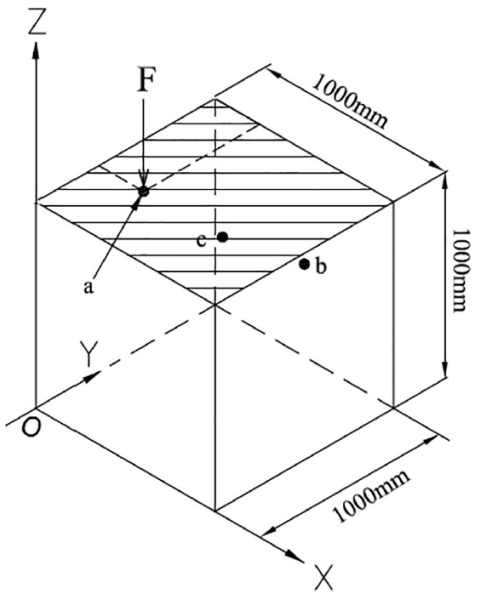

Figure 4.1: The coupled model of plate backed by a cube cavity. A force excitation is applied on the cavity in point A and a two virtual microphones record the pressure values in points B and C.

Modal analysis

In order to validate the model two uncoupled, modal analyses are carried on for the structure and fluid. The aim is to avoid any inaccuracy in the building of the coupled model. The structural shell has been already validated in several works, as in Ferreira et al. [65] for an isotropic plate, and as in Carrera et al. [66,67] and Cinefra et al. [68,69] for an orthotropic one.

For the cavities, a validation is necessary. An analytical solution is available for a box cavity of size a, b and c:

$$\omega_{ijk} = \sqrt{c_f^2 \left[\left(\frac{i\pi}{a} \right)^2 + \left(\frac{j\pi}{b} \right)^2 + \left(\frac{k\pi}{c} \right)^2 \right]} \tag{4.4.1}$$

and results are calculated as described in Appendix B. The first ten natural frequencies are reported in Tab. 4.1 and they are in a perfect agreement with the analytical ones.

Table 4.1: First 10 natural frequencies $[Hz]$ obtained with the analytical solution and the CUF, and the relative error.

Frequency	Analytical $[Hz]$	CUF $[Hz]$	Relative error [%]
1	0	0	0
2	171.5	171.5	0
3	171.5	171.5	0
4	171.5	171.5	0
5	242.54	242.54	0
6	242.54	242.54	0
7	242.54	242.54	0
8	297.05	297.05	0
9	343	343.04	0.02
10	343	343.04	0.02

Frequency response

Firstly, a validation of the Actran coupled model is performed with a literature solution in Puri et al. [70] for an isotropic plate with two different boundary conditions: simply supported edges and clamped edges. The pressure responses of the cavity in points B and C are reported in Fig. 4.2 and compared to the results in [70]. The validating process has been passed. In fact, the main peaks of the frequency response highly coincide with the solution in literature, and this is quite important for the validating process design.

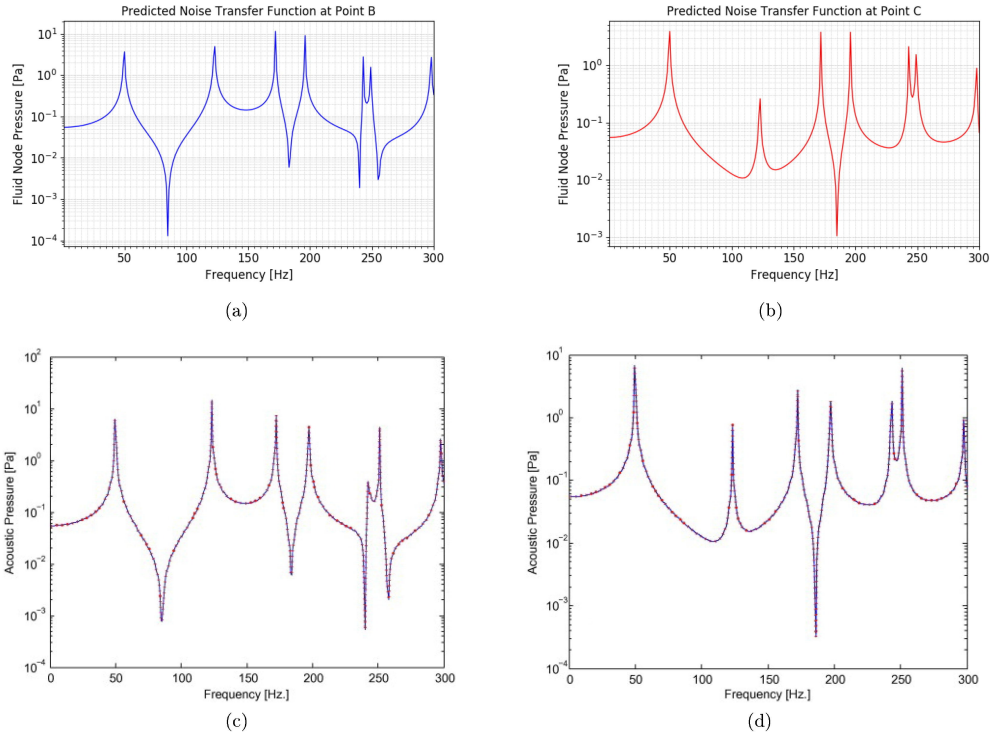

Figure 4.2: The acoustic pressure $[Pa]$ comparison in order to validate the Actran coupled model. (a) Actran Point B. (b) Actran Point C. (c) Puri et al. [70] Point B. (d) Puri et al. [70] Point C.

The main differences between the Actran and MUL2 are in the structural theory, varying from a ESL to a LW approach. It is very likely that the differences between the two software lay in the plate behaviour. Therefore, the structural frequency responses are compared for both structural boundary conditions. A LW2 model is chosen for MUL2, so two points through-the-thickness are considered. The displacements are calculated in the chosen point (0.25, 0.35) m. For the isotropic plate the results are reported in Fig. 4.3, the differences, as expected are small and they slightly increase with a clamped boundary condition, because of an increase in the stiffness of the system, but they remain comparable. Therefore, we expect a small difference for the coupled solution caused by the structure. For an orthotropic multi-layer plate, as we can see in Fig. 4.4, the differences between the results obtained through the two software increase. The LW2 approach used by MUL2 is able to capture the complex dynamic behaviour of the structure, while the ESL approach, exploited by Actran, approximate the properties of the multi-layers laminate with the average properties. The error of the ESL approach increases with the frequency. This gap will interfere with the coupled solution. In general, for both the isotropic and the orthotropic plate, the boundary conditions do not have a significant effect on the difference between the two software, despite the increase in the systems stiffness.

Finally, the coupled frequency response is calculated for a weak and a strong coupling. The plate is simply supported and the two different materials are studied. The pressure frequency response in Pascal for an air-filled cavity is reported in Fig. 4.5 for an isotropic plate and in Fig. 4.6 for a multi-layer plate, while for a strong coupling, so a water-filled cavity, in Fig. 4.7 and Fig. 4.8 respectively. The results reward the MUL2 software approach, in fact the solutions have a better accuracy than those obtained by Actran. Due to the frequency dependent behaviour of the problem and of the solutions, at low frequency there are small differences between the two software, while, for higher frequency the discrepancies increase, in particular for the strong coupling case, due to the reduced wavelength, and for the orthotropic material. This differences are generated by the different approach: LW and the ESL one. In fact, the LW method takes into account multi-layer effects that the ESL method does not cover. Hence, the increase in the differences for a composite plate is due to the Actran ESL approach: the average properties of the plate do not capture the complex kinematic behaviour of the plate and in particular for the water filled cavity, which presents stronger coupling effects. These differences may be considered negligible when dealing with an isotropic material. Moreover, an increase in the number of elements in the Actran mesh, leads to the results in Fig. 4.9. The frequency responses are getting closer to those of MUL2, demonstrating the high level of accuracy of the LW approach.

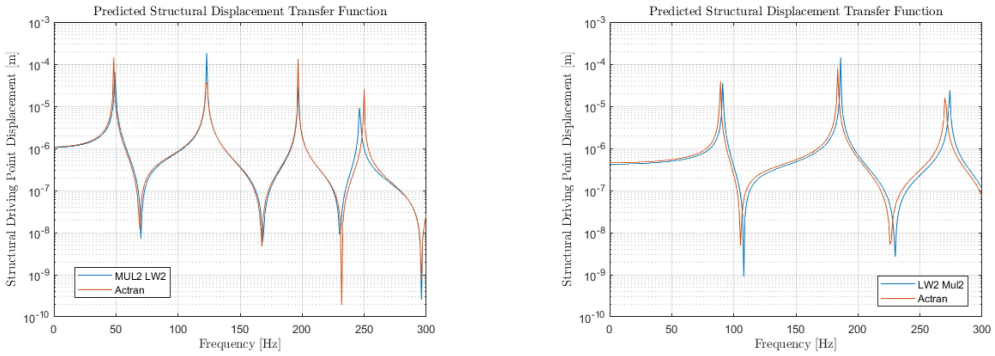

(a) (b)

Figure 4.3: Displacement at (0.25, 0.35) m for the isotropic plate. (a) Simply supported edges. (b) Clamped edges.

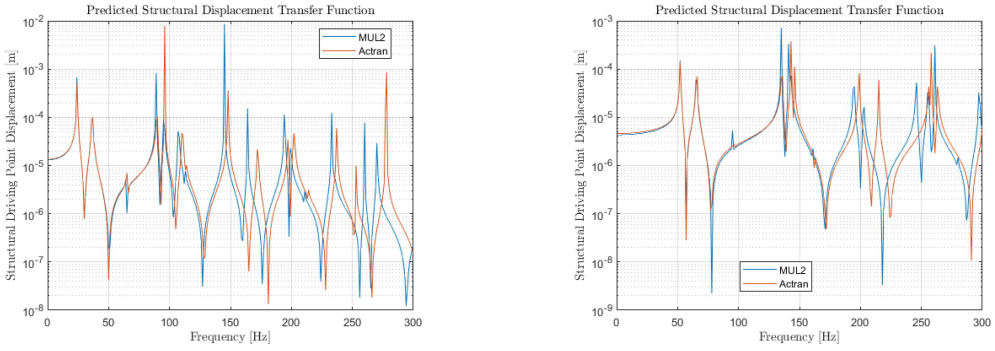

(a) (b)

Figure 4.4: Displacement at (0.25, 0.35) m for the orthotropic plate with different laminations and boundary conditions. (a) $0^o/90^o/0^o$, simply supported edges. (b) $0^o/90^o/0^o$, clamped edges.

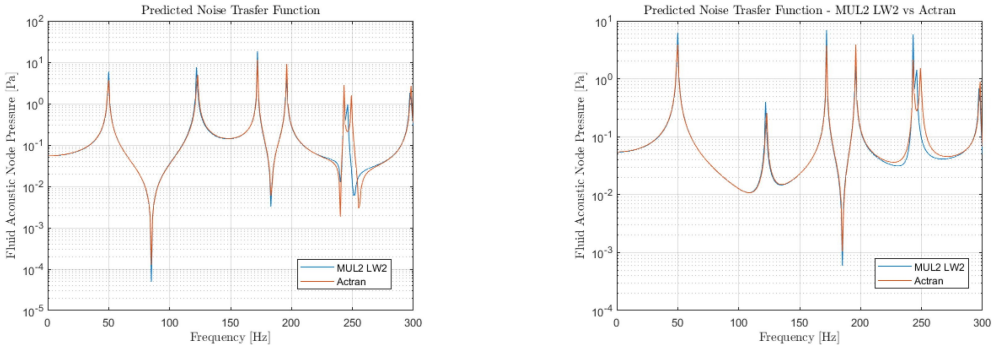

(a) (b)

Figure 4.5: Fluid nodal pressure for a isotropic plate with simply supported edges backed to an air cavity (a) LW2 point B (b) LW2 point C.

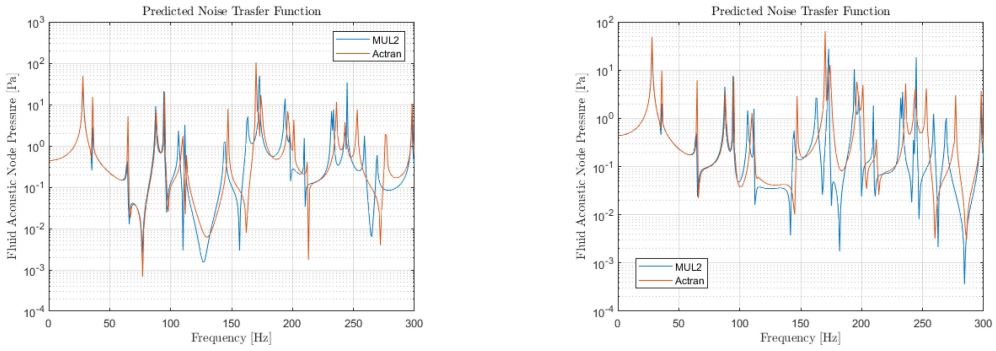

(a) (b)

Figure 4.6: Fluid nodal pressure for orthotropic plate backed to an air cavity ($0^o/90^o/0^o$, simply supported edges). (a) Point B. (b) Point C.

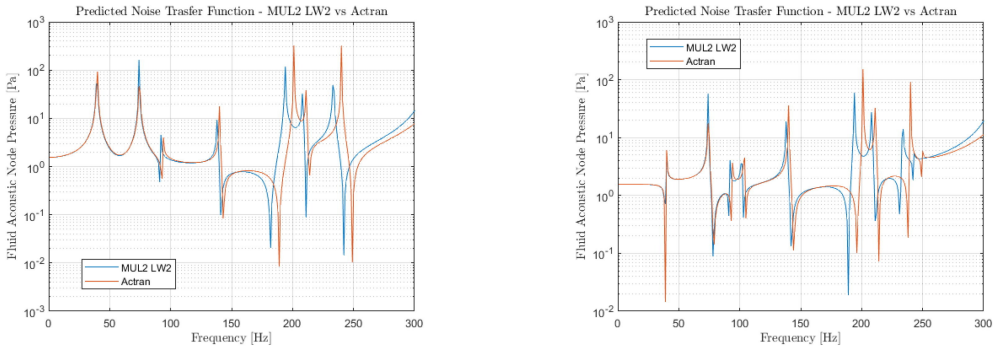

(a) (b)

Figure 4.7: Fluid nodal pressure for a isotropic plate with simply supported edges backed to a water cavity (a) point B (b) point C.

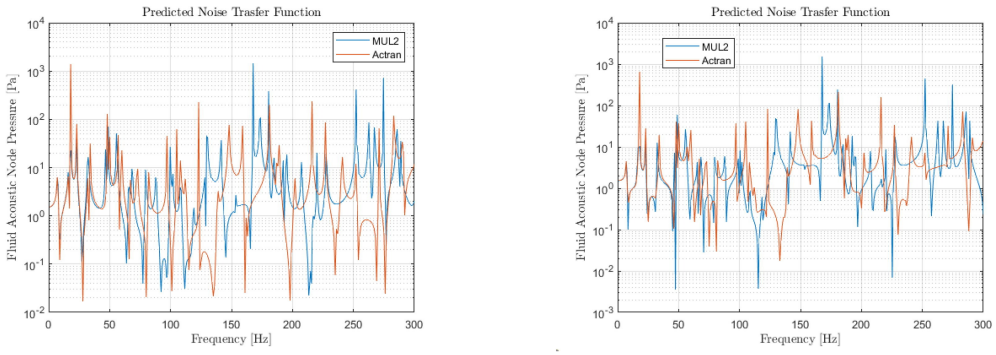

(a) (b)

Figure 4.8: Fluid nodal pressure at point B for an orthotropic plate backed to a water cavity ($0^o/90^o/0^o$, simply supported edges). (a) Point B. (b) Point C.

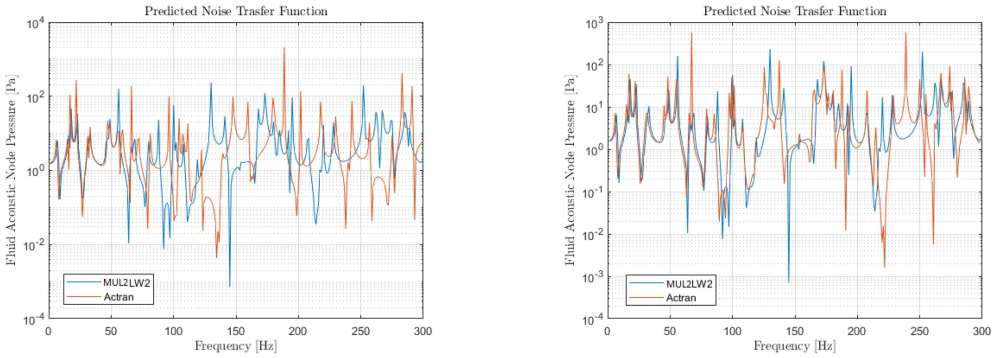

(a) (b)

Figure 4.9: Fluid nodal pressure for an orthotropic plate backed to a water cavity and different structural meshes. (a) 20x20 elements (b) 80x80 elements.

4.4.3 Monopole and free surface

Spherical source: monopole

In the vibro-acoustic system in Eq. 4.3.9, the acoustic loads are not taken into account, because, until now, there were not acoustic sources implemented in MUL2. A first simple source is the monopole, a spherical source which radiates sound equally well in all directions. This source can be simplified as a pulsating sphere. Even if it is a simple source, monopoles are very useful. They can be used to validate vibro-acoustic models, estimate the transmission losses of a plate and they can simulate several acoustic sources, as loudspeaker [71, 72], in particular at low frequency. Moreover, monopoles are used to simulate the engine noise as in the previous cited work by Cinefra et al. [55] or as in the work by Vieira et al. [73].

The system in 4.3.9 can be generalized as in the author's work [74]:

$$\begin{bmatrix} -\omega^2 \boldsymbol{M} + \boldsymbol{K} & \boldsymbol{S} \\ -\rho_f \omega^2 \boldsymbol{S} & -\omega^2 \boldsymbol{Q} + \boldsymbol{H} \end{bmatrix} \cdot \begin{Bmatrix} U \\ P \end{Bmatrix} = \begin{Bmatrix} \boldsymbol{F}_u \\ \boldsymbol{F}_p \end{Bmatrix} \tag{4.4.2}$$

where $\boldsymbol{F}_u$ are the structural external loads and $\boldsymbol{F}_p$ the acoustic load. An acoustic external load is assumed to be defined by its strength, so by its volume velocity $\dot{Q}_s$ or by its power W. For a general source these parameters depend on the radiation directions, for a spherical source there is not dependency on the direction. The acoustic load is defined in terms of fundamental nucleus with the Kronecker Delta δ_K (it is zero except on the position $\boldsymbol{x}_s$, where the value is unity):

$$\int_V \delta p N_j^T(x,\ y\ z) \dot{Q}_s \delta_K(\boldsymbol{x} - \boldsymbol{x}_s) dV = \delta P_j^T \boldsymbol{F}_{p_{sj}} \tag{4.4.3}$$

where the fundamental nucleus is equal to:

$$\boldsymbol{F}_{p_{sj}} = \int_V N_j^T \dot{Q}_s \delta_K(\boldsymbol{x} - \boldsymbol{x}_s) dV \tag{4.4.4}$$

in which for a general source in position $\boldsymbol{x}_s$

$$\dot{Q}_s \cdot e^{i\omega t} = \int_S \dot{u}_f \cdot \boldsymbol{r} dS \tag{4.4.5}$$

where S is the surface on which the flux volume of velocity $\dot{u}_f$ is calculated, and $\boldsymbol{r}$ is the radial vector.

An acoustic monopole is a pulsating sphere that radiates equally in all directions [75,76]. In order to describe the monopole pressure field, the wave equation is transformed in spherical coordinates (θ, ϕ, r). Moreover, the solution only depends on the radial terms, because the sphere pulsates equally in all directions and so the derivatives in θ and ϕ are zero:

$$\frac{\partial^2(pr)}{\partial r^2} - \frac{1}{c_f^2}\frac{\partial^2(pr)}{\partial t^2} = 0 \tag{4.4.6}$$

and the general solution is:

$$p(r,t) = \frac{f\left(t - \frac{r}{c_f}\right)}{r} + \frac{g\left(t + \frac{r}{c_f}\right)}{r} \tag{4.4.7}$$

in which the solution is represented as the sum of two radial waves, one divergent and the other convergent. The convergent wave is incompatible with the boundary conditions of the free field. In a closed cavity the reflection and so the convergent wave is described by the wall boundary conditions. Therefore, the convergent contribution of the spherical wave can be neglected in the monopole description. Moreover, the sound pressure decays with the distance.

Finally, the solution is transformed in Eq. 4.4.7 in the frequency domain:

$$p(r,\omega) = A(\omega)\frac{e^{-ikr}}{r} \tag{4.4.8}$$

where A is the monopole amplitude, that depends on ω, and k the wave number. Moreover, the monopole can be defined from its volume velocity $\dot{Q}_s$ and its acoustic power W respectively:

$$\dot{Q}_s = \frac{4\pi A}{i\omega\rho_f} \tag{4.4.9}$$

$$W = \frac{\rho_f c_f k^2 \dot{Q}_s^2}{8\pi} \tag{4.4.10}$$

In the finite element model the monopole is described as an imposed pressure on a node, which represents the centre of the sphere. In order to validate the previous formulation

and evaluate the CUF advantages, a comparison between MUL2 and Actran is performed. In Actran the monopole is similarly described, between the Carrera's Unified Formulation and commercial software one there is a factor in the pressure equal to 4π due to the definition of the amplitude of the monopole.

The following frequency response analyses between 1 Hz and 1000 Hz are carried on:

- a box cavity filled by air or water with a monopole with different amplitude;
- a box cavity filled by air with three monopoles;
- a cylindrical cavity filled by air with a monopole;
- a plate made by an isotropic or orthotropic material coupled to a box cavity filled by air with a monopole.

The frequency range includes the low frequency and part of the middle frequency in order to validate the formulation in a range wider than those usually applied to FEM analysis in vibro-acoustics.

The FEM model for the frequency response of the cavities are reported in Fig. 4.10. The first geometrical model is a closed cavity 0.75x0.40x0.65 m filled by air (ρ =1.225 kg/m^3 and c =340 m/s) or water (ρ =997 kg/m^3 and c = 1500 m/s) and modeled with 15x8x13 Hexa8 elements with linear interpolation. Two different configurations are selected for the validation:

- one monopole placed in a corner of the cavity (0.05, 0.05, 0.05 m) with a baseline amplitude of 1 N/m;
- three monopoles placed in three different positions (0.05, 0.05, 0.05 m; 0.55, 0.25, 0.15 m; 0.15, 0.15, 0.50 m) with a fixed amplitude equal to 1 N/m for the first two monopoles and equal to 2 N/m for the last.

In the cavity, the pressure is calculated in two points A=(0.71, 0.36, 0.61) m and B=(0.375, 0.200, 0.325) m.

The second cavity is a cylinder filled by air. The elements are Hexa8 (20 on the length and 18 on the diameter) with linear interpolation. In the cavity a monopole is placed at the centre of the cylinder. The amplitude is equal to 1 N/m. In the cavity the pressure is calculated in two points A=(0.010, 0.014, 0.133) m and B=(0.069, 0.072, 0.175) m.

For the coupled mode, the box cavity is the same. The plate is simply supported on its four edges. The plate is placed on the whole upper face of the cavity. The plate's thickness is equal to 0.01 m. The monopole amplitude is 1 N/m and it is placed in a corner of the cavity (0.05, 0.05, 0.05 m). Two direct frequency analyses are performed with different materials for the plate:

(a) **(b)**

Figure 4.10: The two cavity models with the sources (spheres) and the microphones (white points). (a) The box cavity (in black the sphere for the first cases and in white the spheres added in the last case). (b) The cylindrical cavity.

- one layer of aluminum (E =7.2 GPa, ν =0.33, ρ =2700 kg/m^3);
- one layer of an orthotropic material (a polymer material used in additive manufacturing with the following properties $E_1 = E_2$ =1.4 GPa, E_3 = 1.02 GPa, $\nu_{12} = \nu_{23} = \nu_{13}$ =0.35, $G_{23} = G_{13}$ =0.5185 GPa, G_{12} =0.3778 GPa, ρ =1040 kg/m^3 the layer is made of a particular class of orthotropic material: a transversely isotropic material).

The results are calculated in two points. The first one inside the cavity at position A=(0.51, 0.36, 0.51) m and the second one in the plate B=(0.32, 0.19, 0.65) m. Moreover, according to the CUF approach, the isotropic and the orthotropic plates are solved through a three points on the thickness (LW3) interpolation.

The box cavity have already been validated in Section 4.4.2, as well as the plate. Only the cylindrical cavity is validated. For a closed cylindrical cavity there is an analytical solution as proposed in [77,78] based on Bessel's functions. Therefore, this solution can be applied to the closed cavity only for modes defined by the integer m and the positive integer l and n:

$$f_{l,m,n} = \frac{c_f}{2\pi}\left[\xi_{l,m}^2 + \left(\frac{n\pi}{L}\right)^2\right]^{1/2} \tag{4.4.11}$$

in which L is the cylinder length, c_f the speed of sound and the scalar $\xi_{l,m}$ is the $m-th$ zero of the first derivative $l-th$ Bessel's function multiplied by the radius R, so that $J_l'(\xi_{l,m}R) = 0$. Therefore, a comparison between Actran and MUL2 is carried on and with the analytical solution too. As expected, the relative errors in Tab. 4.2 in terms of natural frequencies are negligible. There are two coexistent modes around 1000 Hz, so the frequency maximum limit of the analysis of cylindrical cavity is increased from 1000 to 1100 Hz in order to capture these two modes and to compare the results.

For the two cavities the results are reported in Tab 4.3. The differences between the

Table 4.2: The first ten natural frequencies $[Hz]$ calculated by the analytical method in [77,78], by MUL2 and by Actran with their relative errors and differences between the two software for a cylindrical cavity.

Modes	Analytical [Hz]	MUL2 $[Hz]$	Actran $[Hz]$	MUL2 error [%]	Actran error [%]	MUL2 vs Actran [%]
1	850.00	850.87	850.87	1.03E-01	1.03E-01	2.78E-06
2	996.22	1001.40	1001.27	5.20E-01	5.07E-01	1.28E-02
3	996.22	1001.44	1001.32	5.24E-01	5.12E-01	1.22E-02
4	1309.56	1314.07	1313.98	3.44E-01	3.38E-01	7.42E-03
5	1309.56	1314.11	1314.01	3.47E-01	3.40E-01	7.11E-03
6	1663.97	1663.49	1664.82	2.89E-02	5.11E-02	8.04E-02
7	1663.97	1669.43	1667.70	3.28E-01	2.24E-01	1.04E-01
8	1700.00	1707.00	1707.00	4.12E-01	4.12E-01	2.69E-06
9	1868.50	1868.47	1869.66	1.61E-03	6.21E-02	6.37E-02
10	1868.50	1873.77	1872.22	2.82E-01	1.99E-01	8.24E-02

two software are caused by the different formulation and numerical errors. Although, these deviations are very small, below 0.1% for the pressure in Pascal. From the results it is possible to obtain the following conclusions for the pressure response of a pure acoustic system:

- the differences between the two formulations are not influenced by the monopole amplitude, so we must conclude that there are no issues in the $\boldsymbol{F}_p$ formulation;
- the change of the material from air to water (e.g., increasing the density and the speed of sound of the system) leads to a reduction in the formulations differences, so the gap is included in the mass matrix formulation, which depends on the factor $1/c_f^2$. Despite this conclusion, the gap is still negligible. In general, as reported in Fig. 4.11, the differences between Actran and MUL2 increase near the pressure peaks and deeps, so when there is an high derivative in the pressure response and in correspondence of a natural frequency;
- in the cylindrical cavity the errors seem to rise as reported in Fig. 4.12. This is due to a very small shifting in the frequency of the peaks caused by the natural modes; in order to avoid this discrepancy we decided to compare the areas of the two curves.

Table 4.3: The percentage gap in terms of maximum, average and standard deviation between the two software for all the analysed configurations.

Cavity	Fluid	Monopole(s) amplitude $[N/m]$	Field point A [%]			Field point B [%]		
			Δ_{max}	Δ_{av}	Δ_{SD}	Δ_{max}	Δ_{av}	Δ_{SD}
Box	Air	0.01	1.25E-01	1.03E-03	2.59E-02	1.23E-01	3.31E-04	1.62E-02
Box	Air	0.1	1.25E-01	1.03E-03	2.59E-02	1.23E-01	3.31E-04	1.62E-02
Box	Air	0.5	1.25E-01	1.03E-03	2.59E-02	1.23E-01	3.31E-04	1.62E-02
Box	Air	1	1.25E-01	1.03E-03	2.59E-02	1.23E-01	3.31E-04	1.62E-02
Box	Air	10	1.25E-01	1.03E-03	2.59E-02	1.23E-01	3.31E-04	1.62E-02
Box	Air	100	1.25E-01	1.03E-03	2.59E-02	1.23E-01	3.31E-04	1.62E-02
Box	Water	1	1.51E-03	1.52E-05	5.03E-06	2.05E-04	6.35E-05	8.55E-08
Box	Air	1, 1, 2	2.98E-01	1.44E-03	1.17E-01	1.22E-01	3.08E-04	1.54E-02
Cylinder	Air	1	3.63E+03	6.70E+00	1.33+07	1.00E+02	3.05E-01	1.23E+04
”	”	”		5.27E-02[4]			5.21E-02[5]	

In the coupled case, the results are estimated in terms of both pressure inside the cavity and displacements in the plate. The comparisons between the LW and ESL approach are in Fig. 4.13 for the isotropic plate and in Fig. 4.14 for the orthotropic one. Both results show a good convergence between the two software. Although, as the frequency increases, the displacements tend to diverge. According to the previous studies in Section 4.4.2, the ESL approach is no longer able to correctly model the mechanical behaviour of the plate. This tendency is almost negligible in the isotropic material but becomes significant with orthotropic material. These results, for a single layer plate, do not seem to influence the fluid behaviour, probably due to low drawback of fluid-structure coupling. In fact, unlike the other validation, the external load is in the fluid.

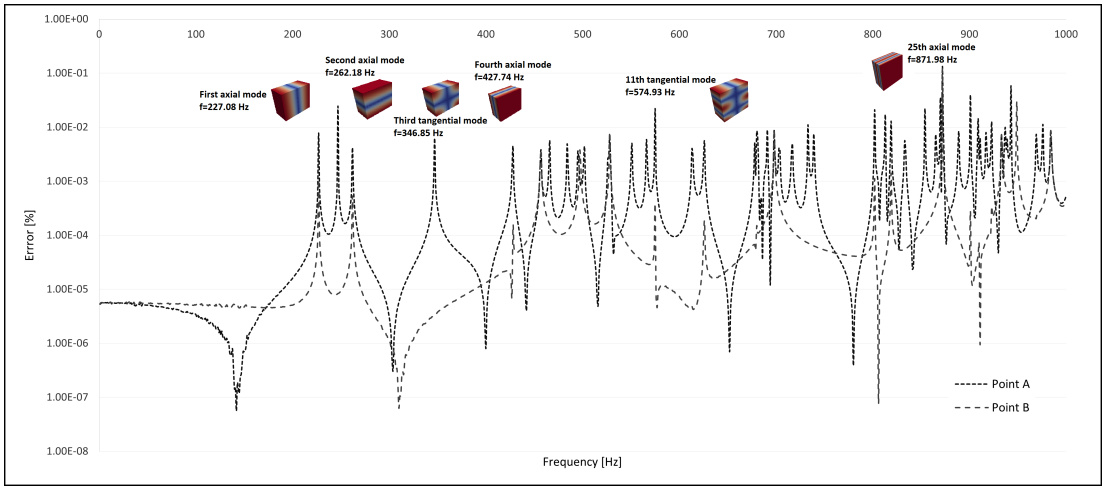

Figure 4.11: The gap [%] in a logarithmic scale between MUL2 and Actran for the two field points in the baseline case of one monopole of amplitude equal to 1 N/m in box cavity. The peaks of the differences correspond to the natural frequency of the system (peak in the pressure value) and deep in the pressure value, so where there is an important increase in the pressure derivative.

Dirichlet boundary condition: free surface

A small addition in MUL2 is the free surfaces, which is defined in the fluid domain of the system Γ_D as Dirichlet boundary condition:

$$(p)_{\Gamma_D} = 0 \tag{4.4.12}$$

This condition does not need any change or addition in the formulation so a fast validation on a cylindrical cavity with a free surface on the two bases is performed, comparing the results with Ansys. The errors are negligible and below the 0.02% for the first six natural frequencies as reported in Tab. 4.4.

[4]Error calculated as comparison between the curves areas.
[5]Ibid.

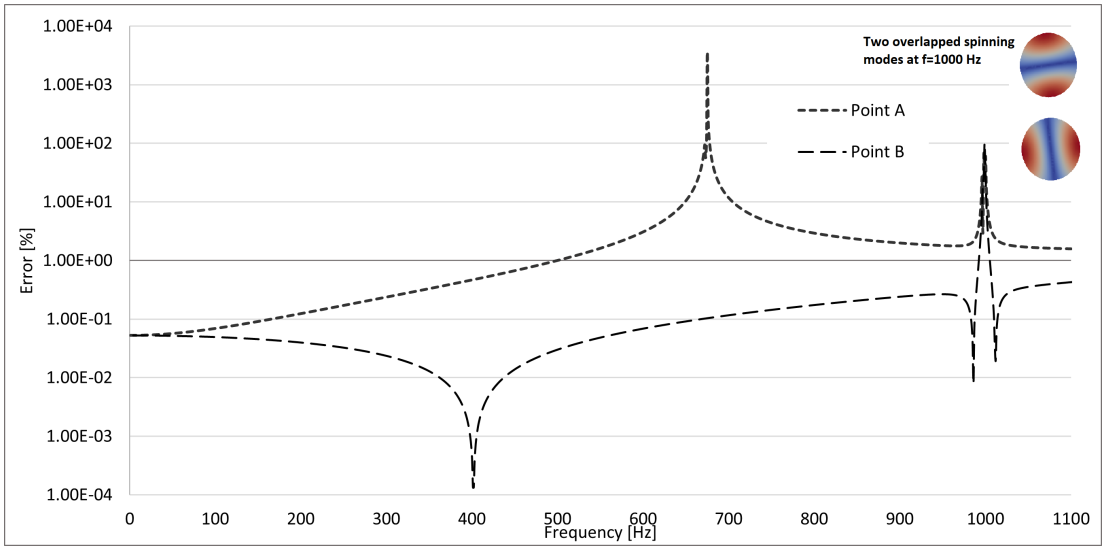

Figure 4.12: The gap [%] in a logarithmic scale between MUL2 and Actran for the two field points in the case of one monopole of amplitude equal to 1 N/m in a cylindrical cavity. The peak of the differences corresponds to the natural frequency of the system (peak in the pressure value) and deep in the pressure value, so for the two coexistent spinning modes at 1000 Hz.

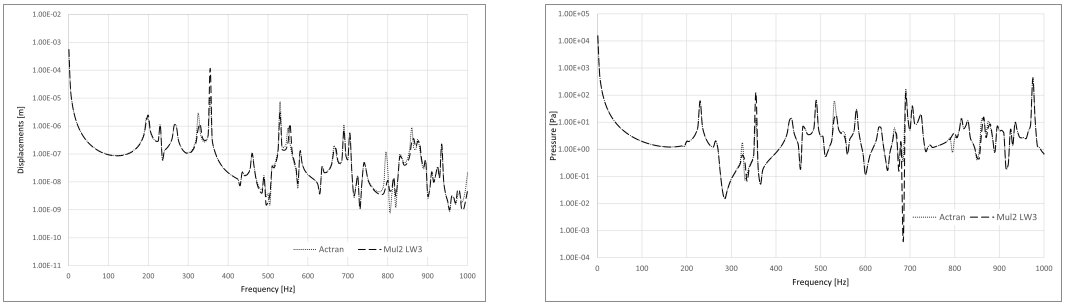

(a) **(b)**

Figure 4.13: The frequency response of the isotropic plate and the coupled cavity calculated by Actran (ESL approach) and MUL2 (LW3 approach). (a) Displacements [m] on the plate at point B. (b) Pressure [Pa] inside the cavity at point A.

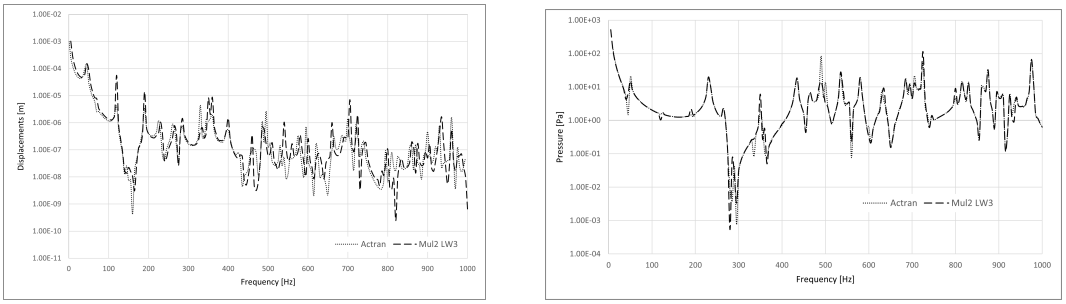

(a) **(b)**

Figure 4.14: The frequency response of the orthotropic plate and the coupled cavity calculated by Actran (ESL approach) and MUL2 (LW3 approach). (a) Displacements [m] on the plate at point B. (b) Pressure [Pa] inside the cavity at point A.

Table 4.4: The first six natural frequencies $[Hz]$ for the cylindrical cavity with two free surfaces on the cylinder's bases. MUL2 results are compared with those obtained by Ansys.

Mode	MUL2 $[Hz]$	Ansys $[Hz]$	Difference [%]
1	8.66E+01	8.56E+01	0.01
2	1.73E+02	1.73E+02	0.02
3	2.21E+02	2.21E+01	0.02
4	2.21E+02	2.21E+01	0.02
5	2.60E+02	2.60E+01	0.01
6	2.67E+02	2.67E+02	0.01

4.4.4 Visco-elastic materials

Visco-elastic materials or in general materials with a damping term play an essential role in N&V absorption. In the vibro-acoustic system Eq. 4.3.9 the damping terms is considered inside the stiffness matrix, which, if the material is visco-elastic, is complex. Therefore, the Young's modulus of a visco-elastic material has to be complex and could be frequency dependant:

$$E(\omega) = E_R(\omega) + E_I(\omega) \tag{4.4.13}$$

and so the loss factor is defined as the ratio between the imaginary and the real part of the Young's modulus:

$$\eta_v = \frac{E_I}{E_R} \tag{4.4.14}$$

The validation process was already done by Filippi et al. [79] for beam structures. In order to validate the CUF for visco-elastic shell in the vibro-acoustics, two steps are followed:

- the comparison of modal results of the a sandwich plate with a visco-elastic core with literature results as those in Fig. 4.15;
- the comparison with Actran of the pressure frequency response of a sandwich plate with a visco-elastic core coupled to a cavity.

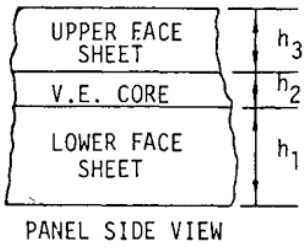

Figure 4.15: The sketch of the sandwich plate with two elastic faces and a visco-elastic core.

In the first step, two cases are selected from literature. The first case is sandwich plate, which has an analytical solution by Abdulhadi reported by Johnson et al. [80] for a simply supported boundary condition. The plate is made by a symmetric sandwich with isotropic faces and a visco-elastic core, see Tab 4.5.

The results for the first five modes are compared to ones of the analytical solution and of the solution proposed by Johnson et al. [80] modelling the core with Hexa8 elements and the faces through Quad4 elements. Moreover, we compare the solutions with a Galerkin based method by Wang et al. [81], an Hamilton principle by Huang et al. [82] and, for the first three modes, on a Reddy's layer-wise theory by Hu et al. [36]. Finally, a comparison between Actran is performed either using shell elements or solid elements for the core. In the CUF model, Quad4 and Quad9 elements are tried with an LW2 approach on the faces and LW3 in the core. The results are reported in Tab 4.6. The CUF approach shows a very good accuracy, in particular with Quad9 elements, greater than those obtained by solid elements in the core by [80] and by Actran.

Table 4.5: Material and geometrical parameters of the simply supported sandwich plate in [80].

Elastic faces	Young's modulus $E_f = 68.9\ GPa$
	Poisson's ratio $\nu_f = 0.3$
	Mass density $\rho_f = 2740\ kg/m^3$
	Thickness $h_f = 0.762\ mm$
Visco-elastic core	Shear modulus $G_c = 0.869\ MPa$
	Poisson's ratio $\nu_c = 0.49$
	Mass density $\rho = 999\ kg/m^3$
	Loss factor $\eta_v = 0.5$
	Thickness $h_c = 0.254\ mm$
Plate size	Length $a = 0.3480\ m$
	Width $b = 0.3048\ m$

A second validation on the first three modes is performed on the plate studied by Li et al. [83] with a semi-analytical solution and by Huang et al. [82] with a method based on the Hamilton principle. The sandwich plate properties are reported in Tab. 4.7. In the results of Tab. 4.8 for a Quad9 model based on CUF with a LW2-LW3 approach, the differences with the semi-analytical solution are negligible, rewarding the CUF-LW approach.

Finally, a coupled model is studied. The plate has the same properties of those in [80] and the cavity is $0.348 \times 0.3048 \times 0.348\ m$ and filled with air. The plate-cavity system is excited by local load equal to $1\ N$ as in the model in Fig. 4.1. The pressure response form $1\ Hz$ to $300\ Hz$ is calculated in two points B=(0.25, 0.25, 0.25) m and C=(0.15, 0.15, 0.15) m. The results are compared to those of an ESL based commercial software, Actran, increasing the number of elements. In Fig. 4.16 the frequency response are shown with a CUF LW3-LW2 approach and Quad4 or Quad9 elements. In Actran we use Quad9 elements and then they are doubled in order to increase the accuracy.

The average differences comparison reward the CUF-LW based approach, in Actran an increase in the number of elements leads to a reduction in the differences between the two approaches: from an average gap of 3.2% to 0.24% so the ESL solution converges to the LW one.

Table 4.6: The first five modes comparison of the sandwich plate in [80]. For each method the natural frequencies f_n and the errors with the analytical solution are given.

		Order				
Approach	Quantity	1	2	3	4	5
Analytical	f_n $[Hz]$	60.3	115.4	130.6	178.7	195.7
Nastran (Johnson)	f_n $[Hz]$	57.4	113.2	129.3	179.3	196
	Err. [%]	4.81	1.91	1.00	0.34	0.15
Reddy's Theory (Hu)	f_n [Hz]	60.24	115.22	130.43	178.46	195.42
	Err. [%]	0.10	0.16	0.13	0.13	0.14
Galerkin (Wang)	f_n $[Hz]$	60.1	115	130.2	178.1	195.1
	Err. [%]	0.33	0.35	0.31	0.34	0.31
Hamilton (Huang)	f_n $[Hz]$	57.27	112.12	127.24	-	-
	Err. [%]	5.02	2.84	2.57	-	-
CUF-LW Q9	f_n $[Hz]$	59.85	114.46	129.60	177.46	194.44
	Err. [%]	0.75	0.81	0.76	0.69	0.64
CUF-LW Q4	f_n $[Hz]$	60.28	116.82	133.75	182.96	205.41
	Err. [%]	0.03	1.23	2.41	2.38	4.96
ESL	f_n $[Hz]$	62.62	123.02	139.75	180.2	198.74
	Err. [%]	3.85	6.60	7.01	0.84	1.55
ESL & solid core	f_n $[Hz]$	61.91	117.8	132.66	172.3	187.79
	Err. [%]	2.67	2.08	1.58	3.58	4.04

Table 4.7: Material and geometrical parameters of the four sides simply supported sandwich plate in [83].

Elastic faces	Young's modulus $E_f = 71\ GPa$
	Poisson's ratio $\nu_f = 0.3$
	Mass density $\rho_f = 2700\ kg/m^3$
	Thickness top face $h_{top} = 0.001\ mm$
	Thickness bottom face $h_{bott} = 0.003\ mm$
Visco-elastic core	Shear modulus $G_c = 0.896\ MPa$
	Poisson's ratio $\nu_c = 0.498$
	Mass density $\rho = 999\ kg/m^3$
	Loss factor $\eta_v = 0.9683$
	Thickness $h_c = 0.001\ mm$
Plate size	Length $a = 0.4\ m$
	Width $b = 0.4\ mm$

Table 4.8: The first three modes comparison of the sandwich plate in [83]. For each method the natural frequencies f_n and the errors with the semi-analytical solution are given.

		Order		
Approach	Quantity	1	2	3
Semi-analytical (Li)	f_n $[Hz]$	94.41	114.01	188.69
Hamilton (Huang)	f_n $[Hz]$	95.09	112.7	187.25
	Err. [%]	0.72	1.15	0.76
CUF-LW Q9	f_n $[Hz]$	94.80	114.01	188.00
	Err. [%]	0.41	0.00	0.37

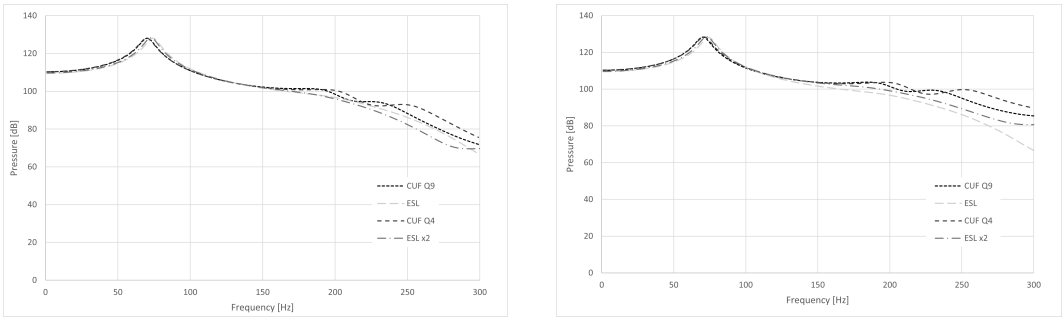

(a) **(b)**

Figure 4.16: The pressure response $[dB]$ as a function of the frequency $[Hz]$ for a sandwich plate with a visco-elastic core baked to an acoustic cavity. A comparison between a LW approach and an ESL one is shown, doubling the elements for the ESL model. (a) Point B. (b) Point C.

4.4.5 A three-dimensional unconventional modelling

Introduction

In the following section, an enhancing of the Carrera's Unified Formulation in curvilinear coordinates is developed and described in the author's work [84]. The aim is to enhance the CUF approach to non-plane geometries, as cylindrical or spherical shell, or more complex ones, as the aircraft fuselage.

The formulation of the shell finite elements used in this work is based on the merging of FEM shape functions and CUF approximating functions into the unique 3D approximating functions employed for both displacements and geometry of the shell element, following the philosophy of non-conventional 2D elements presented in [85]. The resulting 3D approximation is then exploited for the derivation of 3D elements in general curvilinear coordinates, as explained in [86]. The shell elements are particular case of these 3D elements. Therefore, a study case is solved: the study of a multi-layer cylindrical shell (similar to a fuselage structure) coupled to an internal cavity. This example want to be one of the first steps in the exploitation of CUF for studying the vibro-acoustic behaviour of complex structure, following the work by Cinefra [87].

Curvilinear CUF element theory

A similar formulation to those presented in Section 4.1, but generalized for local curvilinear element [58] is reported in this section.

Considering a local curvilinear reference system as represented in Fig. 4.17, a generic shell lays on the local plane $\alpha^1 - \alpha^2$ and the local perpendicular axis to its midsurface is α^3. Along the axis α^3, the thickness h (from $-h/2$ to $h/2$) develops along different layers, each pointed by the index k, so the thickness of each layer is h_k. According to the CUF the three-dimensional field of the displacements of a shell can be split in a two-dimensional field on the shell plane and an expansion on the thickness. The in-plane field is described by the chosen shell model $\boldsymbol{u}_\tau\left(\alpha^1,\ \alpha^2\right)$, while the expansion on the thickness by the function $F_\tau(\alpha^3)$, called the thickness function:

$$\boldsymbol{u}\left(\alpha^1,\ \alpha^2,\ \alpha^3\right) = F_\tau\left(\alpha^3\right)\boldsymbol{u}_\tau\left(\alpha^1,\ \alpha^2\right) \tag{4.4.15}$$

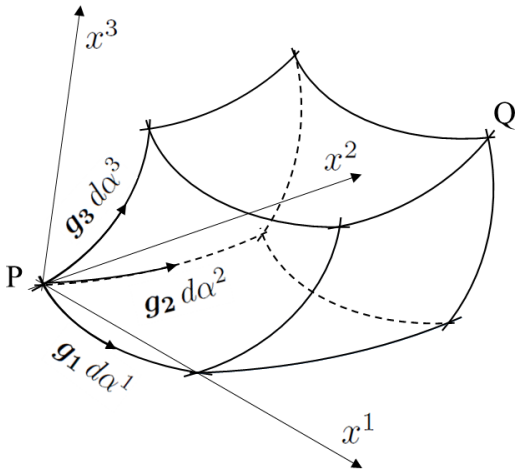

Figure 4.17: Local curvilinear reference system and rectangular Cartesian reference system.

As already explained for local plane reference system, in order to correctly estimate the vibro-acoustic response of a vibrating shell, the thickness functions change according to the layer:

$$\boldsymbol{u}^k\left(\alpha^1,\ \alpha^2,\ \alpha^3\right) = F_\tau^k\left(\alpha^3\right)\boldsymbol{u}_\tau^k\left(\alpha^1,\ \alpha^2\right) \tag{4.4.16}$$

where $\alpha_k^3 \in h_k$. The displacement continuity conditions have to be enforced at the layers interfaces.

In a ESL model the thickness functions are based on Taylor expansion $F_\tau = (\alpha^3)^\tau$ where in a finite expansion the highest order is N and so $\tau = 0, ..., N$ with $N+1$ functions.

In a LW model the thickness functions are expressed by Lagrange interpolation polynomials through the thickness of layer k:

$$F_\tau^k\left(\alpha_k^3\right) = \prod_{i=0, i\neq\tau}^{N} \frac{\alpha_k^3 - \alpha_{k_i}^3}{\alpha_{k_\tau}^3 - \alpha_{k_i}^3} \tag{4.4.17}$$

in which α_k^3 is the adimensional thickness coordinate within layer k (the bottom for $\alpha_k^3 = -1$ and the top for $\alpha_k^3 = 1$). The interpolation points are usually equally spaced in the layer k. In order to guarantee the displacement continuity at the interfaces between the layers, the displacement at the top of a layer must be equal to the one at bottom of the following layer, for the total number of layers N_l. The stress continuity can be obtained when enough Lagrange expansion terms are used.

In a vibration analysis, the displacement field is time dependent and Eq. 4.4.16 has the following formulation:

$$\boldsymbol{u}^k\left(\alpha^1,\ \alpha^2,\ \alpha^3,\ t\right) = F_\tau^k\left(\alpha_k^3\right)\boldsymbol{u}_\tau^k\left(\alpha^1,\ \alpha^2,\ t\right) \tag{4.4.18}$$

In the FEM approximation the physical domain is divided in elements defined by nodes. In order to build the continuous field for the unknowns from the discrete nodal unknowns, the shape functions N_i are introduced. For the shell elements, the displacement field obtained in Eq. 4.4.16 is two-dimensional. The continuous variable of the vibro-acoustic problem, displacement $\boldsymbol{u}_\tau^k$ and pressure p, are calculated from the nodal displacement $\boldsymbol{U}_{\tau i}^k$ and pressure P_i:

$$\boldsymbol{u}_\tau^k\left(\alpha^1,\ \alpha^2,\ t\right) = N_i\left(\alpha^1,\ \alpha^2\right)\boldsymbol{U}_{\tau i}^k(t) \quad i = 1, ..., m_u\ \tau = 1, ..., n_i^k \tag{4.4.19}$$

$$p\left(\alpha^1,\ \alpha^2,\ \alpha^3,\ t\right) = N_i\left(\alpha^1,\ \alpha^2,\ \alpha^3\right)P_i(t) \quad i = 1, ..., m_p \tag{4.4.20}$$

in which i is nodal index inside the element, m_u and m_p the number of structural and fluid nodes respectively, n_i^k is the number of adopted LW expansions in layer k on the corresponding node i. Note that a classical 3D approximation based on 3D Lagrange polynomials is adopted for the acoustic pressure.

On Eq. 4.4.19, we apply the CUF approximation:

$$\boldsymbol{u}^k\left(\alpha^1,\ \alpha^2,\ \alpha^3,\ t\right) = N_i\left(\alpha^1,\ \alpha^2\right)F_\tau^k\left(\alpha_k^3\right)\boldsymbol{u}_{\tau i}^k(t) \tag{4.4.21}$$

In a similar way is possible to obtain $\delta\boldsymbol{u}^k$ and δp:

$$\delta\boldsymbol{u}^k\left(\alpha^1,\ \alpha^2,\ \alpha^3,\ t\right) = N_i\left(\alpha^1,\ \alpha^2\right)F_\tau^k\left(\alpha_k^3\right)\delta\boldsymbol{u}_{\tau i}^k(t) \tag{4.4.22}$$

$$\delta p\left(\alpha^1,\ \alpha^2,\ \alpha^3,\ t\right) = N_j\left(\alpha^1,\ \alpha^2,\ \alpha^3\right)\delta P_j(t) \tag{4.4.23}$$

where indices j and s have the same meaning of i and τ, respectively.

Unconventional 3D shape function

In the following paragraphes, the author tries to summarize the main steps of the derivation of the unconventional 3D shape functions, but the readers are invited to refer to the works [85, 86] for more details.

In the framework of FEM, it is possible to extend the models of Carrera's Unified Formulation to the modelling of generic curvilinear geometries by incorporating the CUF kinematic assumption and the FEM discretization in a unique 3D approximation, as follows:

$$\boldsymbol{u}^k(\alpha^1,\alpha^2,\alpha^3) = (F^k_\tau N_i)\boldsymbol{U}^k_{\tau i} = L^k_{\tau i}(\alpha^1,\alpha^2,\alpha^3)\boldsymbol{U}^k_{\tau i} \tag{4.4.24}$$

where $L^k_{\tau i}(\alpha^1,\alpha^2,\alpha^3) = (F_\tau N_i)$. In this expression, $L_{\tau i}$ represents a non-conventional 3D shape function in which the order of expansion can be different along one of the spatial directions. Similarly, the virtual variation δ of displacements, that will be used in the derivation of governing equations below, can be approximated by:

$$\delta\boldsymbol{u}^k = (F^k_s N_j)\delta\boldsymbol{U}^k_{sj} = L^k_{sj}(\alpha^1,\alpha^2,\alpha^3)\delta\boldsymbol{U}^k_{sj} \tag{4.4.25}$$

Considering this formalism, the volume integrals involved in the governing equations will not be split in 1D and 2D integrals as usual, but the functions $(N_i\,F_\tau)$ and $(N_j\,F_s)$ will be handled as regular 3D shape functions. The Jacobian matrix relative to the transformation from natural coordinates $\alpha^1,\alpha^2,\alpha^3$ to global coordinates x,y,z will be computed in 3D form. However, a formal separation of the coordinates as in Eq. 4.4.16 is still possible and the choice of the CUF/FE approximations follows the same principles, as in conventional shell elements based on CUF.

The results will demonstrate that this particular approach allow us to save degrees of freedom with respect to the use of meshes based on classical 3D finite elements. Indeed, conventional 3D elements employ the same order of expansion in the three spatial directions and this usually implies some limitations on the choice of the aspect ratio of the element by leading to a detrimental increase of the number of elements used.

The interpolation of solid geometry is easily accomplished using an isoparametric procedure. The position vector of the generic point P in the discretized domain is given by:

$$\boldsymbol{x}^k(\alpha^1,\alpha^2,\alpha^3) = L^k_{i\tau}(\alpha^1,\alpha^2,\alpha^3)\boldsymbol{x}^k_{i\tau} \tag{4.4.26}$$

where the Einstein notation has been adopted and a summation on the repeated index $i = 1, ..., n$ is implicit; n is the number of the nodes of the solid element. Hexahedral elements are considered in this work and L_i is the Lagrangian shape function corresponding to node i; $\boldsymbol{x}_{i\tau} = \{x^1_{i\tau}, x^2_{i\tau}, x^3_{i\tau}\}^T$ is the position vector for the node $i\tau$, corresponding to the nodal displacement $\boldsymbol{U}_{i\tau}$ in Eq.4.4.19. The basis of the Cartesian coordinate system, in which $\boldsymbol{x}_{i\tau}$ is defined, is given by the usual unit base vectors $(\boldsymbol{i_1}, \boldsymbol{i_2}, \boldsymbol{i_3})$. From this point on, the formulation of present shell elements follows the same derivation presented in [86] for 3D finite elements in curvilinear coordinates.

Note that, the number of degrees of freedom in these elements is not increased with respect to classical shell elements formulated in the framework of CUF [68, 69].

Procedure in MUL2

Unlike the previous additions, that usually require an enhancement in the formulation and small modification in the procedural part (e.g., the MUL2 code), this new formulation requires an important modification in the pre-processing part and in the matrix calculation. In particular, a main modification is implemented. Traditionally the calculation of the normal along the thickness was simply made on the first node of the shell element, because with plane element all the nodes of an element share the same normal. This is not true for a curvilinear element and it leads to an error in the generation of the through-the-thickness nodes and in a deformation of the 3D element.

In order to calculate the normal for each node we used the properties of the shape function N_i. The in-plane components of the normal $\bar{a}^l_1$ and $\bar{a}^l_2$ in a node can be calculated by the 2D shape function derivative and by the node's global coordinates $\bar{x}_i$:

$$\bar{a}^l_1 = \sum_{i=1}^{mn} \frac{\partial N_i(\xi_l, \eta_l)}{\partial \xi} \bar{x}_i \tag{4.4.27}$$

$$\bar{a}^l_2 = \sum_{i=1}^{mn} \frac{\partial N_i(\xi_l, \eta_l)}{\partial \eta} \bar{x}_i \tag{4.4.28}$$

then the normal along the thickness can be calculated as the cross product of the two in-plane components:

$$\bar{a}^l_3 = \frac{\bar{a}^l_1 \wedge \bar{a}^l_2}{\left\| \bar{a}^l_1 \wedge \bar{a}^l_2 \right\|} \tag{4.4.29}$$

where $\bar{a}^l_1$, $\bar{a}^l_2$ and $\bar{a}^l_3$ represent the normals with respect to $x - y - z$ respectively, $\bar{x}_i$ the vector of global coordinates of the nodes in each element and the partial derivative of the shape functions is performed with respect to the local coordinates ξ and η.

Validation

Two types of validations are carried out:

- the first one aims to validate the procedure of the normal calculation. Therefore, it is based on a simple model made of two Quad9 curvilinear elements. In this way, any procedural problem in the code is avoided in the FEM model validation;
- the second aims to validate the whole theory and it uses a cylindrical curvilinear shell, as a FEM model [84].

The cylindrical shell has the following characteristics:

- radius 1 m, height 2 m, thickness 1 cm;
- clamped on the two edges.

The materials are, as in the previous validation, an isotropic material (aluminium) and a multi-layer sandwich material composed by three layers:

- the top and the bottom faces are made by aluminum and 1 mm thick each;
- the core is made by Nomex and 8 mm thick ($E_1 = E_2 = 1.0\ MPa$, $E_3 = 0.255\ GPa$, $\nu_{12} = 0.49$, $\nu_{13} = \nu_{23} = 0.001$, $G_{12} = 0.1\ MPa$, $G_{13} = 37\ MPa$ and $G_{23} = 10\ MPa$).

The validation is performed comparing the first six modes of the shell with those calculated by Ansys. For the isotropic plate a comparison between a Quad9 ESL model in Ansys and a curvlinear Quad9 LW3 model in MUL2 is made. For the sandwich plate, the shell elements are not accurate enough for the ESL approach. Therefore, the shell is modelled by solid element in the plate core and shell elements on the faces, while for MUL2, a LW3 model for the core and a LW2 for the faces is applied.

The results in Tab. 4.9 are comparable for the isotropic plate. For the sandwich shell exploiting the CUF in Tab. 4.10, the accuracy is similar to those of a solid element. We must consider that for a small model, as the cylindrical shell used in the validation, we have a reduction in DoF from the solid element model (only in the core) to the LW model equal to the 70%.

Finally a coupled analysis is performed, it shows the correct fluid-structure interface performance, in particular there are not modification in interface and fluid part of the formulation or of the code.

Table 4.9: The first six natural frequencies $[Hz]$ for the cylindrical shell calculated exploiting the CUF-LW3 theory (MUL2) and an ESL one.

Mode	CUF-LW3 $[Hz]$	ESL $[Hz]$	Difference [%]
1	133.28	129.91	2.596
2	133.28	129.91	2.596
3	137.18	135.3	1.393
4	137.18	135.3	1.393
5	149.43	145.94	2.388
6	149.43	145.94	2.388

Table 4.10: The first six natural frequencies $[Hz]$ for the cylindrical multi-layer shell calculated exploiting the CUF theory (MUL2) and an ESL-3D one.

Mode	CUF-LW $[Hz]$	ESL-3D $[Hz]$	Difference [%]
1	8.15E+01	7.91E+01	3.048
2	8.15E+01	8.20E+01	0.572
3	8.58E+01	8.30E+01	3.344
4	8.58E+01	8.80E+01	2.469
5	8.89E+01	8.81E+01	0.965
6	8.89E+01	8.82E+01	0.841

Chapter 5

Case study: the windowless concept

5.1 Introduction to the concept

As short-medium air traffic increases, it is necessary to find designs and technologies that allow a reduction in fuel consumption, which leads to cut carbon dioxide emissions and aircraft operating costs. Among the parameters that influence the fuel consumption, the aircraft weight is one of the most important. In the design of the windowless concept, we develop previous researches and studies by the author. The conclusions of this new development are presented in the author's paper [24], based on previous works [88–90].

The main aim of windowless designs is the reduction in fuel consumption, starting with the reduction in weight of the aircraft. This weight reduction is directly related to the elimination of the windows and related reinforcements and, indirectly, it is given by the possibility of lightening other aircraft systems, such as landing gear, wing and rudder, control surfaces, etc. In addition, there could be an increase in the aircraft range and an improvement in its performances. The windowless concept is analysed in the literature for the three following applications:

- cockpit with windowless design [91, 92];
- windowless fuselage for all-wing or blended wing body aircraft [93, 94];
- windowless fuselage for conventional passenger aircraft.

The first type eliminates the cockpit windscreen and replaces it with monitors and 360° visual systems connected to sensors and cameras. These technologies are designed as a future development of ECVFIS (Enhanced Cockpit Visual and Flight Information System). This design, in addition to weight reduction, improves the distribution of pressure

on the aircraft nose and thus decreases the aerodynamic drag. There are also improvements from the safety point of view when dealing with bird strike. The second type consists in the use of monitors instead of windows in the passenger cabin of all-wing aircraft configurations where, due to the particular shape of the wing-fuselage structure it is impossible to have openings, limiting the development of this configuration for passenger transport. Finally, the last category, which is studied in this work, comprises passenger aircraft with traditional configurations in which the windows along the fuselage are removed (except those of the emergency exits) and are replaced inside by lateral internal monitors connected to external cameras, as shown in first prototype of "false window" by [90] in Fig. 5.1; this solution can overcome the issue of a possible sense of claustrophobia felt by passengers. This kind of windowless concept is very efficient and easier to realise with respect to the previous ones for the following reasons:

- it does not require a complete redesign of the passenger cabin and its electrical system;
- it can be directly designed and implemented on the design of existing cabins;
- it does not involve major changes in the interior appearance of the cabin, making passengers more comfortable with respect to the new aircraft and the new interior configuration;
- it can be a benchmark for a windowless concept extended to other configurations, as the previously cited [93] blended wing body concept or for stratospheric passenger vehicle, where the external vision is occluded, as those presented in project H2020 STRATOFLY [95][1] or for geodesic fuselage, where the dense structural net is unsuitable for windows [96].

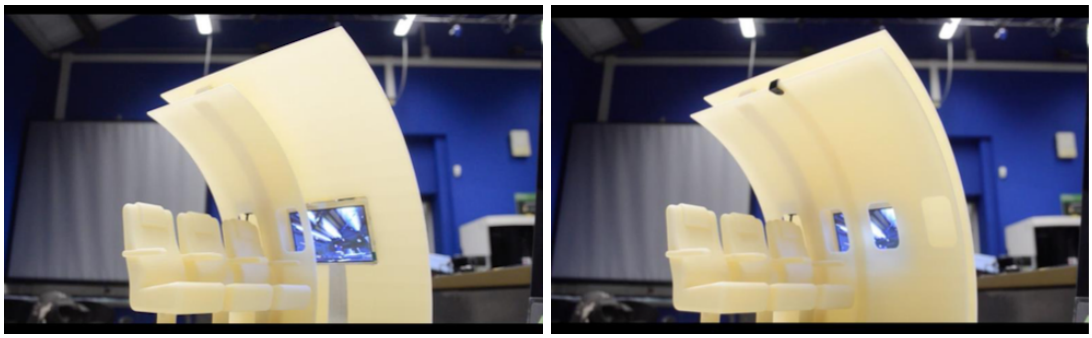

Figure 5.1: Physical scaled prototype for the windowless concept assessment in [90].

Furthermore, the monitors could be larger than the current aircraft windows, allowing an enlarged view of the outer space and creating a wider, albeit virtual, field of vision. We must also consider the lower production costs for a fuselage without windows and greater resistance to fatigue loads. Finally, it is important to emphasise that in recent

[1] `https://www.h2020-stratofly.eu/`

years, this configuration has been introduced to the general public through newspapers and magazines.[2,3]

5.2 Preliminary design

5.2.1 Weight estimation

In a preliminary design environment, the methodology in Fig. 5.2 is followed based on the survey in Section 2.3. The main advantage of this concept in design terms, is that it can be studied on existing aircraft, because it does not require a disruptive change in the configuration. Therefore, it is possible to start from an existing aircraft design and calculate the weight reduction from windows removal. The weight added by monitors and cameras, within the added weight to ”refill” the windows holes is considered too. The number and size of the windows depends on the aircraft model, usually bigger aircraft have more windows, as statistically reported in Section 2.3. In this concept we remove all the windows except those of emergency exit, which are separated by the fuselage structure, as the doors. Then, once the aircraft model is defined within the number and size of the windows, two parallel steps are performed:

- the estimation of windows reinforcements size and weight;
- the definition of the monitors and cameras data (number, model, position, etc).

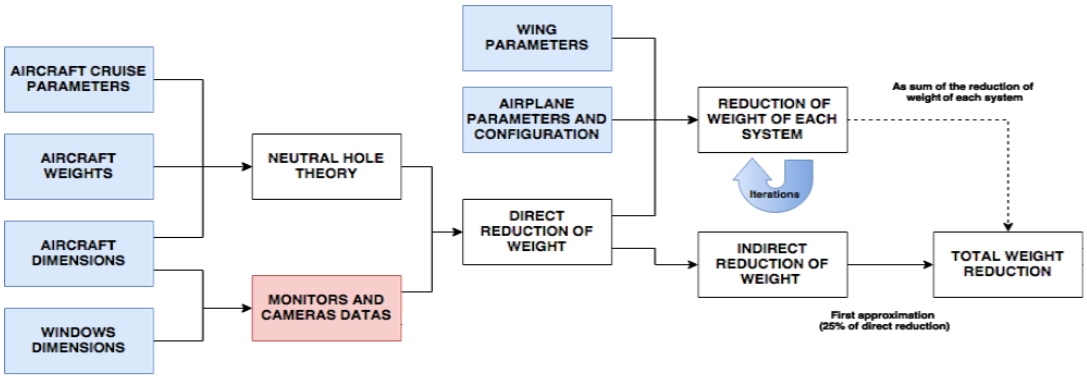

Figure 5.2: Methodology block diagram for the windowless concept analysis.

The first step is done with a simple assumption: weight reduction is the algebraic sum of the weight of the removed elements as panes, metal frames and longitudinal reinforcements, and of added elements, as the visual system and the alloy necessary to ”refill” the holes and the part of stringer that were absent due to the presence of the

[2] https://www.uk-cpi.com/windowless-plane

[3] https://edition.cnn.com/travel/article/maverick-project-rosen-aviation-windowless-cabin/index.html

windows in the traditional cabin. For the structural part, windows are openings on the fuselage skin and they weaken the structure and so the fuselage must be reinforced. The size of the reinforcements are not easy to find for every aircraft model, so a preliminary method is necessary to estimate it. The lack of information on the reinforcements makes it difficult (if not impossible) to create a numerical model of the fuselage. However, to the authors' knowledge, there are not more recent publications than that by Mansfield [97] based on the neutral hole theory to estimate the reinforcements size for a short-medium range aircraft. The main advantage of this theory is the method, which is based on analytical equations. The aluminium alloy of the added part of stringers and fuselage panels depends on the volume and on the material density. The same applies to windows, which are described according to Fig. 3.5 and usually made by Lexan and Plexiglas or other materials as tempered glass.

For the cameras and monitors weight, the fuselage is assumed completely covered by light and flexible monitors, as OLED (Organic Light Emitting Diode), and as shown in the "false windows" concept in Fig. 5.1. Therefore, the monitors number is function of the cabin length (without galleys, doors and toilets). The cameras must be able to capture a wide field of view in order to ensure the depth effect with the false windows design (that could also be mixed with other technologies as eye tracking systems). Taking into account the existing cameras characteristics, it is proposed to place two cameras for each window, as shown in Fig. 5.3. Therefore, the weight of monitors and cameras depends on their manufacturing features and their number.

Finally, the balance of weight to calculate the weight reduction ΔW is given by the following equation:

$$\Delta W = W_p + W_r + W_f - W_a - W_s - W_{mc} \tag{5.2.1}$$

where the terms of the algebraic sum are given in Tab. 5.1.

Table 5.1: The equations to estimate the weight reduction are given for an aircraft with a number of removed windows equal to N_w and a cabin length equal to L_c.

Component	Weight	Equation	Parameters	Geometrical size
Windows panes	W_p	$W_p = N_w \cdot A \cdot [\rho_{lex} \cdot (t_1 + t_2) + \rho_{plex} \cdot t_3]$	ρ_{lex} and ρ_{plex} are the density of Lexan and Plexiglass	A is the area of the windows, t the panes thickness.
Reinforcement belt	W_r	$W_r = 2 \cdot L_c \cdot (t_r - t) \cdot w \cdot \rho_a$	ρ_a is the alloy density	t_r and t are the reinforcement belt and fuselage thickness, w the reinforcement belt height.
Windows frames	W_f	$W_f = \sqrt{2} \cdot k \cdot A_0 \cdot b \cdot \rho_a \cdot N_w$	ρ_a is the alloy density	$k = a/b$ are the main and minor semi-axis of the windows, A_0 is the area of the compacted reinforcement in which the loads are maximum.
Fuselage "refill"	W_a	$W_a = A \cdot t \cdot \rho_a \cdot N_w$	ρ_a is the alloy density	A is the are of the windows, t the panes thickness
Stringers "refill"	W_s	$W_s = V_s \cdot \rho_a \cdot N_w$	ρ_a is the alloy density	V_s is the stringer removed volume
Monitors and cameras	W_{mc}	$W_{mc} = (W_m \cdot N_m + W_c \cdot N_c) \cdot X$	W_m and W_c are the weights of monitors and cameras with their number N_m and N_c, X is the coefficient for the weight of the cables	

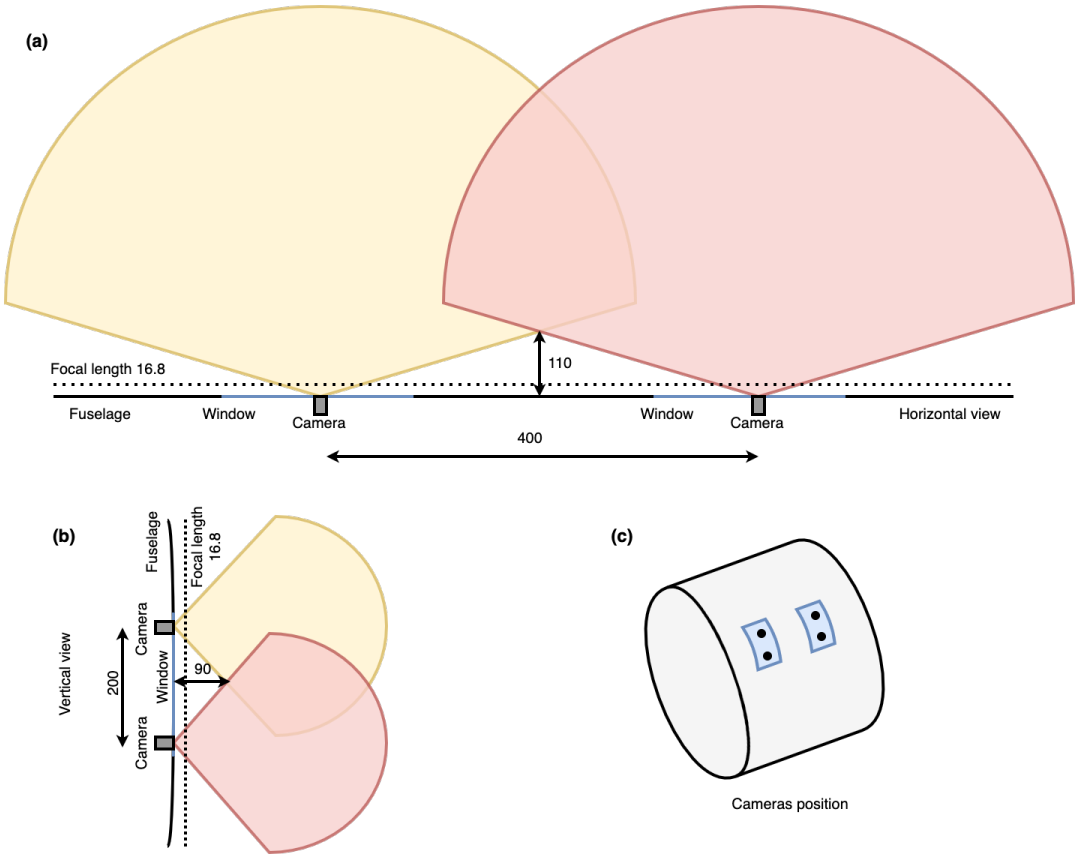

Figure 5.3: Camera position and FOV (Field Of View) [mm]. (a) Camera horizontal FOV. (b) Camera vertical FOV. (c) Camera position on the fuselage.

A reduction in the structural weight of the aircraft leads to a greater saving in the final weight: the so-called snowball effect, which in a very first approximation is assumed equal to the 25% of the original reduction. Therefore, a reduction of other system is calculated through classical method described in Section 2.2. We must understand which systems are lightened. In a preliminary design framework, a lighter aircraft will need less structure to hold the aircraft itself during the phases of flight and during on ground phases, and in particular a lighter wing and landing gear respectively. Moreover, the control surfaces have to be resized for smaller loads. The weights of these systems depend on the empty weight and other parameters as reported in Section 2.2.

5.2.2 Weight reduction

In order to study the weight reduction due to the exploitation of a windowless configuration, we apply the windowless concept to four existing aircraft for short and medium flights [24],[4] refining and enhancing the results previously calculated in [89, 90]. A previous work by the author studies the windowless concept for long-range aircraft [88].

[4]The concept was also proposed at *Tra Visions 2020* competition and presented in the top ten projects for its category `https://2020.travisions.eu/TRAVisions2020/`.

The results are presented for the following aircraft models produced by different industries:

- ATR72, a turboprop aircraft, produce by a joint venture between *Aérospatiale* (now Airbus) and *Aeritalia* (now Leonardo);
- E190, a turbofan aircraft by Embraer;
- A320, a turbofan aircraft by Airbus;
- B737, a turbofan aircraft by Boeing.

The main characteristics of these four aircraft are reported in Tab. 5.2 within the numbers of windows.

Table 5.2: Aircraft models data with windows.

	ATR72	E190	A320	B737
Take-off weight [kg]	22800	47790	73500	79015
Max. Range [km]	1528	4445	6100	7400
Cabin length [m]	19.21	25.76	27.51	29.27
Fuselage width [m]	2.77	3.01	3.95	3.76
Number of windows	54	50	76	80

All windows are removed, except those of the emergency exits, and replaced with 77" OLED screens (weight of 1.9 kg) connected with small external cameras (weight of 0.076 kg). The weight of the cables is conservatively considered the 30% of the weight of the visual system. The weight of this system is reported in Tab. 5.3 within the visual system data. The structural weight reduction (taking in account the monitors and cameras weight) and the total one, considering the reduction of other subsystems is reported in Fig 5.4. Despite the great number of windows and the longer passenger cabin, the B737 presents a lower reduction in weight than the A320, because it has a narrower fuselage, which is the most influencing parameter. The results are more predictable for the ATR and the Embraer models, that are smaller than the Boeing and the Airbus models. As expected, the bigger it is the aircraft the higher is the advantage provided by a windowless configuration.

Table 5.3: Data of the visual system needed to replace the windows.

	ATR72	E190	A320	B737
Number of monitors	20	24	32	34
Number of cameras	108	100	152	168
Visual system weight [kg]	60.1	69.5	94.6	100.6

Finally, a general method for a preliminary estimation of the windowless configuration weight reduction is derived. Firstly, it is possible to estimate the number of windows

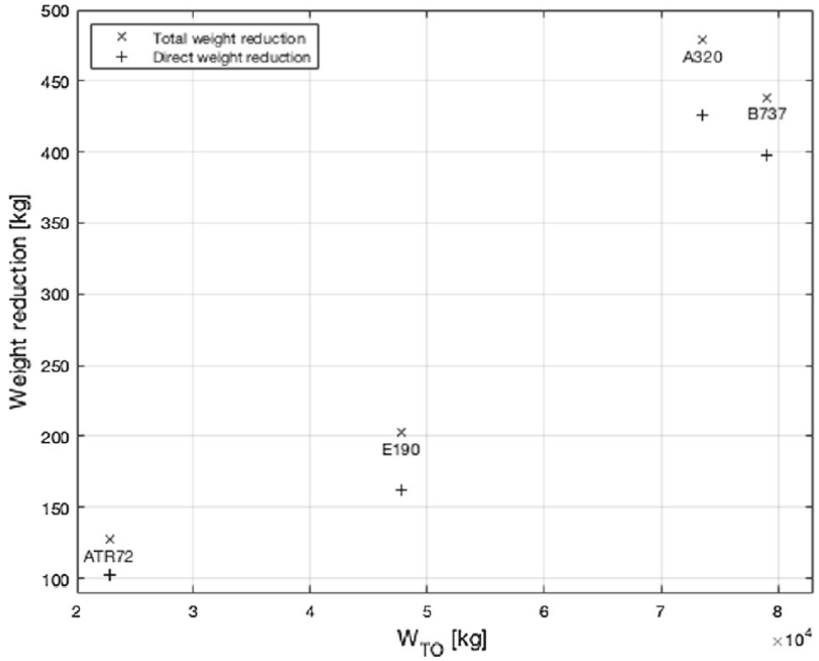

Figure 5.4: Weight reduction, structural and total, for a windowless configuration, for the four different aircraft models, as a function of their maximum take-off weight W_{TO}.

N_w, to have an idea of how many windows are going to be replaced. A simple equation solve this task:

$$N_w = 2\,\frac{L_c - L_e}{d_w} \tag{5.2.2}$$

where L_e is the "empty" cabin length without windows, so occupied by toilets, galleys, wardrobes, emergency exits, and doors. The L_e value can be estimated from the toilets, galleys, wardrobes, emergency exits, and doors lengths, and for short-medium range aircraft is between 4 m and 5 m. The parameter d_w is the space between each window, in a very first approximation can be equal to 0.5 m. In order to calculate the total weight reduction ΔW due to the exploitation of a windowless fuselage, the previous equations, as Eq. 5.2.1, those in Tab. 5.1 and those from [97], are used. Therefore, we obtain a correlation function between the cabin size (length and width) and the weight reduction $\Delta W = f\,(L_c, d_c)$. A general results for the structural weight reduction for a windowless configuration as function of the number of windows (and so according to Eq. 5.2.2 to the cabin length), for different cabin widths, is reported in Fig 5.5. These results are obtained for different fuselages, according to the survey performed in Section 2.3.

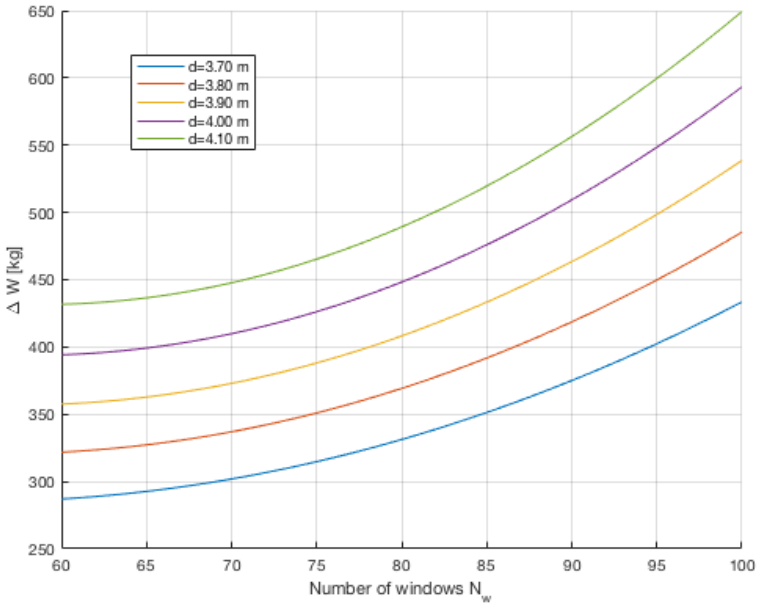

Figure 5.5: The weight reduction ΔW as function of the removed windows N_w, and so according to Eq. 5.2.2 of the fuselage length, for different fuselage diameters.

5.3 Noise assessment

5.3.1 Introduction

As described in Chapter 1, sustainability refers to the environment and economic, in the last years the economic sustainability has been extended to human sustainability, including comfort. Therefore, an important aspect to consider when dealing with comfort is the noise level, in particular in aircraft, which are traditionally noisy. In Section 5.2 the weight reduction assessment method is defined for the windowless configuration. In this one, we built the noises assessment method. In particular, we focus on low frequency noise, which is traditionally difficult to stop with conventional materials or solutions.

5.3.2 Vibro-acoustic model

In order to study the N&V spread in passenger cabin, we exploit two different models of aircraft, a first one enhanced starting from the CASTLE consortium [50] and a second one in collaboration with DLR. As described in Chapter 3, the three main issues in numerical model are the accuracy, the computational cost and maximum frequency. These three elements are deeply linked and two different trade-offs are performed.

Turboprop aircraft from CASTLE project

The first model is defined in the author's works [98, 99] and based on a preliminary work in [100]. This model starts from the CASTLE FEM model of a fuselage barrel of a turboprop aircraft, as briefly described in Section 3.5.2. The choice for a turboprop aircraft falls within the types of aircraft for which the windowless concept is conceived. The model is developed in Actran.

From a physical point of view the turboprop high-wing aircraft fuselage is a 20 m cylindrical barrel, with an external diameter of 3.45 m and a passenger cabin height of 2.26 m. The model is composed by the following components:

- the fuselage structures (panels, stringers, frames, deck panels and support). Each one of these elements is modeled in a monolithic way and connections between them are built at node level;
- the windows and their reinforcements (the windows belts and frames), in particular for windows a multi-layer panes is used to simulate the different materials, the air gap is neglected. Moreover, the aircraft doors are modelled too;
- the cabin interiors as the lining panel, the seats and the luggage compartments;
- the acoustic cavities;
- the bulkhead frames for the imposition of the boundary conditions;
- the fluid-structure interfaces, which are manually generated.

The structural elements and the windows are modelled in a classical way: shell elements for the panels and beam elements for the stringers and frames. In particular for the panels, any local modes is neglected. The cabin interiors require a different formulation due to their characteristics:

- the lining panel is a sandwich plate made of fiberglass and Nomex. The trim panel core (Nomex with a density equal to 48 kg/m^3) has a thickness of 6 mm, while the fiberglass plates (density equal to 1940 kg/m^3) have a thickness of 0.48 mm each, with a single layer thickness of 0.24 mm and an orientation of the fibers equal to 0° and 90°. In order to capture the complex kinematic behaviour of the plate, the Nomex core is modelled with solid elements, while the faces with shell elements. This choice greatly increases the number of DoF and so the computational cost of the problem. The panels are connected to the fuselage and the floor through beam elements, that roughly simulate the rivets and the shock absorbers;
- the seats are modelled as a solid volume, on which a non-normalized impedance boundary condition is imposed, similar to the method in [44]. The impedance

frequency dependant values are given by the producer, the Geven company[5] and reported in Fig. 5.6. The seats supports and masses are neglected. The passenger cabin includes eighteen rows with five seats each and an aisle between them;

- the overhead compartments are two monolithic components (one per side), modelled with shell elements and made of a plastic isotropic material.

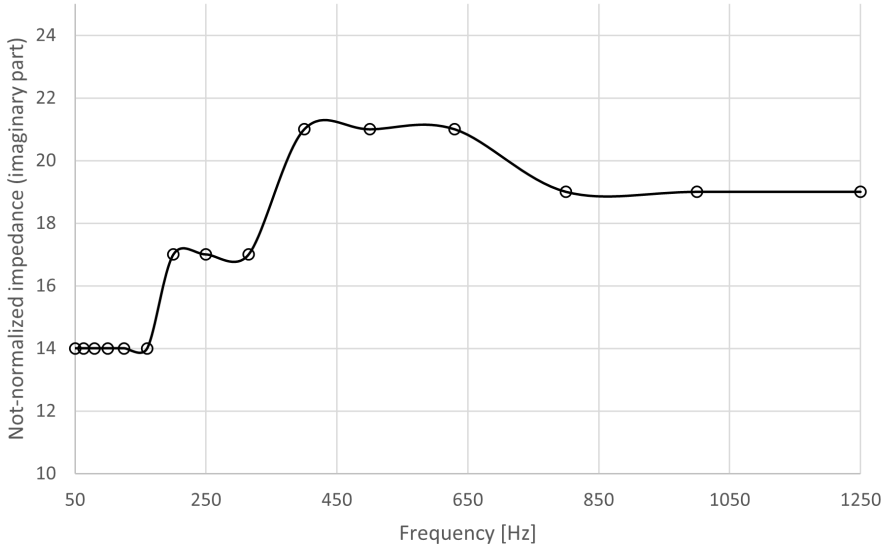

Figure 5.6: The frequency dependant imaginary impedance values applied to the seats volume.

The acoustic cavities (passenger cabin, cargo hold, the gap between the fuselage skin and the lining panel and the two volumes inside the luggage compartments) exploit solid elements and non-homogeneous interfaces is created between them and the structural components. Finally, a frame around the bulkhead positions is created to fix the model with clamped boundary conditions on the edges. The bulkhead panels are not considered and a wall boundary condition is automatically imposed on the cavities edges in the numerical model. A summary of the elements of the numerical model is reported in Tab. 5.4. The size of the elements is derived according to Appendix A for a maximum frequency of 300 Hz. A general view of the FEM fuselage in Actran is given in Fig. 5.7. A modal validation of the fuselage structure was already performed by [50], although it was not possible to validate the new model due to the absence of experimental data or literature results. Therefore, only local convergence tests are carried on, which are in accordance with the elements size criterion in [101, 102].

Once the model is defined, the acoustic excitation must be selected, in particular we choose to evaluate both external and internal sources.

For the external source, a predominant contribution is given by the propellers, their contribution was calculated in the CASTLE framework by CIRA in [50]. The calculated

[5] `https://www.geven.com/`

loads represent the complex pressure field generated at Blade Passage Frequency (BPF) by two 8-blades propellers rotating clockwise with 20 degrees relative phase angle in the first three harmonics, that occur at 100 Hz, 200 Hz and 300 Hz according to the number of blades and propeller rotational per minute (RPM) at cruise velocity (provided by LNDVEL). The aerodynamic pressure has been calculated using Blade Element Momentum Theory (BEMT) and consequently, from the aerodynamic pressure, the acoustic pressure distribution over the fuselage external skin has been computed through a FW-H (Ffowcs Williams and Hawkings) approach. The pressure field at 100 Hz is reported in Fig. 5.8. Therefore, for an external source the analysis is performed at the three harmonic frequencies.

For the internal source, at the author's knowledge, no information from literature is available except the test campaign in the work by Hu et al. [36], that is not exportable to the numerical model as a source. Therefore, a generic spherical source, a monopole with a constant amplitude, is placed in the centre of passenger cabin. The aim is to study the noise spread from a position inside the passenger cabin and the system absorption properties and not the transmission loss from an external source, where the acoustic wave travel through the panels of the fuselage and of the cabin. There are no limitation on the frequency range from the source, so the analysis is performed from 1 Hz to 300 Hz.

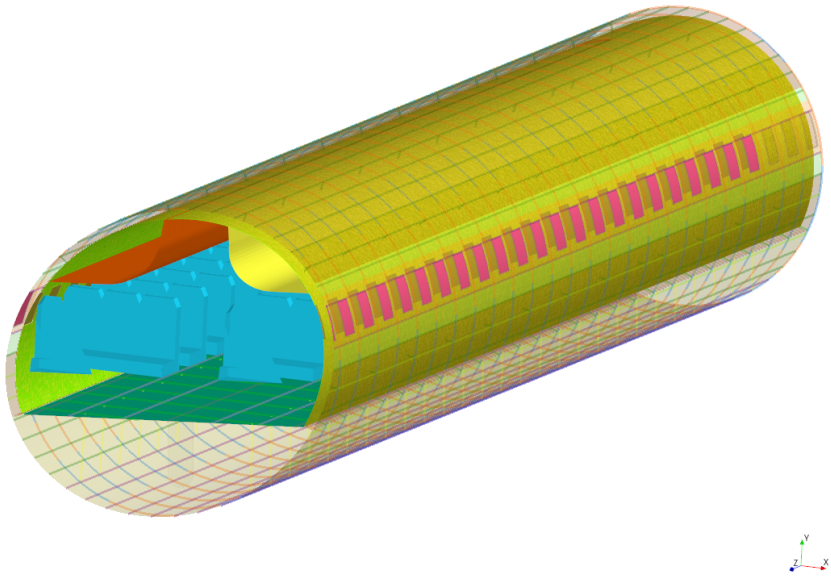

Figure 5.7: The FEM model of the fuselage in Actran: the passenger cabin components are visible, as seats, luggage compartments and lining panel, within windows.

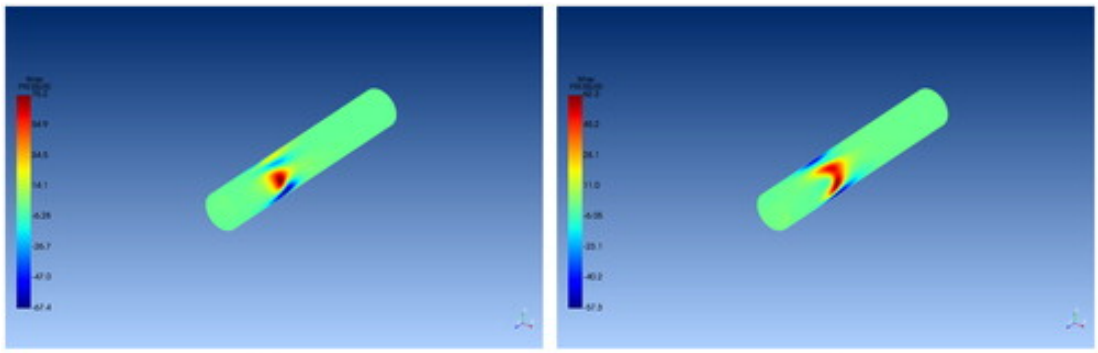

Figure 5.8: The complex pressure field $[Pa]$ around the fuselage generated by the propellers at the first harmonic frequency, 100 Hz, as expected there is an increase in the load near the propellers positions. (a) Real part. (b) Imaginary part.

The CPACS based fuselage barrel

In order to test the proposed noise reduction solutions in Section 5.4, a generic windowless fuselage barrel for short-medium range turbofan aircraft is built. The model is defined through CPACS in XML files (see Section 2.4.2). This model has an high degree of accuracy in the components description; however some components are missing. Moreover, while the previous model was built in a traditional way, from geometry file to the FEM mesh, the current one is generated from the CPACS file as described by Walther et al. [30]. This new process is very reliable and flexible and allows to have a standard description of fuselage for data exchange or MDO. Therefore, the FEM model is built in Ansys, from the XML and geometry files. The CPACS files contain information on the components materials, sizes and connections. In particular the FEM generation is partially automatized through a Python script. Ansys is chosen as software because the automatic fluid-structure interface generation simplifies the pre-processing operations in a complex and irregular structure.

The model is a fuselage barrel of 8 m length and a radius of 2 m. The fuselage sizes are equal to those in the Airbus's Acoustic Lab in Hamburg.[6] The model, according to the CPACS definition, is divided in a primary structure, and a secondary structure. Moreover, the acoustic cavities are defined too.

The primary structure was partially validated for very low frequencies in previous studies comparing the modal response to experimental one from the Acoustic Lab. The structure includes the fuselage skin, the frames and stringers, the deck panels and supports, the cargo hold deck and supports, and the connections between the components (e.g., the rivets). In this case each component is independent and linked to others through rivets and contacts (e.g., an impenetrability condition), that transmit the energy from a component to an other. The fuselage is windowless.

[6] `https://zal.aero/en/innovation-rt/infrastructure/`

The secondary structure is very detailed and represents the cabin skin. It includes the lining panels as described in Fig. 3.2. Therefore, there are the sidewall panels, with a recess to accommodate the passenger shoulder, the cow panels above the passenger head, the dado panels at foot height, and the ceiling panels. Moreover, the overhead luggage compartments are included too. As for the primary structures, these components are independently defined and connected.

The mesh is automatically built from the criterion in Appendix A for a maximum frequency of 250 Hz. The whole structural model is made by two dimensional elements. In particular from the previous validation, the use of beam elements in the frames and stringers is discarded, because they lead to a numerical increase in the stiffness of the system. Moreover, the lining panels are modelled with two dimensional elements for computational reason, in fact the FEM model is already very computationally heavy and with solid element in the panel core it would be unsolvable. Rivets and shock absorbers are modelled with Ansys connections elements (MPC184 and COMBI250)[7] defined by their stiffness. In particular it is possible to have an high degree of accuracy in the connection definition of the secondary structure thanks to study of the aircraft fuselage itself at DLR in Hamburg. In particular, we can define three classes of connections:

- primary structure rivets, they connect the primary structure elements and have an high stiffness. Their properties and position depends on the fuselage barrel in the Acoustic Lab;
- secondary structure connections, that fix the overhead luggage compartment to the primary structure, in particular to the frames. These connections are rigid beams and have to hold the luggage compartments in position, their stiffness is still high due to the luggage compartments weight and loads;
- shock absorbers, their characteristic and size are given in Appendix C. These components have to absorb vibrations from the primary structure and also from the independent frequency response of the panels. They connect the cabin panels to stringers and frames of the fuselage. Their properties are derived from Appendix C. However, no damping information is available, as for other connection elements. Therefore, a value equal to the 1% of the stiffness can be used as a first try.

Acoustic cavities are always modelled by solid elements and Ansys automatically creates fluid-structure interfaces. In this model there are ten cavities as shown in Fig. 5.9:

- the passenger cabin cavity;

[7] See the Ansys user's manual for the elements formulation.

- the cargo hold cavity, which include the the gap between the lining panels and the fuselage skin;
- eight cavities (four per side) for eight overhead luggage compartments.

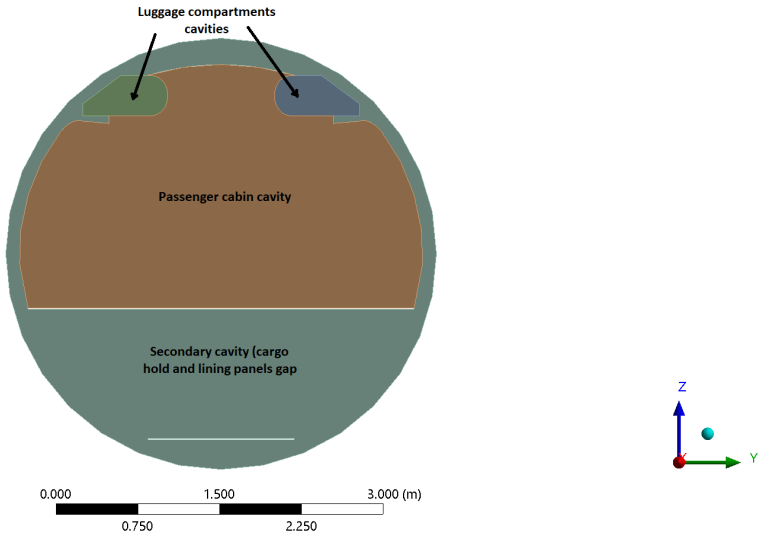

Figure 5.9: The acoustic cavities of the Ansys model, where there is no separation from the cargo hold and the gap between the fuselage and the passenger cabin, unlike the model in Actran. Moreover, the luggage compartments cavities are separated for each compartment (four per side).

A summary on the type of elements is reported in Tab. 5.4. comparing them with the elements of the previous FEM model from CASTLE project. The rendering of the model is reported in Fig. 5.10.

Table 5.4: The elements dimension and the materials type for each components of the FEM model in Actran and the model in Ansys based on CPACS.

	Actran model		Ansys model	
Component	Element dimension	Material type	Element dimension	Material type
Fuselage skin	2D	Orthotropic	2D	Isotropic
Frames and stringers	1D	Orthotropic	2D	Isotropic
Windows reinforcements	1D/2D	Orthotropic	-	-
Windows	2D	Multi-layer	-	-
Decks	2D	Orthotropic	2D	Multi-layer
Decks supports	1D	Orthotropic	2D	Isotropic
Rivets	1D (partial)	Isotropic	1D	COMBI250/MPC184
Shock absorbers	-	-	1D	COMBI250/MPC184
Lining panels	2D and 3D core	Multi-layer	2D	Multi-layer
Luggage compartments	2D	Isotropic	2D	Multi-layer
Seats	3D (as BC)	Impedance	-	-
Acoustic cavities	3D	Fluid	3D	Fluid
Fluid-structure interfaces	2D	-	2D	-

The material applied to the primary structure is aluminium (according to the real fuselage barrel) and a composite material based on CFRP for the deck and cargo hold

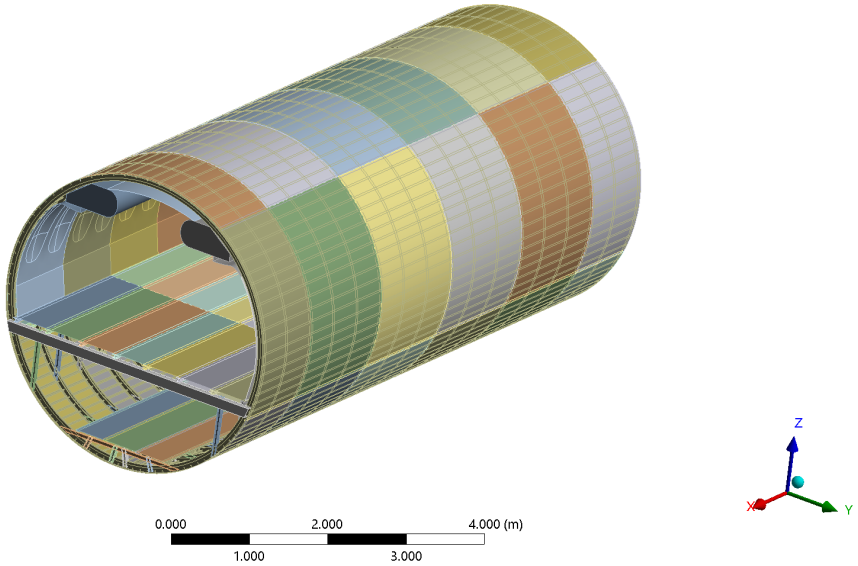

Figure 5.10: The FEM model of the fuselage structure derived from CPACS. The different colors show the several single components of the model.

floors. The secondary structure materials depend on the panels, but in general their are composed by rigid material as fiberglass with a low density core, similarly to the lining panel in the previous FEM model (fiberglass and Nomex). These values are given by DLR and stored in CPACS.

The acoustic sources are not available for this fuselage and a random pressure is applied on the external panels of the barrel.

Strengths and weaknesses of the two FEM models

As summarized in Fig. 3.8, the main trade-off in a vibro-acoustic FEM model is between the number of DoF and the computational cost. The CASTLE and CPACS based models have the following main differences:

- the maximum frequency obtainable from the mesh (300 Hz for the former and 250 Hz for the latter);
- the description of the lining panels, on one hand the CASLTE based model exploits solid elements for the core of the sandwich panel, while the other uses shell elements, with a probable reduction in the accuracy. On the other hand, the CASTLE model consumes a lot of DoF in the core description. Moreover, in this model, the local modes of each panels are not considered
- the definition of the components connections. In the CASLTE model, only few necessary connections are created between the lining panel and the fuselage. However, the main components have a monolithic description and connection between

different components are solved merging the nodes. In the CPACS based model, the connections are accurately assessed and so there is a correct and realistic description of the local modes and of the energy transfer between different components. The presence of thousands of rivets and shock absorbers lead to an increase in complexity of the problem and number of DoF;

- the passenger cabin components. The CASTLE FEM model is derived from a design process for a defined aircraft, so more information are available on the interior materials, from Geven, an industrial partner inside the CASTLE consortium. Therefore, it has been possible to model the seats. Moreover, for the windows, in the CPACS based model, due to the high degree of precision in the connections, at this point, it is not possible to correctly model the windows, because there is a lack of information on them and on their reinforcements. Therefore, only the windowless fuselage is studied.

Other two points, that are not related to the DoF trade-off, must be taken in account:

- the CASTLE model has a real source definition for low frequencies;
- the CPACS based model has been developed in the framework of CPACS for future developments, optimizations or MDO processes.

5.3.3 Windowless configuration in acoustics

The windowless configuration is not designed as a noise reduction solution. However windows are hole in the fuselage, so they change the vibro-acoustic behaviour of the structure. The windows influence is more important at high frequency as studied in [50]. A preliminary study is performed on simple plate-cavity model, in order to understand the windows material frequency response compared to the one of a classical aluminum fuselage. In Fig. 5.11 the frequency response in Pascal is obtained with a LW approach, the two curves have a similar average behavior and so we do not expect a significant change at low frequency in the noise inside the cabin from a traditional configuration to a windowless one. It is important to underline that we are considering the windows built as in the CASTLE model, so without the air gap between the panes.

On the CASTLE based model two analyses are performed:

- definition of the baseline configuration for the three harmonic frequencies (100 Hz, 200 Hz and 300 Hz);
- evaluation of the noise spread in the cabin applying a windowless configuration for the three harmonic frequencies.

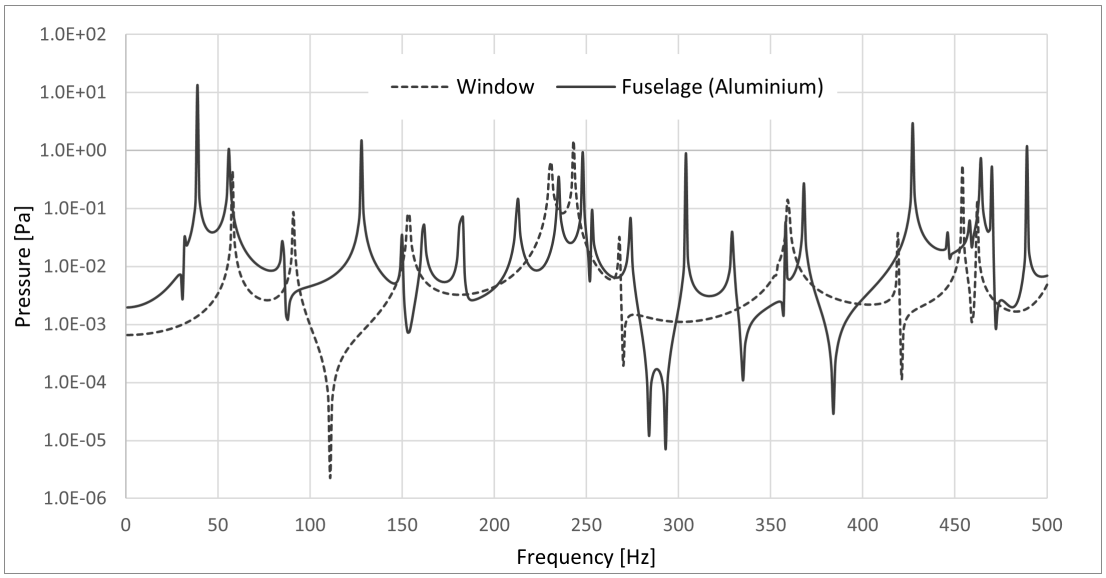

Figure 5.11: The frequency response of a cavity coupled to a plate obtained with the CUF-LW approach. The aim is to compare the fuselage material response and windows materials in the low frequency range.

The results are calculated in terms of SPL at the positions of the seated passenger's heads (1.20 m from the floor). Moreover, the OASPL is calculated on the frequency range. Finally, the A filter (dBA) is chosen to take in account the human ear sensibility.

The multifrontal massively parallel solver (MUMPS) in Actran has been chosen to find the solution of direct frequency response. This solver is based on well-known LU decomposition of an algebraic system:

$$\boldsymbol{Z}x = \boldsymbol{B} \tag{5.3.1}$$

and it assembles $\boldsymbol{Z}$ matrix and then factorizes it to find the lower $\boldsymbol{L}$ and upper $\boldsymbol{U}$ matrix:

$$\boldsymbol{Z} = \boldsymbol{LU} \tag{5.3.2}$$

This solver has been preferred to KRYLOV solver which works better with materials and boundary conditions that have a simple relation with the frequency. Unconventional materials or impedance boundary conditions, have instead frequency dependant properties.[8]

The pressure maps in terms of SPL are completely reported in the author's works [98, 99]. In this thesis, the OASPL maps for each analysis on the measured positions are reported.

The OASPL on the three frequencies is equal to 87.76 dBA for the baseline configuration with windows. At low frequencies, the exploitation of a windowless configuration does

[8]See Actran 20 Users Guide.

not lead to a reduction in the noise. Indeed, the OASPL increases of 0.10 dBA, by almost 0.11% (the absolute value is equal to 87.86 dBA). This result is quite predictable according to Fig. 5.11, where the average frequency responses of the fuselage material and the one of the windows are very similar. The pressure maps are reported in Fig. 5.18(a) and (b) respectively.

Therefore, the windowless configuration does not show any advantage in noise reduction at low frequency. Another noise reduction solution must be found and studied.

5.4 Noise reduction solution

5.4.1 Introduction

In order to improve the acoustic comfort in the passenger cabin, a noise reduction solution must be exploited. In this work, we focus on low frequency noise and on two noise reduction solutions. The two main factors to consider during the solution design are:

- the transmission loss (or the noise reduction) over the frequency spectrum;
- the weight (and if it is relevant, the volume), because an increase in weight with respect to the baseline aircraft is not desirable.

Other factors are the regulations, the production phase and precision, within the sustainability of the solution.

Two main solutions are studied for low frequencies: the exploitation of two different acoustic metamaterials in the passenger cabin lining panel in order to obtain high level of absorption;

5.4.2 Acoustic metamaterials (AMM)

The design and study of an insulating material is performed according to this process:

- design of the material;
- high accuracy analysis by a CUF-LW approach in MUL2, as described in Section 4.4, in order to understand the complex kinematic behaviour of the material, in particular for sandwich plate. If necessary, an homogenizing process is performed;
- application (if it is possible) of the new acoustic solution in the fuselage FEM model described in Section 5.3.2 in order to understand its behaviour in the complex fuselage environment.

In an acoustic metamaterials (AMMs), as briefly described in Section 3.5.2, it is possible to manipulate the acoustic behavior, resulting in negative effective mass density and negative effective bulk modulus based on localized resonance mechanisms and dispersion properties [103]. Furthermore AMMs, due to negative mass density, demonstrate excellent performances at low frequencies. These materials have properties "beyond" those of conventional materials. They are artificial structures with periodically or non-periodically arranged sub-wavelength elements. The acoustics properties of these materials, as the density and bulk modulus, can be influenced through inclusions artificially fabricated in a specified host medium or surface. Therefore, an AMM is usually made by a series of inclusions and a host. The elementary cell of the AMM is called meta-atom.

From the properties of the host and of the inclusions, it is possible to obtain the properties of the AMM as a function of frequency (for example the effective mass density and the bulk modulus). Conceptually it is a similar process to those applied for composite materials. The homogenization is necessary, because it is numerically impossible to model the meta-atoms in a macro-structure (as a fuselage) without exceeding in the computational cost. Homogenization has two important hypotheses that could lead to errors or differences between numerical analyses and experiments (for example in the anechoic chamber or in the impedance tube):

- the AMM plate is infinitely extended;
- for a periodic AMM, the meta-atoms are perfectly replicated in all the AMM.

A sketch of the AMM structure and homogenization is reported in Fig. 5.12.[9]

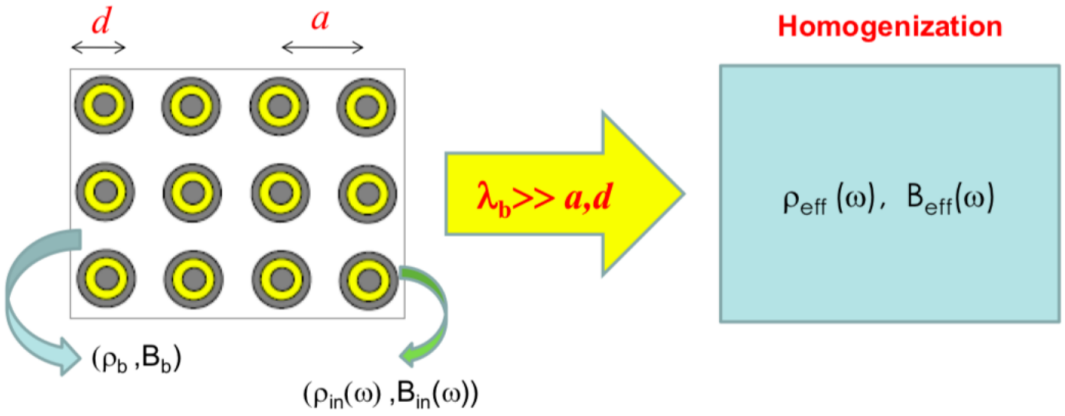

Figure 5.12: The structure of a periodic AMM with inclusions embedded in a host. The two materials have very different properties (as density ρ and compressibility bulk modulus B). The homogenized material has effective properties which are frequency dependant. Two important parameters of the AMM are the inclusions size and position.

In this work, two AMMs are considered, the first one come from the CASTLE project and it was studied and homogenized with a CUF approach by Cinefra et al. [51].

[9] From the presentation *Review on acoustic metamaterials* of Josè Sanchez-Dehesa.

The material is made of a melamine foam with aluminium cylindrical inclusions, as reported in Fig. 5.13. The sample consists in a melamine foam plate, pierced with aluminium inclusions, and a composite material skin in order to increase mechanical strength and protect the material, such as in sandwich plate. The advantages of using melamine (formaldehydemelamine-sodium bi-sulfite copolymer) are high sound absorption capability, low weight, good thermal insulation properties, and flexibility at very low temperatures; moreover, this material is fireproof. Aluminum is used because of its proven efficiency in aeronautics. The results from FEM analysis in [51], for the transmission loss are reported in Fig. 5.14 and show for the sandwich panel, a high TL in the low frequency range, compared to classical material for the lining panel as Nomex. The homogenized properties of the material in [51] are frequency dependant and complex, as an example the complex Young's modulus in the direction 11 is reported in Fig. 5.15 (refer to Fig. 5.13 for the reference system). An important factor in this material is the density, which is equal to those of Nomex (e.g. 48 kg/m^3) to not increase the aircraft weight. In particular, this result has been obtained refining the volume fraction (the ratio between the volume occupied by the inclusions and the host) up to the value of 0.015. The previous results are also confirmed by CUF in MUL2 thanks to modification in Section 4.4.

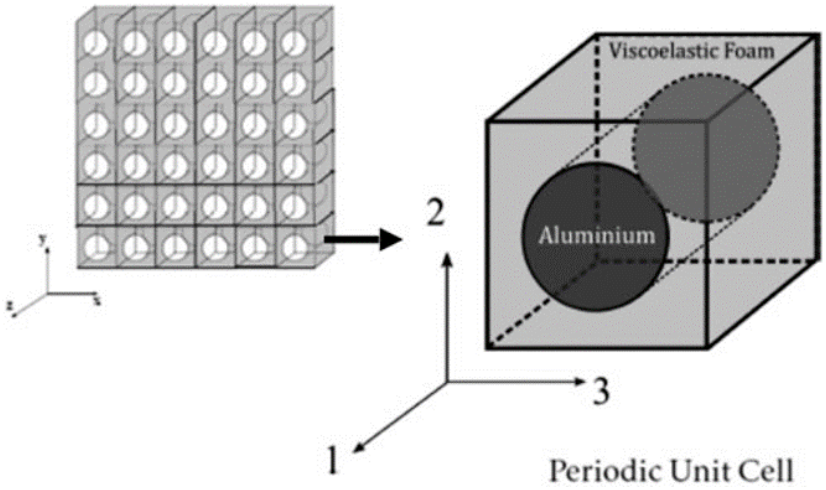

Figure 5.13: The AMM designed in [51], composed by a melamine foam (the visco-elastic foam) and aluminium cylindrical inclusions.

The second material is a micro-perforated sandwich panel, Fig. 5.16, in an additive material, preliminary studied in the author's work [104], and produced and designed from a literature case study by Nunes et al. [105]. The additive manufacturing allows an high accuracy in the production of a material with periodic meta-atoms. The mismatch between theoretical AMM and real produced one, usually leads to important differences in the numerical and experimental results. The aim of this AMM is to achieve high performances below 2000 Hz. Some geometrical parameters, such as perforation ratio and diameter of holes, are considered to realize different models and see the differences in

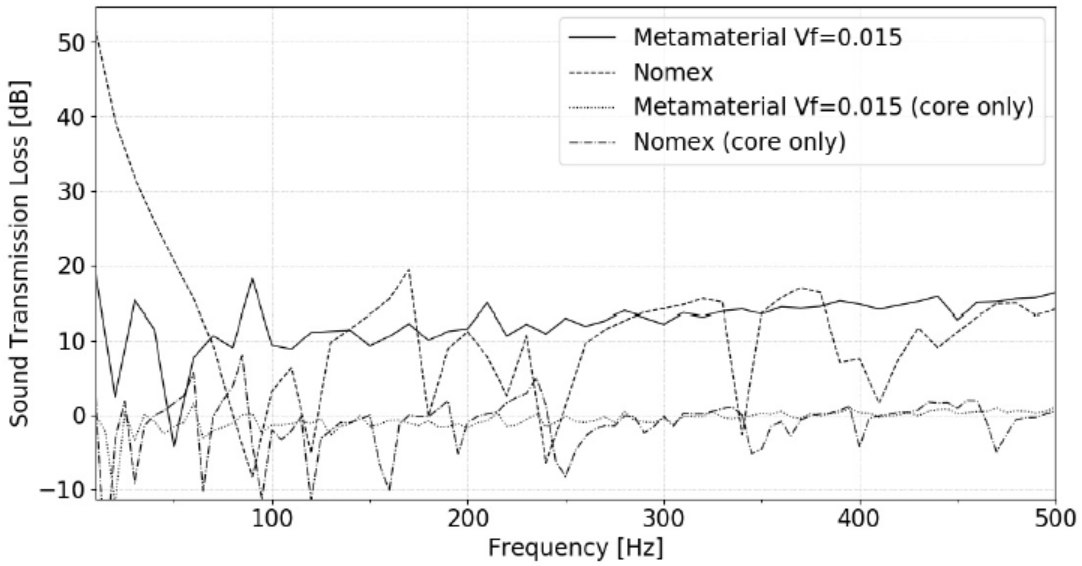

Figure 5.14: The TL of the AMM in [64] with a volume fraction equal to 0.015, both for only the core and the sandwich panel, compared to those of the classical lining panel material, Nomex, both alone and in the sandwich panel.

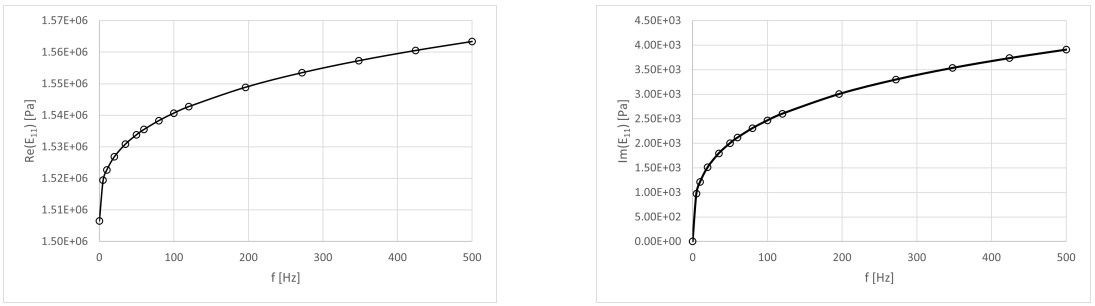

(a) **(b)**

Figure 5.15: The Young's module $[Pa]$ for direction 11 of the first AMM as function of the frequency $[Hz]$. (a) The real part. (b) The imaginary part.

the sound transmission loss. The models are produced by means of Fused Deposition Modelling using an Acrylonitrile Butadiene Styrene (ABS Plus p430) material on a commercial additive manufacturing system. The design process of this AMM is performed in two main steps:

- definition of the mechanical and acoustic properties of the additive material (ABS Plus p430), in the author's works [104, 106], performed in the prototyping laboratory of the *Università di Bologna*;
- design and study of the AMM [104].[10]

In the first step, the mechanical properties of the prototype material are derived through

[10] A final paper on this AMM is under production, for further information see `https://amslaurea.unibo.it/25941/`.

a test campaign. In fact, the nominal raw material data sheets are not reliable for after printing sample, whose mechanical properties depend on several manufacturing parameters. An extensive test campaign is performed in [106] on several samples to evaluate the influence of two different parameters: layer thickness and part interior density. Uni-axial tension tests and quasi-static tests are used to evaluate the material response to static and quasi-static loading and compressive properties. The tests are performed with a universal testing machine. Thanks to this work and the work by Rezayat et al. [107], the mechanical properties of the material are derived. The AMM made of this material is studied for different configurations, in particular the design parameter is the perforation ratio, which evaluates the number and the size of the hole on the plates. The materials is studied using the CUF approach in MUL2, thanks to the enhancement presented in Section 4.4. The AMM best design shows an higher value of TL between 1000 Hz and 2000 Hz as reported in Fig. 5.17, so outside the low frequency range. The density is equal to 1040 kg/m^3, but it would not require the fiberglass faces, having a better mechanical resistance than the previous AMM. A better TL at low frequency could be reach with a foam or a glass wool inside the cavities, although this will lead to an increase in weight.

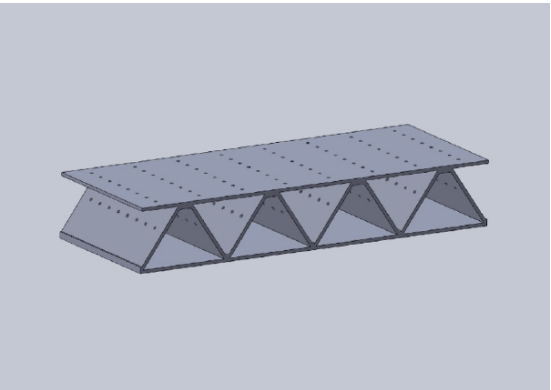

Figure 5.16: The model of the second AMM produced by additive manufacturing, a double perforated plate. The design parameters are the holes position and size.

5.4.3 Results

The noise assessment is reported for the two different numerical models, the former built from the CASTLE project and developed in Actran, the latter created from DLR and based on CPACS and developed in Ansys.

CASTLE Project based FEM model

On the CASTLE based model as defined in Section 5.3.3, the noise reduction solutions are studied in the following cases:

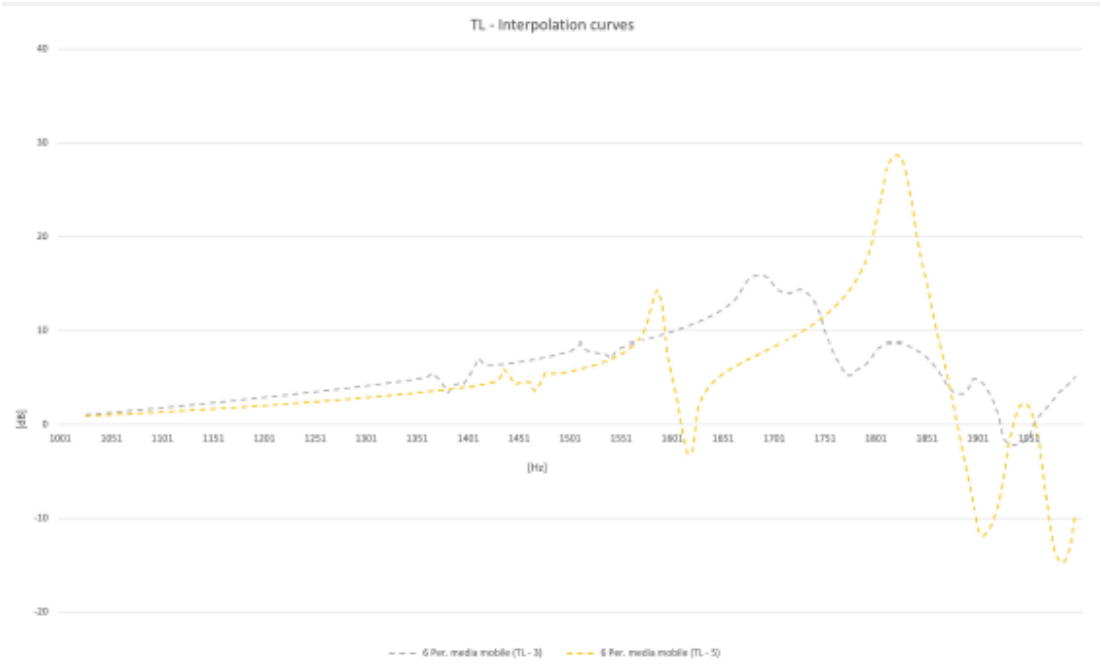

Figure 5.17: The TL for two design of the AMM. In this case, the TLs given by a different perforation ratios are analyzed. Increasing the perforation ratio, the overall TL shift its peaks towards lower frequencies; while on the opposite the increment of the hole diameter shifted the peaks towards higher frequencies. In addition, as predictable higher values of perforation ratio and diameter of the holes produced an increase in the TL.

- evaluation of the noise reduction applying an AMM by [51] in the cabin lining panel for the three harmonic frequencies on windowed fuselage;
- evaluation of the noise spread in the cabin applying a windowless configuration and an AMM in the lining panel for the three harmonic frequencies;
- definition of the baseline configuration for a monopolar internal source (from 1 Hz to 300 Hz);
- evaluation of the noise reduction applying an AMM by [51] in the cabin lining panel for a monopolar internal source (from 1 Hz to 300 Hz).

The OASPL on the three frequencies is equal to 87.76 dBA for a lining panel made of Nomex as calculated in Section 5.3.3, and it is equal to 81.60 dBA for a lining made of AMM [51]. The OASPL, for a windowless aircraft, on the three frequencies is equal to 87.85 dBA for Nomex, and it is equal to 81.78 dBA with the AMM. Therefore, the AMM is acoustically more efficient than the Nomex, as expected. In fact, there is a mean reduction of 6.15 dBA, equal to 7.01% of total OASPL. Taking in account the logarithmic nature of the decibel scale, the sound pressure is almost halved. Finally, for a windowless configuration, the positive effect of the AMM on the noise is similar to those obtained for a conventional aircraft. The results in terms of pressure maps are reported in Fig. 5.18(c) and (d) and compared to those of a baseline configuration and

windowless one.

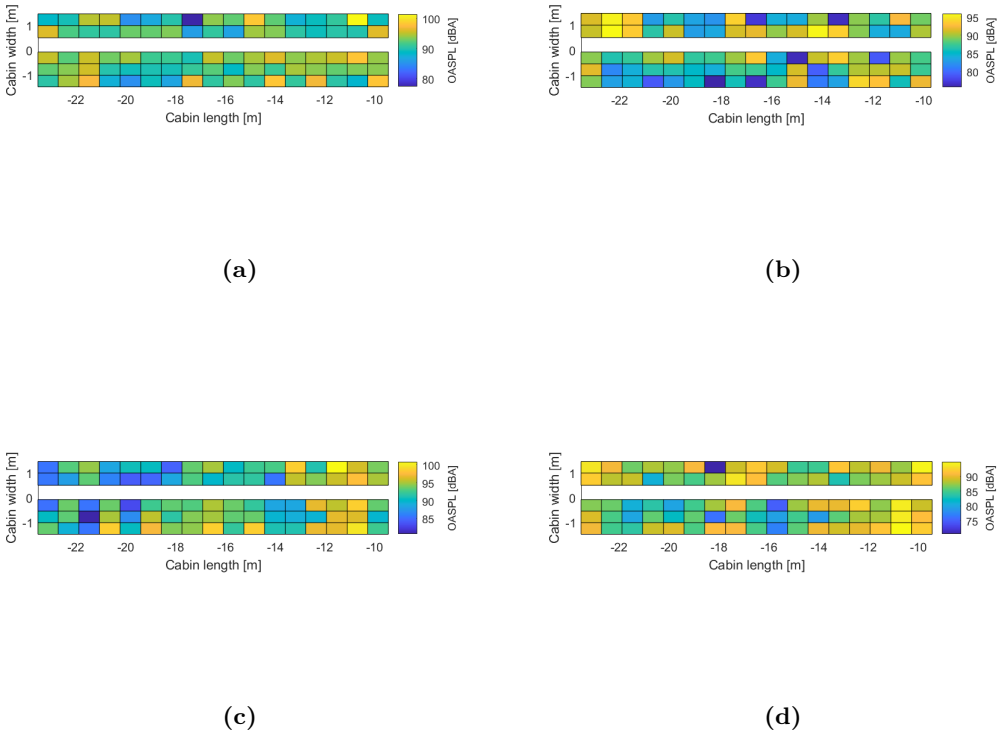

Figure 5.18: The OASPL [dBA] maps on the positions of the seated passenger's heads in fuselage under an external complex pressure field. The cabin of the model is composed by eighteen rows with five seats each one (from the bow on the right to the aft on the left). There is an increase in OASPL near the propeller position between row 2 and 5. (a) Lining panel core in Nomex in traditional fuselage. (b) Lining panel core in AMM in traditional fuselage. (c) Lining panel core in Nomex in a windowless fuselage. (d) Lining panel core in AMM in a windowless fuselage.

For in internal monopole placed at the centre of the cabin, the results in terms of OASPL between the Nomex and the AMMs are similar to the previous one. In particular for a monopole of an amplitude equal to 1 N/m^2, the perceived noise is equal to 89.10 dBA for the plain configuration and to 83.80 dBA for a configuration with the AMM in lining panel core. Therefore, there is a reduction in the OASPL of 5.30 dBA, corresponding to a relative reduction of 6.32%. According to the previous results, the windowless configuration is not studied for an internal source, because a relevant variation in the acoustic behaviour of the fuselage at low frequency from a traditional configuration is not expected. Numerical results are calculated for an amplitude equal to 0.5 N/m^2 in order to discover any change in the results, although the conclusions are similar to the previous ones. An analysis studies the behaviour of several internal sources in the passenger cabin, five monopoles, the results are similar to the those obtained for a

single monopole, with a more homogeneous pressure distribution. The pressure maps are reported in Fig. 5.19.

A final summary of the results in terms of average OASPL is reported in Tab. 5.5.

Table 5.5: The average OASPL [dBA] in the passenger cabin for the four types of sources exploited with different acoustic solutions and configurations.

Acoustic load	Nomex	AMM	Windowless	Windowless+AMM
External pressure	87.76	81.60	87.85	81.78
Monopole (1 N/m^2)	89.10	83.80	-	-
Monopole (0.5 N/m^2)	83.10	78.50	-	-
5 Monopoles (0.1 N/m^2)	83.17	75.26	-	-

CPACS based FEM model

The windowless fuselage barrel model has been previously validated for the primary structure. The high flexibility of the model due to the CPACS language allows to study different configurations for the lining panel changing both the materials and the layers thickness. The mesh, the geometry and the fluid-structure interfaces are changed according to the new materials.

The analyses are carried from 0 Hz to 250 Hz. We study the acoustic behaviour in the passenger cabin for three cases:

- baseline configuration, so using the materials given by DLR for the lining panels;
- we replace the core of the lining panels with the AMM by [51]. In particular is applied on the dado, sidewall, cowl and ceiling panels, but not on the overhead compartments. This last component is a completely separated components with its particular requirements. The luggage compartment has to carry the stresses due to the loading and unloading of luggage by passengers and crew, and the stresses during flight, instead of insulate the cabin from noise;
- the additive printed AMM is tested too. However, the frequency range of the analysis is out of its design range (above 1000-1200 Hz) and the aim is to study its behaviour at very low frequency.

The boundary conditions applied to the model are the following:

- a pressure applied on the external surface, in a similar way to the one applied on the previous model, but with a random value;
- auto-imposed wall conditions on the two sides of the fuselage barrel (to roughly simulate the bulkheads) as in the previous model;

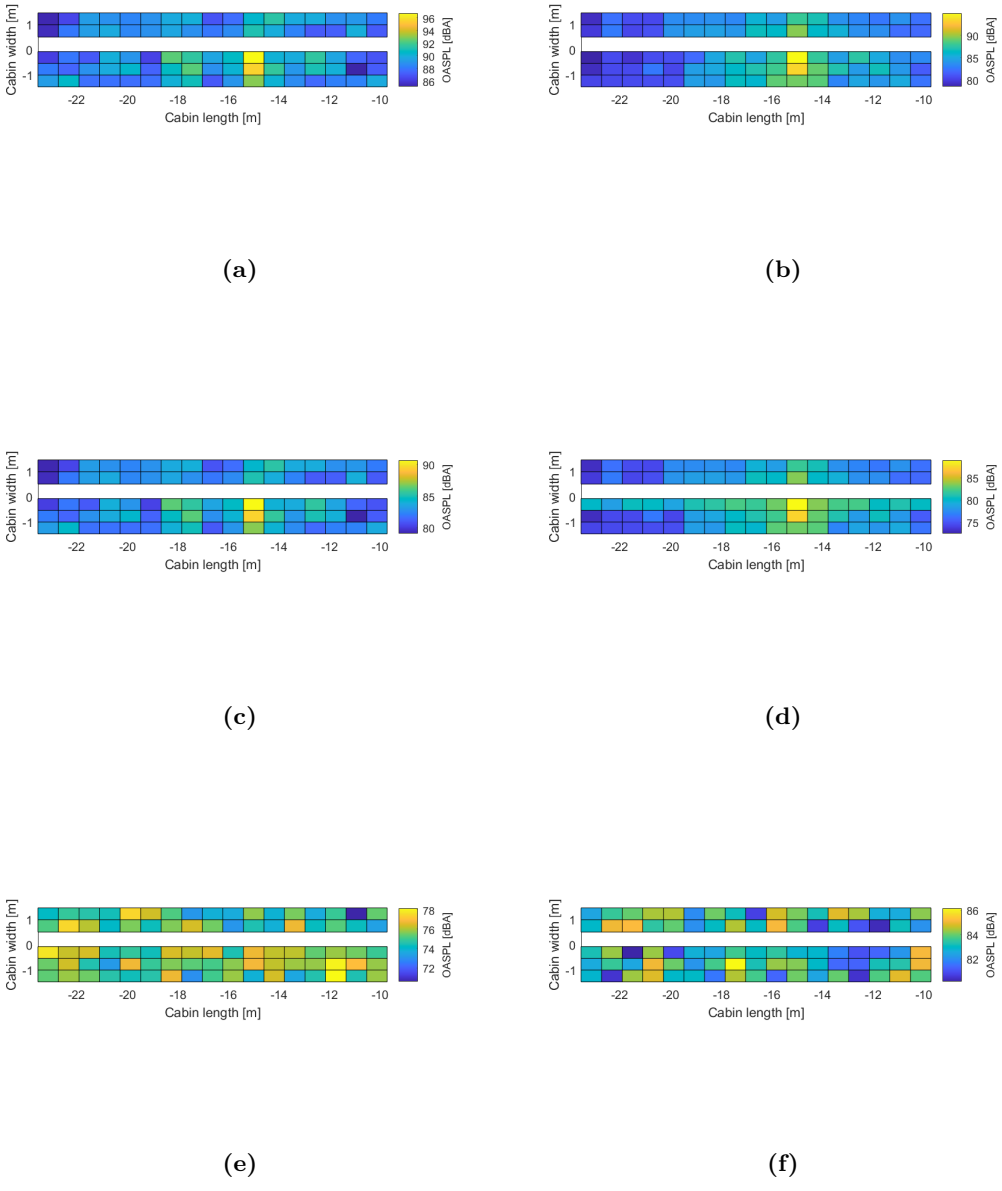

Figure 5.19: The OASPL $[dBA]$ maps on the positions of the seated passenger's heads in traditional fuselage loaded by internal monopolar sources. The cabin of the model is composed by eighteen rows with five seats each one (from the bow on the right to the aft on the left). For the first four cases there is an increase in OASPL around the monopole position at the centre of the cabin. (a) Lining panel core in Nomex for one monopole with unitary amplitude. (b) Lining panel core for one monopole with unitary amplitude. (c) Lining panel core in Nomex for one monopole with the amplitude equal to 0.5 N/m^2. (d) Lining panel core in AMM for one monopole with the amplitude equal to 0.5 N/m^2. (e) Lining panel core in Nomex for five monopoles with the amplitude equal to 0.1 N/m^2. (f) Lining panel core in AMM for five monopoles with the amplitude equal to 0.1 N/m^2.

- connections as joints (see MPC184 and COMBI250 formulation for joints)[11] between two components to accurately simulate the transfer of energy. In Fig. 5.20 the visualization and stiffness table of the two joints is reported. The first joint in Fig. 5.20(a) connects a sidewall panel to a frame, it is a shock absorber with a lower stiffness than the following joint. The second one in Fig. 5.20(b) connects an overhead luggage compartment to a frame. Moreover, there are the thousands of rivets between frames, stringers, fuselage panels and decks supports.

The solver is direct (*sparse*), which allows to use the smallest amount of virtual memory, which is the main limitation in this analysis. In order to solve the huge FEM model, the computer has to allocate the mass and stiffness matrices, before effectively solving the vibro-acoustic system. The matrix allocation is done exploiting the RAM and then the available virtual memory. [12]

The results are expressed in terms of average OASPL on the passenger cabin and with pressure maps. The acoustic pressure is calculated in dBA.

The OASPL on the frequency range is equal to 62.03 dBA for a lining panel made of the baseline material, similar to Nomex, and it is equal to 57.58 dBA for a lining panale made of AMM [51]. Therefore, the AMM is acoustically more efficient than the honeycomb material. In fact, there is an average reduction in 4.45 dBA, equal to 7.18% of total OASPL. On one hand the absolute reduction for this model is lower than the one for CASTLE based model, on the other hand the relative percentage reduction is very similar. Three main reasons could lead to these differences in the results:

- the model is built in a different way, with an increase in the accuracy of the components and connections description. Nevertheless, the shell model applied on the lining panels could not accurately understand the kinematic behaviour of the AMM;
- in the CASTLE model the overhead compartments are built on the monolithic lining panel, so the rear part of the overhead is a part on the panel and it is made of Nomex or AMM, while the front side by its own material. In the CPACS based model the overhead compartments are an independent component, both the rear and the front. Therefore, the part of the cabin closed by the luggage compartment is not shielded from incoming noise by the AMM;
- the range from 251 Hz to 300 Hz is missing respect to the previous model.
- for different acoustic loads, as demonstrate in the results for the monopolar source in the CASTLE model, the reduction in OASPL does not change for different types of loads and intensity, while the absolute values do.

[11] `https://www.mm.bme.hu/~gyebro/files/ans_help_v182/ans_elem/Hlp_E_MPC184.html`
[12] See the Ansys user's manual.

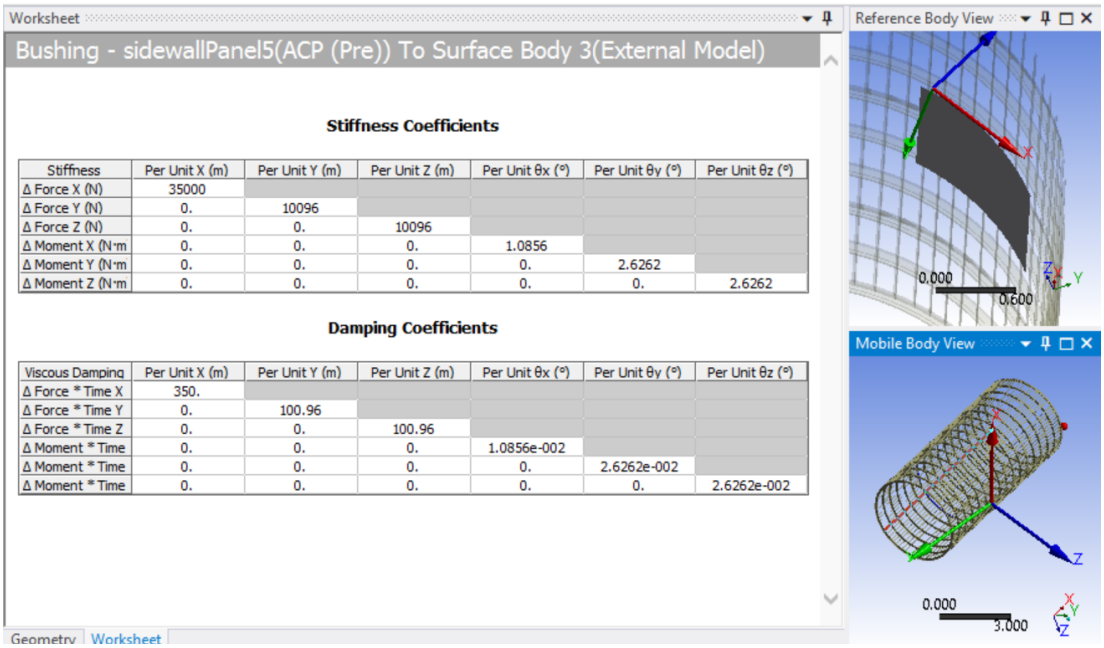

(a)

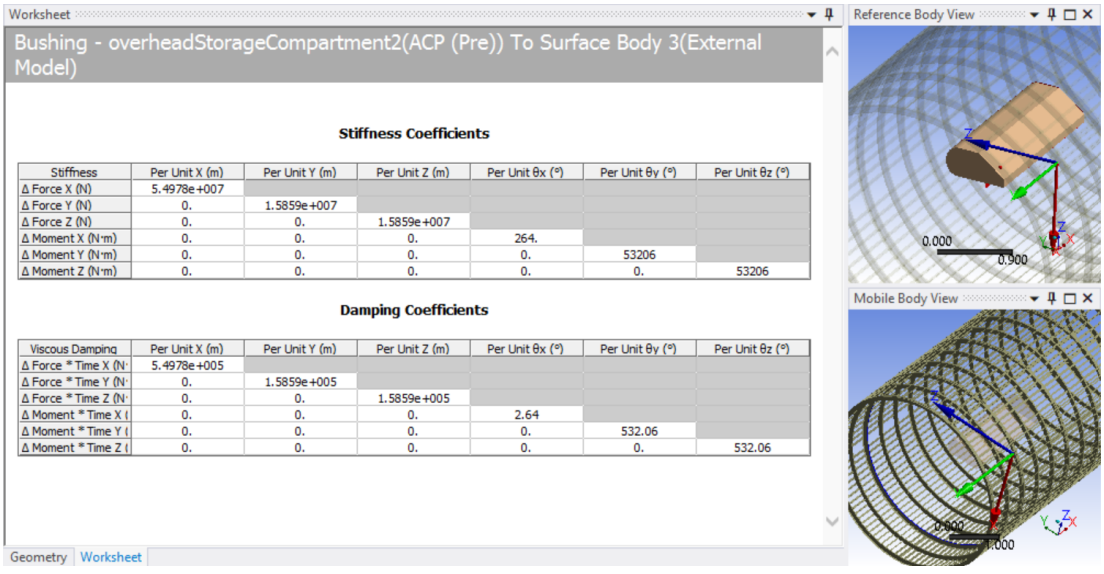

(b)

Figure 5.20: The connection between the primary and secondary structures as defined in Ansys for a MPC184 element, on the left the stiffness and damping table and on the right the two components connected. The damping is roughly approximated as the 1% of the stiffness. (a) The shock absorber between a sidewall panel and a fuselage frame. (b) The bar between a overhead luggage compartment and a fuselage frame.

Finally, the OASPL, for a lining panel exploiting the additive AMM, is equal to 65.12 dBA. In this case, the AMM completely replaces the lining panels materials. At low frequencies, the exploitation of this AMM in the lining panels does not lead to a reduction in the noise in accordance to the material TL, which has an high value above 100 Hz. The results in terms of pressure maps are reported in Fig. 5.21 and a summary of the average OASPL in Tab. 5.6.

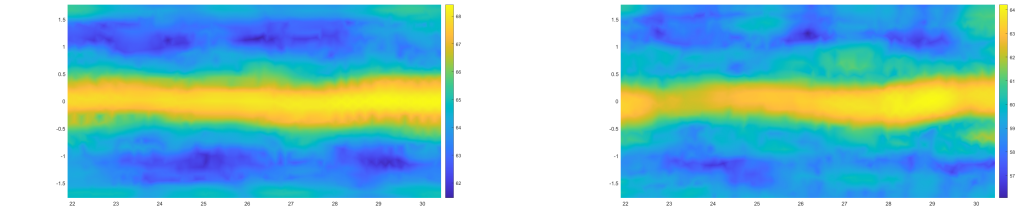

(a) **(b)**

Figure 5.21: The OASPL [dBa] maps for the passenger cabin calculated from the CPACS based model for two configurations of the linings panels (except the overhead luggage compartments). (a) The lining panels core is made of its original material provided by DLR and similar to Nomex. (b) The lining panels core is made of the AMM by [51].

Table 5.6: The average OASPL [dBA] in the windowless passenger cabin for the three types of materials exploited in the lining panels.

Material	OASPL
Baseline	62.03
AMM [51] in the core	57.58
Additive AMM	65.12

5.5 Sustainability analysis

5.5.1 Fuel consumption calculation

The windowless configuration impact on the environment is evaluated in terms of fuel consumption, both due to the reduction in weight and to the installation of new electronic devices. Therefore, the methodology in Fig. 5.2 is updated in Fig. 5.22 with the addition of the fuel consumption evaluation.

The fuel consumption $\dot{m}_p$ caused by the presence of the new electronic devices (e.g., the monitors and cameras) is estimated with the method proposed by Scholtz et al. [108], with the following equation:

$$\dot{m}_P = k_p \cdot SFC \cdot (N_c \cdot P_c + N_m \cdot P_m) \tag{5.5.1}$$

where N_c and N_m are the cameras and monitors number respectively, P_c and P_m their

power consumption which depends on the device model. The SFC is the thrust specific fuel consumption and it depends on the engine design, for modern aircraft it is assumed equal to $1.6 \cdot 10^{-5}$ $kg/(Ns)$. The shaft power factor k_p is calculated from the aircraft speed (the Mach's number) and the cruise altitude through a statistical equation proposed in [108]:

$$\begin{aligned} k_p =& 0.0057 + 4.60 \cdot 10^{-8} \cdot \frac{1}{m} \cdot h - 0.0106 \cdot M - 4.44 \cdot 10^{-13} \cdot \frac{1}{m^2} \cdot h^2 + \\ &+ 1.85 \cdot 10^{-7} \cdot \frac{1}{m} \cdot h \cdot M + 0.0049 \cdot M^2 \end{aligned} \tag{5.5.2}$$

where M is Mach number and h the altitude, that can be approximated to 0.8 and 10000 m or derived from a preliminary design process.

Finally, once the weight reduction and the fuel consumption due to monitors and cameras are estimated, it is possible to calculate with preliminary method in Section 2.2, such as the fuel fractions, the total fuel consumption reduction. Moreover, the emissions, in terms of CO_2 or NO_X, and the operating costs savings are estimated based on general data for jet fuel.

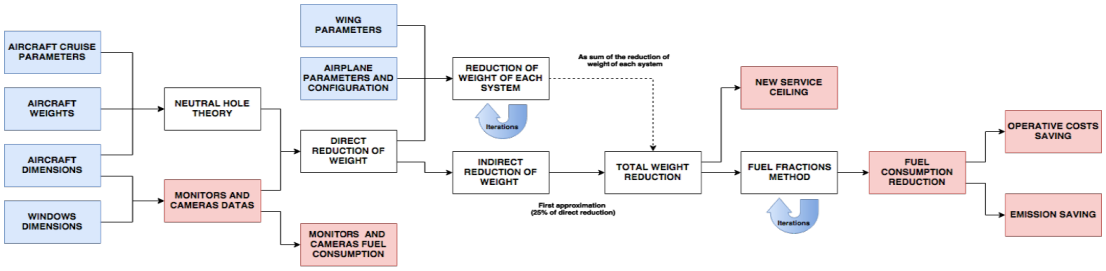

Figure 5.22: Updated methodology block diagram for the windowless concept analysis including the fuel consumption estimation.

5.5.2 Sustainability assessment

The fuel consumption of the visual system after one hour, considering all cameras and monitors on, is reported in Tab. 5.7 within the visual system data, assuming an average power consumption equal to 96 W for each monitor and 2.8 W for each camera.

Table 5.7: Data of the visual system needed to replace the windows and their fuel consumption.

	ATR72	E190	A320	B737
Number of monitors	20	24	32	34
Number of cameras	108	100	152	168
Fuel consumption $[l/hr]$	0.36	0.41	0.59	0.60

For the four aircraft models, the amount of fuel consumed due to monitors and cameras is very low and consequently negligible.

The emissions and operating cost savings are roughly based on the average emissions

and costs of jet fuel per liter for one year. Therefore, we assume that for one liter of fuel, 2.53 kilograms of CO_2 are emitted and an average price for jet fuel is used. A windowless A320 approximately saves 0.06 kilograms of CO_2 per kilometer, the B737 0.55 kg/km, the ATR72 0.02 kg/km and the E190 0.03 kg/km. These results become encouraging considering the whole aircraft fleet of each model[13] exploiting a windowless configuration, as reported in Fig 5.23. There are 4111 A320s, 4258 B737s, 991 ATR72s and 546 E190s, for example for the A320 the daily emission saving would be 1.89 million kilograms of CO_2 and the daily operating cost saving is around 309 thousand dollar.

In order to summarize the results according to the double sustainability concept (economic and environmental), a medium-haul aircraft, exploiting a windowless configuration, such as the A320 or the B737, produces 0.70% less polluting emissions than a traditional one and it is 0.72% cheaper. A regional turboprop, such as the ATR72, is 0.5% cheaper. A short-range aircraft, such as the E190, is 0.34% cheaper. According to the Air Transport Action Group (ATAG) report data,[14] the exploitation of a windowless configuration on regional and short range aircraft (e.g., domestic flights) would reach a reduction almost equal to to 0.5% of the total emissions.

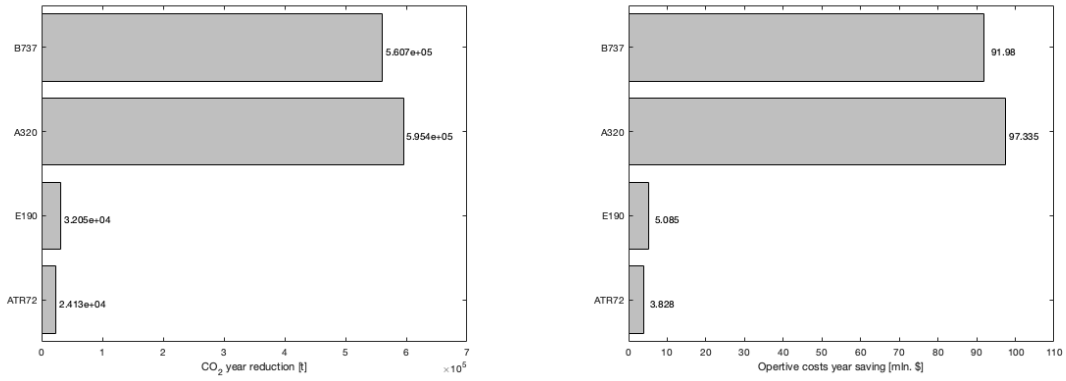

(a) **(b)**

Figure 5.23: The advantages of a windowless configuration exploited by the actual fleet of the four aircraft models considered in the study case. (a) Emissions reduction. (b) Operating costs saving.

[13] According to the companies reports in 2020.
[14] `https://www.atag.org/`

Conclusions

In this work the sustainability concept in aircraft is declared in its two main aspects: the environmental and the economical one. The two types of sustainability are defined in terms of emissions reduction and comfort increase. In particular, for a commercial passenger aircraft we focus, on one hand, on fuel consumption saving due to a reduction in the empty weight of the aircraft and, on the other hand, on the increase in the acoustic comfort (e.g., the noise reduction) of passengers and crew. In order to achieve these results, two different design methods and solutions are exploited due to the different disciplines for the assessment of the reductions in weight and noise.

The weight reduction is obtained through a preliminary design method, refining the preliminary equations for weight estimation. The chosen solution is a windowless configuration, where the removal of windows and reinforcements from the fuselage structure leads to an important reduction in weight and in emissions. This reduction takes in account the weight decrease of other subsystems due to the lighter structure. Moreover, in order to avoid any visual comfort issue, the windows are replaced with monitors connected to external cameras. Their weights and fuel consumption is considered too. The windowless configuration is tested for four aircraft models and the results are very positive with a reduction of around the 0.3-0.6% of the maximum take-off weight. Moreover, this concept is studied as a baseline for more advanced and disruptive configurations, where the absence of windows is caused by the design of the aircraft, as geodesic fuselage, blended wing body aircraft or stratospheric vessels. The preliminary design tools exploited in the analysis allow a high flexibility in the aircraft design. These tools are used to estimate the weight of both the reinforcement and the visual system (cameras, monitors and cables).

The noise reduction solution needs a deeper analysis, using different numerical tools. At this state of art, it is not possible to accurately estimate the noise spread in the passenger cabin through preliminary design analytical or semi-analytical equations, because the problem is complex and depends on several factors coupled together, as the structure of the fuselage and of the cabin, the type of aircraft, which influences the acoustic sources, the connections between the several structural components, etc. The main problem in noise reduction is at low frequency, where traditional solutions are limited by weight and volume. Innovative and advanced solutions use a new class of

materials, the acoustic metamaterials, which can reach high insulating performances at low frequency with very low weight. Therefore, in this work, we choose to study this kind of solution with the Finite Element Method. The kinematic complexity of these materials, as well as those of sandwich and multi-layers plates used in the aircraft structures, is represented using a powerful formulation, the Carrera's Unified Formulation, which enables a class of Layer Wise theories for studying this kind of structures. In this work, this formulation is expanded to the vibro-acoustic problem and several validations are performed within modifications in the related code, MUL2. This software, developed by *Politecnico di Torino*, is used for preliminary evaluation between the acoustic performances of metamaterials and traditional materials used in the aircraft cabin lining panels. The noise reduction solutions are applied to two aircraft FEM models, which are refined in this work for vibro-acoustic problem:

- a FEM model of a turboprop aircraft derived from the CASTLE European project;
- a FEM model of a turbofan aircraft based on the standard language for aircraft design and optimization CPACS.

When complex numerical analyses are performed, two issues are the model accuracy and flexibility. The first model has an high level of precision in modelling the lining panel kinematic through solid elements and it applies real external acoustic sources. Nevertheless, a low flexibility in the design is possible due to the simplified geometry and how the data are stored. The second model is developed in CPACS and then through a script it is exported in a commercial software for the analysis. This process allows to easily modify the design from the CPACS files and then to reload them in a semi-automatically way. The model has an high degree of accuracy in the components and connections description. However, the computational cost is high and in order to reduce it, the lining panels structural approach is simplified to a shell model. In this two models the noise reduction solutions are tested. The results are encouraging and in agreement with the preliminary analysis performed in MUL2. In particular the first AMM studied shows an important noise reduction at low frequency.

In the end, the results can be dived in quantitative and qualitative one. The former refers to the estimation of the advantages of different solutions to improve sustainability of future aircraft, a so-called case study for emissions and noise reduction. The latter refers to the creation of a flexible and accurate method for weight reduction estimations for a windowless concept and for the calculation of acoustic performances for new noise reduction solutions.

On one hand, the quantitative results for the application of CUF framework in vibro-acoustics show the following conclusions:

- Layer Wise theories in the frame of CUF are able to model the kinematic beha-

viour of multi-layer structures with a lower computational cost than model with solid elements and with a greater accuracy than Equivalent Single Layer theories with shell elements. This result is transferred to vibro-acoustic field, where there is fluid-structure coupling, which increase the differences between LW and ESL models;

- new parts in the CUF are added and implemented in MUL2, as acoustic sources, boundary conditions and new unconventional shape functions for curvilinear elements. These additions are fully validated.

On the other hand, we obtain the following conclusions for the study cases on weight and noise reduction:

- the windowless concept is applicable to aircraft through a visual system integration and there is an important reduction in weight, hence in emissions and operating costs. In terms of noise reduction, at low frequency, the windowless concept does not show any advantage;
- acoustic metamaterials applied on the aircraft lining panels show an effective reduction in OASPL (and SPL) inside the cabin.

If the previous results are very encouraging for the proposed solutions, the qualitative conclusions lay the foundations for developing and enhancing several concepts for the design processes. In particular for the weight estimations, the following conclusions are derived:

- it is possible to develop a relative simple model in the preliminary design framework for estimation of emissions saving due to the reduction in the empty weight of the aircraft. This model is based on a mix of preliminary design analytical equations and statistical correlations. For new configurations the equations and correlations must be evaluated individually in order to understand if they are still valid or must be updated;
- the windowless concept, at preliminary level, is feasible and can lead to an advancement in the sustainability challenge, that the aviation sector is facing.

For the noise estimation we reach the following conclusions:

- computational cost and accuracy are important issues in vibro-acoustics. They strongly affect and limit the size (degrees of freedom) and the frequency range of a FEM model, in particular when dealing with multi-layer materials. This issue can be solved exploiting advanced numerical approach, as those enhanced by CUF. This formulation allows to use reduced order shell elements with the

same accuracy of solid elements. This approach can also solve the numerical increase in stiffness of the CPACS based model, underlined in previous validation, for beam elements applied on stringers and frames. The DoF reduction in an aircraft fuselage/cabin numerical system can be estimated with a preliminary comparison between LW model and ESL-solid model. A conventional FEM model of a fuselage uses solid elements for the fluid, shells for the floors and the fuselage skin, solid elements for the core of sandwich materials, AMM or advanced multi-layer materials (as those in the ling panel) and, in order to avoid errors, shells for stringers and frames. The exploitation of a LW approach in the CUF framework, makes it possible to use shell elements for advanced multi-layer materials and beam elements for the stiffeners. The relative reduction of DoF would be almost equal to the 70% for the lining panel only (from a solid elements to shells elements), according to the author's work [84]. For the stiffeners, the switch from shells to beams can lead to relative reduction in DoF roughly estimated between 30% and 40%. Therefore, the total reduction in DoF and in the computational cost in the fuselage system would be very significant;

- the vibro-acoustic theory can be included in CUF framework (and in MUL2);
- next to accuracy and computational cost, at preliminary design phase, the model must be flexible in order to try several acoustic solutions or to share data to other research groups, for example in a MDO process, but not only. This problem is solved using a standardized language for aircraft system, CPACS, which can be also used to generate vibro-acoustic model, as done in this work;
- new solutions, as acoustic metamaterials, have to be studied to stop noise at low frequency.

In this work several aspects of the design of new sustainable aircraft are investigated and solutions effectiveness is evaluated. The idea is to create a framework for further studies on emissions and noise reduction, based on an enhancing of the proposed solutions. The final purpose is to integrate in a MDO tool the weight estimation process and the vibro-acoustics analysis for noise assessment at low frequency, for example using the CPACS framework. However, there are still some further developments and studies to be carried on, both on the framework and on the case study:

- with regard to the windowless concept, we must extend it to other configurations. The visual system must be completely defined through mock-up in order to study the connection between monitors and cameras;
- the main idea in vibro-acoustics is to use the CUF framework for completely analyze the fuselage behaviour, in order to do that in MUL2, non homogeneous interface must be created. In this way it will be possible to export the mesh directly from the geometry files or better from CPCAS to MUL2, saving thousands

of degrees of freedom. A reduction in the computational cost give us more design freedom in the model creation, allowing to add other components of the fuselage and cabin. Moreover, other minor issues must be solved, as the integration of frequency dependant boundary conditions and material properties or infinite elements;

- the optimization of acoustic metamaterials must be carried on, in particular it will be challenging to study active metamaterials, with piezoelectric actuators. Active metamaterials could lead to increase the design frequency range with higher performances than the passive ones. However, the energy consumption must be evaluated;

- in this work, we focus on low frequency. A very promising future developments will be the integration of FEM analysis for low frequency with high frequency simulation performed by SEA methods;

- the creation of a tool for noise assessment through a human in the loop process could be done in virtual or augmented reality environment. This is important in order to have subjective measurement of the acoustic comfort, coupled to the ergonomics, visual and thermal comfort, of the users in a quasi-real environment. Therefore, the auralization concept, preliminarily designed and tested in this work, must be developed to a further step in order to validate noise reduction solutions or new cabin configurations from the user point of view.

Bibliography

[1] D. Albalate, G. Bel, and X. Fageda. Competition and cooperation between high-speed rail and air transportation services in europe. *Journal of Transport Geography*, 42, 07 2014.

[2] J. Jupp. The design of future passenger aircraft - the environmental and fuel price challenges. *The Aeronautical Journal*, 120:37–60, 01 2016.

[3] A. Hall, T. Mayer, I. Wuggetzer, and PRN. Childs. Future aircraft cabins and design thinking: Optimisation vs. win-win scenarios. *Propulsion and Power Research*, 2, 06 2013.

[4] A. Sarkar. Evolving green aviation transport system: A hoilistic approah to sustainable green market development. *American Journal of Climate Change*, 01, 01 2012.

[5] G. Brasseur, M. Gupta, B. Anderson, S. Balasubramanian, S. Barrett, D. Duda, G. Fleming, P. Forster, J. Fuglestvedt, A. Gettelman, R. Halthore, S. Jacob, M. Jacobson, A. Khodayari, KN. Liou, M. Lund, R. Miake-Lye, P. Minnis, S. Olsen, and C. Zhou. Impact of aviation on climate: Faa's aviation climate change research initiative (accri) phase ii. *Bulletin of the American Meteorological Society*, 97:150709110621006, 07 2015.

[6] M. Campagna, A. Frattolillo, S. Pili, G. Marcias, N. Angius, C. Mastino, P. Cocco, and G. Buonanno. Environmental exposure to ultrafine particles inside and nearby a military airport. *Atmosphere*, 7:138, 10 2016.

[7] N. Hudda, M. Simon, W. Zamore, and J. Durant. Aviation-related impacts on ultrafine particle number concentrations outside and inside residences near an airport. *Environmental Science & Technology*, 52, 02 2018.

[8] M. Basner, W. Babisch, A. Davis, M. Brink, C. Clark, S. Janssen, and S. Stansfeld. Auditory and non-auditory effects of noise on health. *The Lancet*, 383(9925):1325 – 1332, 2014.

[9] MP. De Looze, LFM. Kuijt-Evers, and J. Van Dieen. Sitting comfort and discomfort and the relationships with objective measures. *Ergonomics*, 46(10):985–997, 2003. PMID: 12850935.

[10] NA. Stanton, WC. Li, and D. Harris. Editorial: Ergonomics and human factors in aviation. *Ergonomics*, 62(2):131–137, 2019. PMID: 30601105.

[11] PR Bassett and SJ Zand. Noise reduction in cabin airplanes. *Transactions of the A.S.M.E.*, pages 49–56, 1934.

[12] S. Pennig, J. Quehl, and V. Rolny. Effects of aircraft cabin noise on passenger comfort. *Ergonomics*, 55(10):1252–1265, 2012. PMID: 22849320.

[13] L. Bourikas, S. Gauthier, N. Khor Song En, and P. Xiong. Effect of thermal, acoustic and air quality perception interactions on the comfort and satisfaction of people in office buildings. *Energies*, 14(2), 2021.

[14] DP. Restuputri, K. Purnamasari, N. Afni, S. Legtria, E. Shoffiah, M. Septia, and I. Masudin. Evaluation of aircraft cabin comfort: Contributing factors, dissatisfaction indicators, and degrees of influence. *AIP Conference Proceedings*, 2453(1):020047, 2022.

[15] L. Pang, Y. Qin, D. Liu, and M. Liu. Thermal comfort assessment in civil aircraft cabins. *Chinese Journal of Aeronautics*, 27(2):210–216, 2014.

[16] S Bagassi, F Lucchi, F De Crescenzio, and S. Piastra. Design for comfort: aircraft interiors design assessment through a human centered response model approach. In *31th ICAS 2018 Proceedings*, 2018.

[17] F. De Crescenzio, S. Bagassi, and F. Starita. Preliminary user centred evaluation of regional aircraft cabin interiors in virtual reality. *Scientific Reports*, 11, 05 2021.

[18] D. Kiehn, J. Autenrieb, and N. Fezans. Coast - a simulation and control framework to support multidisciplinary optimization and aircraft design with cpacs. In *33th ICAS 2022 Proceedings*, 2022.

[19] E. Torenbeek. *Synthesis of Subsonic Airplane Design*. Springer Netherlands, 2013.

[20] D. Raymer. *Aircraft Design: A Conceptual Approach, Sixth Edition*. AIAA Education Series, 09 2018.

[21] LR. Jenkinson, D. Rhodes, and P. Simpkin. *Civil Jet Aircraft Design*. AIAA education series. American Institute of Aeronautics and Astronautics, 1999.

[22] P. Sforza. *Commercial Airplane Design Principles*. Butterworth-Heinemann, Boston, 2014.

[23] O. Gur, W. Mason, and J. Schetz. Full configuration drag estimation. *American Institute of Aeronautics and Astronautics*, 2009.

[24] MC. Moruzzi and S. Bagassi. Preliminary design of a short-medium range windowless aircraft. *International Journal on Interactive Design and Manufacturing (IJIDeM)*, 14(3):823–832, Sep 2020.

[25] A. Papageorgiou, M. Tarkian, K. Amadori, and J. Ölvander. Multidisciplinary design optimization of aerial vehicles: A review of recent advancements. *International Journal of Aerospace Engineering*, 2018:4258020, May 2018.

[26] L. Boggero, T. Lefebvre, WJ. Vankan, B. Beijer, V. Saluzzi, and B. Nagel. The agile4.0 mbse-mdao development framework: overview and assessment. In *33th ICAS 2022 Proceedings*, 2022.

[27] A. Rizzi, M. Zhang, B. Nagel, D. Boehnke, and P. Saquet. Towards a unified framework using cpacs for geometry management in aircraft design. In *50th AIAA Aerospace Sciences Meeting*, 2012.

[28] M. Alder, E. Moerland, J. Jepsen, and B. Nagel. Recent advances in establishing a common language for aircraft design with cpacs. In *7th CEAS 2020 Proceedings*, 2020.

[29] JN. Walther and PD. Ciampa. Knowledge-based automatic airframe design using cpacs. *Transportation Research Procedia*, 29:427–439, 2018. Aerospace Europe CEAS 2017 Conference.

[30] JN. Walther, C. Hesse, M. Alder, JYC. Biedermann, and B. Nagel. Expansion of the cabin description within the cpacs air vehicle data schema to support detailed analyses. *CEAS Aeronautical Journal*, Aug 2022.

[31] A. Filippone. *Aircraft Noise: Noise Sources*, page 470–532. Cambridge Aerospace Series. Cambridge University Press, 2012.

[32] LL. Beranek. The noisy dawn of the jet age. *Sound and Vibration*, 41:94–99, 2007.

[33] D. Casalino, F. Diozzi, R. Sannino, and A. Paonessa. Aircraft noise reduction technologies: A bibliographic review. *Aerospace Science and Technology*, 12(1):1–17, 2008. Aircraft noise reduction.

[34] W. Dobrzynski. Almost 40 years of airframe noise research: What did we achieve? *Journal of Aircraft*, 47(2):353–367, 2010.

[35] F. Zangeneh-Nejad and R. Fleury. Active times for acoustic metamaterials. *Reviews in Physics*, 4:100031, 2019.

[36] N. Hu, H. Buchholz, M. Herr, C. Spehr, and S. Haxter. Contributions of different aeroacoustic sources to aircraft cabin noise. In *19th AIAA/CEAS Aeroacoustics Conference*, 2013.

[37] M. Norambuena, M. Böswald, and Y. Govers. Vibro-acoustic analysis of flight test data comprising fuselage vibrations, external pressure and interior cabin noise measurements. In *54th AIAA Aerospace Sciences Meeting*, 2016.

[38] K. Ozcan and S. Nemlioglu. In-cabin noise levels during commercial aircraft flights. *Canadian Acoustics - Acoustique Canadienne*, 34, 12 2006.

[39] HP Lee, S. Kumar, S. Garg, and KM Lim. Assessment of in-cabin noise of wide-body aircrafts. *Applied Acoustics*, 194:108809, 2022.

[40] CD. Zevitas, JD. Spengler, B. Jones, E. McNeely, B. Coull, X. Cao, SM Loo, AK Hard, and JG. Allen. Assessment of noise in the airplane cabin environment. *Journal of Exposure Science & Environmental Epidemiology*, 28(6):568–578, Nov 2018.

[41] C. Hesse. Active control of composite fuselage type structures with enclosed acoustic cavity. *Journal of Fluids and Structures*, 81:565–573, 2018.

[42] PC. Herdic, BH. Houston, MH. Marcus, EG. Williams, and AM. Baz. The vibro-acoustic response and analysis of a full-scale aircraft fuselage section for interior noise reduction. *The Journal of the Acoustical Society of America*, 117(6):3667–3678, 2005.

[43] A. Grewal, D. Zimcik, R. Lapointe, A. Grewal, D. Zimcik, and R. Lapointe. Vibro-acoustic modelling in aircraft cabin noise transmission and control. In *38th Structures, Structural Dynamics, and Materials Conference*, 1997.

[44] C. Blech and S. Langer. Wave-resolving aircraft fuselage model for cabin noise predictions under distributed fluid loadings. In *XI International Conference on Structural Dynamics*, pages 2437–2445, 01 2020.

[45] B. Aloufi, K. Behdinan, and J. Zu. Theoretical vibro-acoustic modeling of acoustic noise transmission through aircraft windows. *Journal of Sound and Vibration*, 371:344–369, 2016.

[46] JK. Henry and RL. Clark. Noise transmission from a curved panel into a cylindrical enclosure: Analysis of structural acoustic coupling. *The Journal of the Acoustical Society of America*, 109(4):1456–1463, 2001.

[47] Y Liu. On the bem for acoustic wave problems. *Engineering Analysis with Boundary Elements*, 107:53–62, 2019.

[48] FJ. Fahy, WG Price, and AJ. Keane. Statistical energy analysis: a critical overview. *Philosophical Transactions of the Royal Society of London. Series A: Physical and Engineering Sciences*, 346(1681):431–447, 1994.

[49] G. Wang, YX. Zhang, ZB. Guo, and ZG. Zhou. A novel hybrid deterministic-statistical approach for the mid-frequency vibro-acoustic problems. *Applied Mathematical Modelling*, 83:202–219, 2020.

[50] P. Vitiello, D. Bianco, B. Galasso, S. Ameduri, R. Lombardi, M. Cinefra, G. Petrone, and C. Colangeli. Innovative passive n&v concepts definition, studies and numerical models delivery for optimization. *AIR-CIRA-RPT(O B-4.4.6.2-1)-0001*, 2018.

[51] M. Cinefra, G. D'Amico, AG. De Miguel, M. Filippi, A. Pagani, and E. Carrera. Efficient numerical evaluation of transmission loss in homogenized acoustic metamaterials for aeronautical application. *Applied Acoustics*, 164:107253, 2020.

[52] D. Magliacano, G. Petrone, F. Franco, and D. De Rosa. Numerical investigations about the sound transmission loss of a fuselage panel section with embedded periodic foams. *Applied Acoustics*, 182:108265, 2021.

[53] V. Giannella, R. Citarella, M. Barbarino, P. Vitiello, D. Bianco, and G. Petrone. Passive noise control oriented design of aircraft headrests. In *3rd Euro-Mediterranean Conference on Structural Dynamics and Vibroacoustics*, 02 2020.

[54] I. Dimino, C. Colangeli, J. Cuenca, P. Vitiello, and M. Barbarino. Active noise control for aircraft cabin seats. *Applied Sciences*, 12(11), 2022.

[55] M. Cinefra, S. Passabì, and E. Carrera. Fem vibroacoustic analysis in the cabin of a regional turboprop aircraft. *Advances in Aircraft and Spacecraft Science*, 5:477–498, 07 2018.

[56] M. Cinefra and G. Petrone. Sea analysis in the cabin of a regional turboprop with metamaterial lining panels. In *AIAA Scitech 2019 Forum*, 2019.

[57] G. Petrone, G. Melillo, A. Laudiero, and S. De Rosa. A statistical energy analysis (sea) model of a fuselage section for the prediction of the internal sound pressure level (spl) at cruise flight conditions. *Aerospace Science and Technology*, 88:340–349, 2019.

[58] E. Carrera, M. Cinefra, M. Petrolo, and E. Zappino. Finite element analysis of structures through unified formulation. *Wiley*, 2014.

[59] S Santhosh, MC Moruzzi, F De Crescenzio, and S Bagassi. Spatial sound system to aid interactivity in a human centred design evaluation of an aircraft cabin environment. In *XXVI AIDAA Congress Proceedings*, 2021.

[60] S. Santhosh, MC. Moruzzi, F. De Crescenzio, and S. Bagassi. Auralization of noise in a virtual reality aircraft cabin for passenger well being using human centred approach. In *33th ICAS 2022 Proceedings*, 2022.

[61] M. Cohen, J. Villegas, and W. Barfield. Special issue on spatial sound in virtual, augmented, and mixed-reality environments. *Virtual Reality*, 19(3):147–148, Nov 2015.

[62] M. Schoeffler, JL. Gernert, M. Neumayer, S. Westphal, and J. Herre. On the validity of virtual reality-based auditory experiments: a case study about ratings of the overall listening experience. *Virtual Reality*, 19(3):181–200, Nov 2015.

[63] MP. Arunkumar, J Pitchaimani, KV. Gangadharan, and MC. Leninbabu. Vibro-acoustic response and sound transmission loss characteristics of truss core sandwich panel filled with foam. *Aerospace Science and Technology*, 78:1–11, 2018.

[64] M. Cinefra, MC. Moruzzi, S. Bagassi, E. Zappino, and E. Carrera. Vibro-acoustic analysis of composite plate-cavity systems via cuf finite elements. *Composite Structures*, 259:113428, 2021.

[65] AJM. Ferreira, CMC. Roque, E. Carrera, and M. Cinefra. Analysis of thick isotropic and cross-ply laminated plates by radial basis functions and a unified formulation. *Journal of Sound and Vibration*, 330(4):771–787, 2011.

[66] E. Carrera, M. Cinefra, G. Li, and GM. Kulikov. Mitc9 shell finite elements with miscellaneous through-the-thickness functions for the analysis of laminated structures. *Composite Structures*, 154:360–373, 2016.

[67] E. Carrera, M. Cinefra, and G. Li. Refined finite element solutions for anisotropic laminated plates. *Composite Structures*, 183:63–76, 2018. In honor of Prof. Y. Narita.

[68] M. Cinefra and E. Carrera. Shell finite elements with different through-the-thickness kinematics for the linear analysis of cylindrical multilayered structures. *International Journal for Numerical Methods in Engineering*, 93(2):160–182, 2013.

[69] M. Cinefra and S. Valvano. A variable kinematic doubly-curved mitc9 shell element for the analysis of laminated composites. *Mechanics of Advanced Materials and Structures*, 23(11):1312–1325, 2016.

[70] R. Srinivasan Puri, D. Morrey, AJ. Bell, JF. Durodola, EB. Rudnyi, and JG. Korvink. Reduced order fully coupled structural–acoustic analysis via implicit moment matching. *Applied Mathematical Modelling*, 33(11):4097–4119, 2009.

[71] N. Trompette and M. Guerich. An experimental validation of vibro-acoustic prediction by the use of simplified methods. *Applied Acoustics*, 66(4):427–445, 2005.

[72] C. Marchetto, L. Maxit, O. Robin, and A. Berry. Vibroacoustic response of panels under diffuse acoustic field excitation from sensitivity functions and reciprocity principles. *The Journal of the Acoustical Society of America*, 141:4508–4521, 06 2017.

[73] A. Vieira, M. Snellen, AM.N. Malgoezar, R. Merino-Martinez, and DG. Simons. Analysis of shielding of propeller noise using beamforming and predictions. *The Journal of the Acoustical Society of America*, 146(2):1085–1098, 2019.

[74] MC. Moruzzi, M. Cinefra, and S. Bagassi. Analysis of an acoustic monopole source in a closed cavity via cuf finite elements. *Aerotecnica Missili & Spazio*, Aug 2022.

[75] JL. Migeot, JP. Coyette, and L. Grègory. Acoustics. *IJK Numerics*, pages 101–105, 2016.

[76] LE. Kinsler, AR. Frey, AB. Coppens, and JV Sanders. Fundamentals of acoustics. *Wiley*, pages 127–130, 2000.

[77] LD. Pope. On the transmission of sound through finite closed shells: Statistical energy analysis, modal coupling, and nonresonant transmission. *The Journal of the Acoustical Society of America*, 50(3B):1004–1018, 1971.

[78] A. Rona. The acoustic resonance of rectangular and cylindrical cavities. *Journal of Algorithms & Computational Technology*, 1(3):329–356, 2007.

[79] M. Filippi, E. Carrera, and AM. Regalli. Layerwise Analyses of Compact and Thin-Walled Beams Made of Viscoelastic Materials. *Journal of Vibration and Acoustics*, 138(6), 07 2016. 064501.

[80] CD. Johnson and DA. Kienholz. Finite element prediction of damping in structures with constrained viscoelastic layers. *AIAA Journal*, 20(9):1284–1290, 1982.

[81] G. Wang, S. Veeramani, and NM. Wereley. Analysis of Sandwich Plates with Isotropic Face Plates and a Viscoelastic Core . *Journal of Vibration and Acoustics*, 122(3):305–312, 01 1999.

[82] Z. Huang, Z. Qin, and F. Chu. Vibration and damping characteristics of sandwich plates with viscoelastic core. *Journal of Vibration and Control*, 22(7):1876–1888, 2016.

[83] EQ Li, Y. Lei, GJ Tang, and L. Daokui. Dynamic analysis of a constrained layer damping beam by transfer function method. *Zhendong yu Chongji/Journal of Vibration and Shock*, 26:75–78, 02 2007.

[84] MC Moruzzi, M Cinefra, S Bagassi, and E. Zappino. Vibro-acoustic analysis of multi-layer cylindrical shell-cavity systems via cuf finite elements. In *33th ICAS 2022 Proceedings*, 2022.

[85] M. Cinefra. Non-conventional 1d and 2d finite elements based on cuf for the analysis of non-orthogonal geometries. *European Journal of Mechanics/A Solids*, 88:104273, 2021.

[86] M. Cinefra. Formulation of 3d finite elements using curvilinear coordinates. *Mechanics of Advanced Materials Structures*, pages 1–10, 2020.

[87] M. Cinefra. Free-vibration analysis of laminated shells via refined mitc9 elements. *Mechanics of Advanced Materials and Structures*, 23(9):937–947, 2016.

[88] S Bagassi, F Lucchi, and MC. Moruzzi. Preliminary design of a long range windowless aircraft concept. In *31th ICAS 2018 Proceedings*, 2018.

[89] S. Bagassi, F. Lucchi, and MC. Moruzzi. The windowless concept: preliminary design of short-medium range windowless aircraft. In *XXIV AIDAA Congress Proceedings*, 2017.

[90] S. Bagassi, F. Lucchi, and F. Persiani. Aircraft preliminary design: a windowless concept. In *5th CEAS 2015 Proceedings*, 2015.

[91] J. Zaneboni and B. Saint Jalmes. Aircraft with a cockpit including a viewing surface for piloting which is at least partially virtual. In *U.S. patent no. 2014/0180508*. Airbus, March 6 2014.

[92] C. Berth, G. Huttig, and O. Lehmann. Research on integrated collimated cockpit visual and flight information system. In *26th ICAS 2008 Proceedings*, 2008.

[93] HR. Liebeck. Design of the blended wing body subsonic transport. *Journal of Aircraft*, 41:10–25, 01 2004.

[94] Z. Van Der Voet, F. Geuskens, TJ. Ahmed, B. Ninaber Van Eyben, and A. Beukers. Configuration of the multibubble pressure cabin in blended wing body aircraft. *Journal of Aircraft*, 49:991–1007, 07 2012.

[95] N. Viola, R. Fusaro, B. Saracoglu, C. Schram, V. Grewe, J. Martinez, M. Marini, S. Hernandez, K. Lammers, A. Vincent, D. Hauglustaine, B. Liebhardt, F. Linke, and C. Fureby. Main challenges and goals of the h2020 stratofly project. *Aerotecnica Missili & Spazio*, 100(2):95–110, Jun 2021.

[96] ZJ. Goraj, M. Kowalski, and B. Goliszek. Stress, strain and displacement analysis of geodetic and conventional fuselage structure for future passenger aircraft. *Aircraft Engineering and Aerospace Technology*, 91(6):814–819, Jan 2019.

[97] EH. Mansfield. On the design of a row of windows in a pressurized cylindrical fuselage. *ARC/R&M*, 3360:1–10, 1964.

[98] MC. Moruzzi, M. Cinefra, and S. Bagassi. Vibroacoustic analysis of an innovative windowless cabin with metamaterial trim panels in regional turboprops. *Mechanics of Advanced Materials and Structures*, 28:1–13, 2019.

[99] MC. Moruzzi, M. Cinefra, S. Bagassi, and E. Carrera. Attenuation of noise in the cabin of a regional aircraft by metamaterial trim panels. In *32th ICAS 20020 Proceedings*, 2021.

[100] MC. Moruzzi, M. Cinefra, E. Carrera, M. Barbarino, P. Vitiello, and S. Bagassi. Vibroacoustic analysis in the cabin of a regional turboprop with innovative materials by actran. In *XXV AIDAA Congress Proceedings*, 2019.

[101] S. Marburg. Six boundary elements per wavelength: Is that enough? *Journal of Computational Acoustics*, 10(01):25–51, 2002.

[102] P. Langer, M. Maeder, C. Guist, M. Krause, and S. Marburg. More than six elements per wavelength: The practical use of structural finite element models and their accuracy in comparison with experimental results. *Journal of Computational Acoustics*, 25(04):1750025, 2017.

[103] S. Chen, Y. Fan, Q. Fu, H. Wu, Y. Jin, J. Zheng, and F. Zhang. A review of tunable acoustic metamaterials. *Applied Sciences*, 8(9), 2018.

[104] MC. Moruzzi, S. Bagassi, M. Cinefra, M. Corsi, and M. Rossi. Design of additively manufactured metamaterial for cabin noise and vibrations reduction. In *XXVI AIDAA Congress Proceedings*, 2021.

[105] JP. Nunes and JF. Silva. Sandwiched composites in aerospace engineering. In *Advanced Composite Materials for Aerospace Engineering*, pages 129–174. Woodhead Publishing, 2016.

[106] M. Corsi, S. Bagassi, MC. Moruzzi, and L. Seccia. Correlation between production parameters and mechanical properties of abs plus p430 fused deposition material. *Proceedings of the Institution of Mechanical Engineers, Part C: Journal of Mechanical Engineering Science*, 236(5):2478–2487, Mar 2022.

[107] H. Rezayat, W. Zhou, A. Siriruk, D. Penumadu, and SS. Babu. Structure–mechanical property relationship in fused deposition modelling. *Materials Science and Technology*, 31(8):895–903, 2015.

[108] D. Scholtz, R. Seresinhe, I. Staack, and C. Lawson. Fuel consumption due to shaft power off-takes from the engine. In *Workshop on aircraft system technologies*, 2013.

Acknowledgments

I'm deeply indebted to my colleagues Marzia Corsi and Sandhya Santhosh and professors Francesca De Crescenzio and Leonardo Seccia for their help and collaboration in these three years. Moreover, I am also grateful to Christian Hesse for his valuable assistance during my period at DLR in Hamburg. Many thanks to Vito Bonaventura of Geven, for helpful information on the cabin design. Last but not least, the completion of my PhD would not have been possible without the support of my supervisor, professor Sara Bagassi.

Appendix A

Element size criterion

In order to fully characterize the vibro-acoustic behaviour of a system (structural or acoustic) in a FEM framework, the element size must be able to capture the minimum wavelength of the problem. The minimum wavelength definition of a system depends on the system properties and on the maximum frequency of the analysis f_{max}.

For an acoustic cavity defined by its speed of sound c_f the minimum wavelength is equal to:

$$\lambda = \frac{c_f}{f_{max}} \tag{A.0.1}$$

For a structural plate the equation depend on the bending wavelength and the speed of sound:

$$\lambda_{bend} = \frac{c_{bend}}{f_{max}} \tag{A.0.2}$$

where the definition of c_{bend} depend on the material type and is a function of the Young's modulus for isotropic materials and of the shear modulus for orthotropic materials within the Poisson's ratio.

The minimum element h size able to capture λ or λ_{bend} is:

$$h = \frac{\lambda_{min}}{k} \tag{A.0.3}$$

where k is the number of elements per wavelength, so the chosen criterion. According to the validation work by Marburg [101] and Langer et al. [102] for linear elements at least 6 or 7 elements are necessary, while for quadratic elements 3 or 4. Therefore, to increase the maximum frequency of an analysis, the element size must be reduced, within the rise of the number of DoF and the computational cost, because:

$$h \propto \frac{1}{f_{max}} \tag{A.0.4}$$

Appendix B

Analytical solutions for modal extraction

In order to validate simple vibro-acoustic systems, as those used to enhance the CUF approach or to preliminary study the material properties, analytical solutions are available. A software to calculate the frequencies and the modal shapes is built in Python. The aim is to speed up the validation process and avoid errors in the non-differential equations resolution.[1]

The library includes simple structures made of an isotropic material and acoustic cavities filled by fluid:

- beam (an edge free and one clamped, both edges clamped);
- rectangular plate (opposite edges simply supported, all edges simply supported, opposite simply supported and clamped respectively);
- circular plate (clamped);
- cylindrical shell (both edges simply supported)
- box closed cavity;
- cylindrical closed cavity.

For the cylindrical shell and cavity the solution is based on Bessel functions [78]. Fig. B.1) reports an example of the interface of the software for a plate. The outputs are the natural frequencies, in the format of a text file, and their modal shapes, colour maps, as reported in Fig. B.2 for the first mode of a beam with a clamped edge and of a simply supported plate.

[1] The first step of the software development is reported in `https://amslaurea.unibo.it/27013/`.

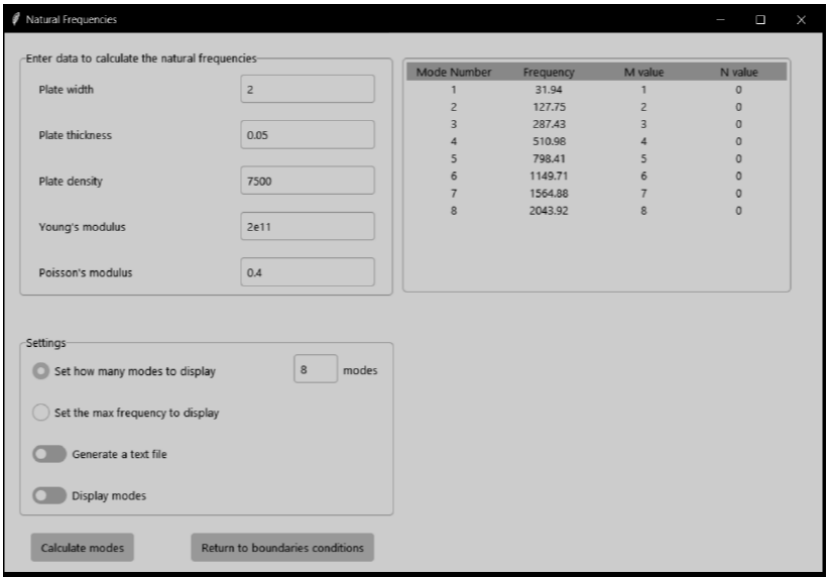

Figure B.1: The software interface for the plate modal extraction: on the top left the inputs, as the plate geometry and the material properties, on the bottom left the output option, as the number of modes and visualization features, on the top right the natural frequencies, calculated by the software.

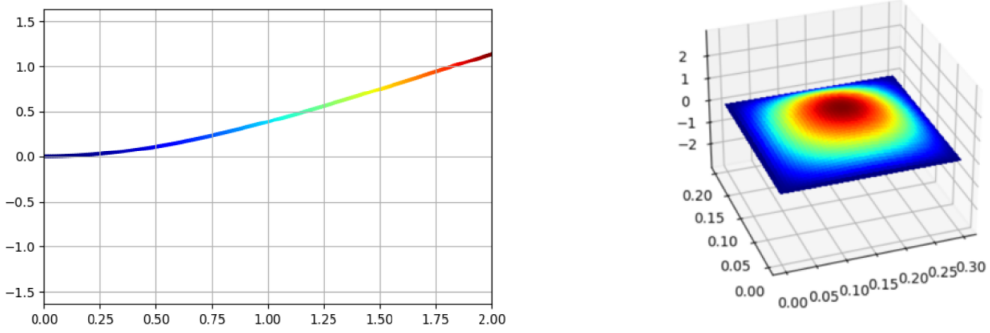

(a) **(b)**

Figure B.2: The visualization of the modal shape for the first natural frequency. (a) A beam with a clamped edge. (b) A simply supported plate.

Appendix C

Shock absorber properties

The shock absorber data sheet is reported. These components connect the several lining panels to the primary structure of fuselage, usually the frames. Therefore, shock absorbers play an important role in the vibrations absorption and more generally in the vibro-acoustic behaviour of the structure.

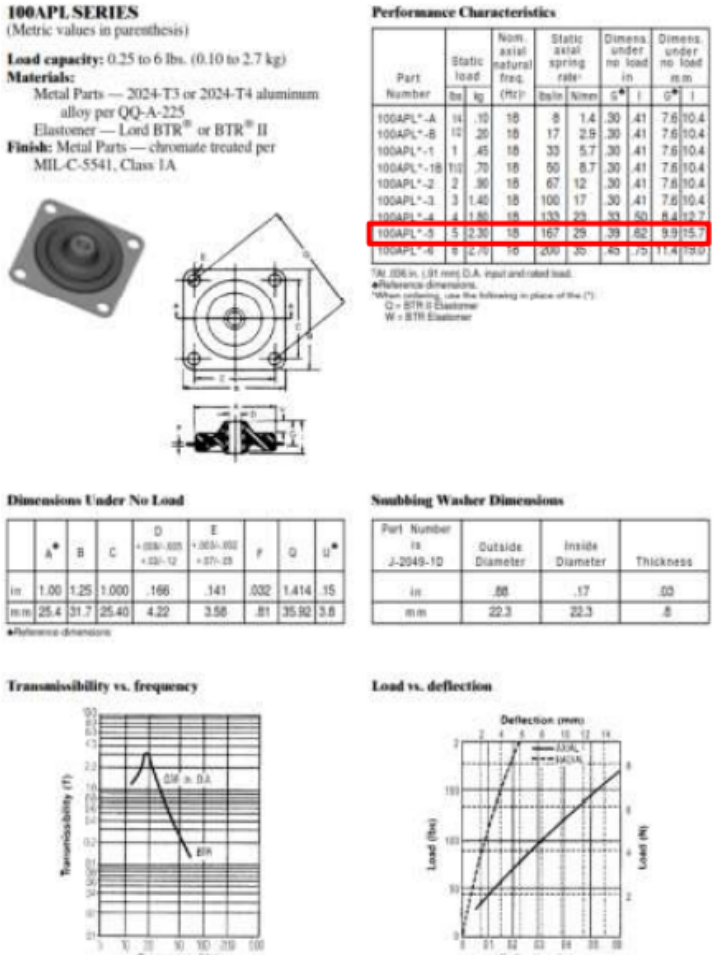

100APL SERIES
(Metric values in parenthesis)

Load capacity: 0.25 to 6 lbs. (0.10 to 2.7 kg)
Materials:
Metal Parts — 2024-T3 or 2024-T4 aluminum alloy per QQ-A-225
Elastomer — Lord BTR® or BTR® II
Finish: Metal Parts — chromate treated per MIL-C-5541, Class 1A

Performance Characteristics

Part Number	Static load lbs	Static load kg	Nom. axial natural freq. (Hz)†	Static axial spring rate lbs/in	Static axial spring rate N/mm	Dimens. under no load in G*	Dimens. under no load in I	Dimens. under no load mm G*	Dimens. under no load mm I
100APL*-A	¼	.10	18	8	1.4	.30	.41	7.6	10.4
100APL*-B	½	.20	18	17	2.9	.30	.41	7.6	10.4
100APL*-1	1	.45	18	33	5.7	.30	.41	7.6	10.4
100APL*-1B	1½	.70	18	50	8.7	.30	.41	7.6	10.4
100APL*-2	2	.90	18	67	12	.30	.41	7.6	10.4
100APL*-3	3	1.40	18	100	17	.30	.41	7.6	10.4
100APL*-4	4	1.80	18	133	23	.33	.50	8.4	12.7
100APL*-5	5	2.30	18	167	29	.39	.62	9.9	15.7
100APL*-6	6	2.70	18	200	35	.45	.75	11.4	19.0

†At .036 in. (.91 mm) D.A. input and rated load.
♦Reference dimensions.
*When ordering, use the following in place of the (*):
C = BTR II Elastomer
W = BTR Elastomer

Dimensions Under No Load

	A*	B	C	D	E	F	G	U*
in	1.00	1.25	1.000	.166	.141	.032	1.414	.15
mm	25.4	31.7	25.40	4.22	3.58	.81	35.92	3.8

♦Reference dimensions

Snubbing Washer Dimensions

Part Number is J-2049-10	Outside Diameter	Inside Diameter	Thickness
in	.88	.17	.03
mm	22.3	22.3	.8

Transmissibility vs. frequency

Load vs. deflection